OAK RIDGE NATIONAL LABORATORY LIBRARIES

3 4456 0566301 0

ORNL/Sub-81/70519/1

ornl

OAK
RIDGE
NATIONAL
LABORATORY

UNION
CARBIDE

UTILIZATION OF AMORPHOUS METALS IN ELECTRIC MOTORS

OAK RIDGE NATIONAL LABORATORY
CENTRAL RESEARCH LIBRARY
CIRCULATION SECTION
4500N ROOM 175
LIBRARY LOAN COPY
DO NOT TRANSFER TO ANOTHER PERSON
If you wish someone else to see this report, send in name with report and the library will arrange a loan.
UCN-7969 (3 9-77)

October 1983

POWER SYSTEMS TECHNOLOGY PROGRAM

OPERATED BY
UNION CARBIDE CORPORATION
FOR THE UNITED STATES
DEPARTMENT OF ENERGY

Printed in the United States of America. Available from
National Technical Information Service
U.S. Department of Commerce
5285 Port Royal Road, Springfield, Virginia 22161
NTIS price codes—Printed Copy: A07 . Microfiche A01

This report was prepared as an account of work sponsored by an agency of the United States Government. Neither the United States Government nor any agency thereof, nor any of their employees, makes any warranty, express or implied, or assumes any legal liability or responsibility for the accuracy, completeness, or usefulness of any information, apparatus, product, or process disclosed, or represents that its use would not infringe privately owned rights. Reference herein to any specific commercial product, process, or service by trade name, trademark, manufacturer, or otherwise, does not necessarily constitute or imply its endorsement, recommendation, or favoring by the United States Government or any agency thereof. The views and opinions of authors expressed herein do not necessarily state or reflect those of the United States Government or any agency thereof.

ORNL/Sub-81/70519/1
Dist. Category UC-97C

UTILIZATION OF AMORPHOUS METALS IN ELECTRIC MOTORS

L. A. Johnson

October 1983

Prepared by

GENERAL ELECTRIC COMPANY
CORPORATE RESEARCH AND DEVELOPMENT
P.O. Box 8
Schenectady, New York 12301

for

OAK RIDGE NATIONAL LABORATORY
Power Systems Technology Program
Energy Division
(under Subcontract No. 70519C)
Date Published: March 1984
operated by

UNION CARBIDE CORPORATION
for the
U.S. DEPARTMENT OF ENERGY
ASSISTANT SECRETARY FOR CONSERVATION AND RENEWABLE ENERGY
DIVISION OF ELECTRIC ENERGY SYSTEMS

Contract No. W-7405-eng-26

TABLE OF CONTENTS

		Page
I.	Introduction	2
II.	Executive Summary	4
III.	Amorphous Metal Helical Ribbon	6
	III.1 Summary of Results	9
	III.1.2 Property Assessment	9
	III.1.3 Conductor Slot Casting	10
	III.1.4 Conductor Slot Formation	11
	III.2 Detailed Results and Discussion	13
	III.2.1 Helical Ribbon Casting	13
	III.2.2 Property Assessment	16
	Annealing and Measurement Methods	16
	Properties of Multilayer Samples	26
	Effect of Stacking Pressure	27
	Annealing Under Load	30
	Annealing Under Flattening Load	33
	Bonding	33
	III.2.3 Conductor Slot Casting	37
	Shallow Grooved Patterns	40
	Deep Open Grooved Patterns	50
	Metal Filled Groove Patterns	52
	Glass Filled Groove Patterns	67
	III.2.4 Conductor Slot Forming	89
	Hot Wire Forming	92
	I^2R Stylus Forming	93
	Electron Beam Heating	98
	Hot Die Punching	110

LIST OF TABLES

No.	Title	Page
I.	D-C and A-C Properties of Helix Samples	24
II.	D-C Properties Under Various Conditions of Anneal and Measurement	34
III.	A-C Properties of Multilayer Samples	35
IV.	A-C Properties Reseating and Retesting Sample 073081 H-1-TL4	36
V.	Losses With Various Bonding Treatments	38
VI.	Thick Film Pastes Used to Fill Slots	86
VII.	Effect of Beam Writing Parameters	104
VIII.	Bead Thickness Next to Kerf on Melted Samples	105
IX.	Effect of Beam Current on Mark Intensity	108

LIST OF FIGURES

No.	Title	Page
1.	Schematic of helical ribbon casting	8
2.	Schematic of conductor slot casting in a helical ribbon	8
3.	Air casting equipment	14
4.	Fixtures for annealing and measuring d.c. properties	18
5.	Typical d.c. hysteresis loops	20
6.	A.C. measurement fixture	21
7.	Effect of measuring 180^0 sample without a return flux path	22
8.	A.C. measurements of straight samples	25
9.	Fixture for annealing and measuring under axial load	28
10.	Effect of applying axial load to sample annealed under load	29
11.	Sample annealed under axial load of 20 psi	31
12.	Ten-layer sample before and after anneal	32
13.	Effect of bonding sample rings with various agents	39
14.	Effect of groove depth on cast slots	42
15.	Helical ribbon cast over unfilled groove pattern	43
16.	Detail of slot registry	43
17.	Reduced stacking factor due to slot burr	44
18.	Helical ribbon cast over open groove pattern	46
19.	Cross section of ribbon cast over 8 Mil parallel groove	48
20.	Cross section of ribbon cast over 8 mil radial groove	48
21.	Effect of ribbon thickness on slot casting	49
22.	Effect of casting on braze alloy inserts	53
23.	Ribbon cast over metal inserts	55
24.	Ribbon cast over narrow metal insert	57
25.	Groove filling with plasma sprayed metal	59
26.	Ribbon cast over plasma sprayed insert	61
27.	Particles in ribbon cast over plasma sprayed insert	63
28.	Air pocket in ribbon cast over plasma sprayed insert	63
29.	Thermal conductivity of insert materials	65
30.	Surface bubbles in glass filled grooves	69
31.	Cross sections of glass filled grooves	70

32. Surface bubbles in glass insert grooves 71
33. Glass insert before casting 72
34. Casting wheel with glass filled grooves 73
35. Movie frame of casting over glass inserts 75
36. Glass insert after casting 75
37. Ribbon cast over glass insert 77
38. Glass particle on ribbon of figure 37 77
39. Ribbon cast over glass inserts 78
40. Schematic of molten metal wetting of casting wheel and glass insert 80
41. Ribbon cast over glass insert 82
42. High magnification of figure 41 82
43. High magnification of figure 42 83
44. Ribbon cast over glass insert 83
45. Thick ribbon cast over glass insert 84
46. Cross section of "thick film" glass insert 87
47. Ribbon cast over ceramic insert 90
48. Erosion of ceramic insert 90
49. High magnification of ceramic insert erosion 91
50. Ribbon scribed with 20 amp stylus 95
51. Transverse cracks in scribed ribbon 95
52. Samples marked with electron beam at one inch per second 100
53. Sawtooth beam modulation 101
54. Cross section of ribbons with electron beam traces 102
55. Cross section of ribbons with electron beam traces 106
56. Stress relief from fracture of crystallized line 109
57. Fracture of electron beam line 111
58. Holes made in ribbon with hot die punch 113

Foreword

This final report covers work sponsored by the Division of Electrical Energy Systems of the United States Department of Energy under subcontract 86X-70518C (formerly 40X-70519C) from Oak Ridge National Laboratory, M. O. Pace, Project Manager, and was prepared by the Corporate Research and Development, General Electric Company, Schenectady, New York, L. A. Johnson, Principal Investigator. The duration of this contract was from February 1981 to November 1982.

The direct contributors to this project have been P. G. Frischmann, S. J. Kelly, R. P. Laforce, L. C. Perocchi, A. C. Rockwood, J. R. Wilcox and L. A. Wojcik.

I. INTRODUCTION

In the past several years, glassy metal, or amorphous metal, alloys with excellent soft magnetic characteristics have become available. These alloys, produced in thin strip, are the result of very rapid cooling of liquid alloy such that no crystalline structure appears in the material. Measured losses at 60 Hz are an order of magnitude less than those of nonoriented silicon iron. This low loss coupled with the long-range potential for low cost has generated interest in application of these materials for magnetic cores for stationary and rotating equipment.

It is estimated that more than 35×10^9 kWhrs of electrical energy are lost annually in the U.S.A. in the core laminations of motors. Analysis and experimental measurements indicate that if amorphous metals were used in motors, these motor iron losses could be reduced by as much as 80%. Such a reduction in these losses would provide a benefit of 28×10^9 kWhrs conserved with an approximate value of $1100 million (at $.04/kWhr) annually after complete replacement.

The principal hurdle which must be overcome to realize these potential savings is the development of a cost effective method for forming motor cores from amorphous metal. Two characteristics of the material in its presently available forms make its use in motors using standard design and manufacturing methods prohibitively costly. These characteristics are its thin gauge (0.001 to 0.002 inches) and its high hardness (~700 Vickers). The thin gauge means that about 15 to 20 times as many laminations must be punched and handled compared to present core material. The high hardness has been shown to lead to unacceptably low punching die life. Together these aspects would make the cost of using amorphous metals by standard approaches unacceptable.

Thus, the objective of this work has been to establish the feasibility of producing amorphous metal in a form which could be utilized in a motor core at low cost while retaining its excellent magnetic properties. The approach taken was to develop a process for casting amorphous

metal in the form of a continuous helical ribbon in order to avoid the necessity of handling individual laminations. A second objective was to either 1) establish the feasibility of directly casting conductor slots in the amorphous metal ribbon or 2) develop a means for rapid, inexpensive formation of the conductor slots after casting the helical ribbon.

II. EXECUTIVE SUMMARY

The major obstacle to realizing the large energy savings potential from the use of amorphous metals in motors is the cost of forming and assembling this unique new material into a motor core. Efforts to accomplish this assembly by the traditional method of lamination cutting and stacking have been technically successful, and the performance results have confirmed the more than five-fold reduction in core loss potential from utilizing amorphous metals. However, an analysis of the costs associated with this direct materials substitution approach indicate that the additional costs exceed the energy savings benefit. Thus, in order to realize the energy savings potential of amorphous metals in motors, innovative methods must be developed to produce the material in a form which can be converted to a motor core at low costs while retaining the excellent intrinsic magnetic properties. The objective of this contract effort has been to demonstrate the feasibility of a cost effective method of producing amorphous metals in a form useful as a motor core.

In a preceding contract from the U.S. Department of Energy (DE-AC01-78ET29313) a method was developed to produce a solid composite material of about 90 volume percent amorphous metal flake in a polymeric binder. However, it was discovered during this work and other parallel fundamental studies that the compaction-thermal cycle of the consolidation process resulted in an irrecoverable, intrinsic degradation of the magnetic properties due to a stress induced directional ordering. This ordering anisotropy caused the compacted composites to exhibit magnetic properties that were unacceptable for motor application.

In the present contract a second alternative approach was examined. The objective of this approach was to establish the feasibility of directly casting amorphous metal in the form of a continuous helix. Such a continuous helix, bonded into a cylindrical form, would serve as a motor stator core. A second objective of this approach was to either 1) establish the feasibility of casting conductor slots directly in the edge of the helical ribbon or 2) develop a means for rapid, inexpensive

formation of the conductor slot after casting the helical ribbon.

This approach offers substantial economic advantage. All lamination punch operations along with the individual stacking of laminations would be eliminated. Also, the amount of scrap would be significantly reduced.

It was established that helical ribbon with good properties could be made. This was demonstrated by the casting of many helical samples seven inches in diameter and one-half to one inch wide with as many as 120 layers. Methods for simultaneously casting conductor slots were examined. Two methods were found to accomplish this. However, each suffered a different single deficiency which made it impractical for scaleup. One method consisted of casting the helical ribbon on a wheel that contained the conductor slot pattern in the form of a shallow continuous groove. This produced ribbon of the desired shape and form except it had burrs approximately 0.0002" high at the edge of the slots. This prevented tight, uniform packing of the helix. A second method avoided the burr problem by filling the groove pattern with a low conductivity material. This produced good, slotted helical ribbon with no burr, but the casting wheel had insufficient durability for continuous production.

Thus, several methods for forming the slots after the ribbon was cast were explored. Of all of the methods explored electron beam cutting had the best success when measured by both technical and economic criteria.

It is our judgment that the methods developed in this contract could be successfully extended to a viable manufacturing process for the production of amorphous metals in a form useful for motor application. A few key engineering tasks would require demonstration. These include: 1) effective cooling of the casting wheel, 2) development of a ribbon catching and winding method, 3) development of ribbon handling equipment for continuous electron beam cutting, and 4) a method of bonding, clamping and annealing the helical stator core.

III. AMORPHOUS METAL HELICAL RIBBON

The objective of this approach was to determine the feasibility of casting amorphous metal ribbon in the shape of a helix with properties suitable for motor applications. The tasks included 1) determination of the casting parameters required to produce a helical ribbon, 2) evaluation of the magnetic properties, 3) developing methods for patterning a wheel for producing motor slots in as-cast ribbon, and 4) assessing methods for forming conductor slots in ribbons after casting.

Task I: Helical Ribbon Casting

The planar flow casting methods previously developed for casting straight ribbon on the outer periphery of a casting wheel were adopted and extended for casting helical ribbon. In order to produce a ribbon in helical form the casting was done on the flat side of the casting wheel as shown schematically in figure 1. Optimization of the casting process was focused principally on those aspects which differ from straight ribbon casting. These process parameter variables included nozzle geometry and positioning, wheel speed, surface conditioning and ribbon removal.

Task II: Property Assessment

The magnetic and physical properties were measured and evaluated as a function of the processing conditions. Physical measurements included dimensional characteristics, surface and edge irregularities, and degree of uniformity. Magnetic properties were established by measurement of both the d.c. and a.c. magnetic properties. Included in this task was the evaluation of stacking, bonding and annealing and their effects on properties.

Task III: Conductor Slot Casting

The objective of this task was to establish the feasibility of directly casting in the edge of the ribbon shapes simulating conductor slots. The approach taken to achieve the direct-cast conductor slots was to incorporate a low thermal conductivity or non-wetting pattern in the surface of the casting wheel so that this pattern created a slow quenched, brittle pattern in the ribbon which could be broken out to create the conductor slots. This process is illustrated schematically in figure 2. Three different approaches were pursued to produce a pattern in the casting substrate that would provide a lower quench rate. These included: 1) a shallow grooved pattern with no filler material in the grooves, 2) a deep, narrow grooved unfilled pattern or filled with a low thermal conductivity, bonded glass or ceramic or 3) filled with a low thermal conductivity, bonded metal.

Task IV: Conductor Slot Forming

This task was established as an alternative approach to the preceding task. Knowing that there was a risk of not achieving completely satisfactory results by direct casting, the objective of this task was to explore and evaluate methods of forming conductor slots in helical ribbon after casting. Four approaches were pursued: 1)cutting the slots with a hot wire, 2) hot punching, 3) local resistance heating of the ribbon, and 4) electron beam cutting. All of these approaches are based on one of two concepts. First, at elevated temperatures below the crystallization temperature the amorphous ribbon becomes soft, thus punching or slitting might be accomplished without excessive die wear. Second, locally crystallized regions of the ribbon are brittle and can be broken clearly without any tool wear and without creating a burr.

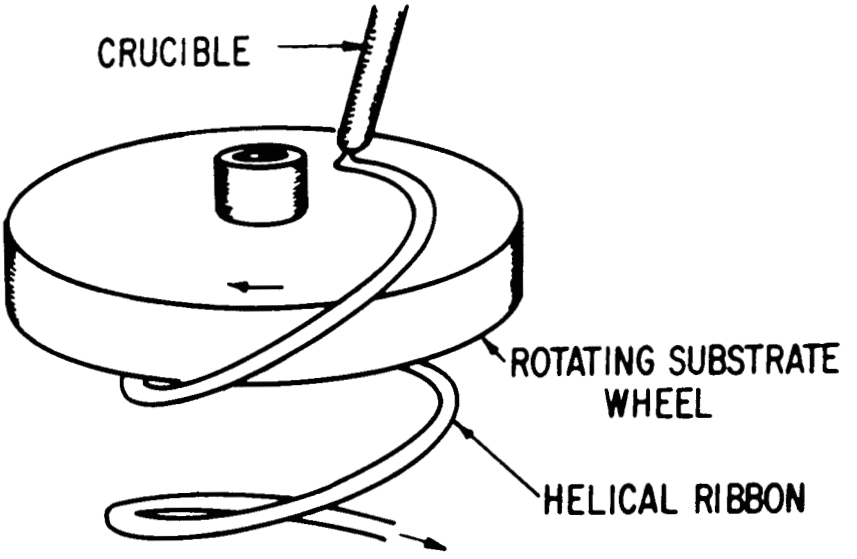

Figure 1. Schematic representation of helical ribbon casting.

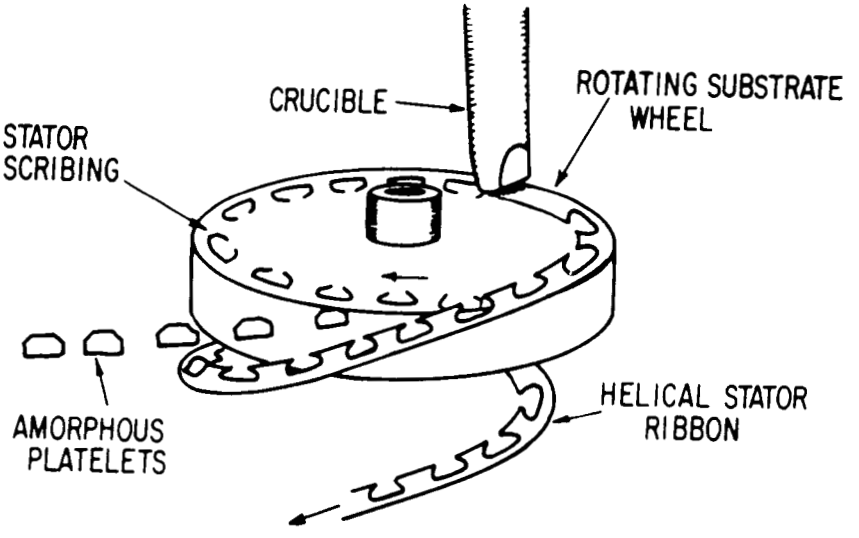

Figure 2. Schematic representation of conductor slot casting in a helical ribbon.

III.1 Summary of Results

III.1.1 Helical Ribbon Casting

The major difference between straight and helical ribbon casting is the variable tangential velocity (proportional to the radius) of the helical casting. This leads to a ribbon that is slightly thicker on the inside diameter than the outside diameter. This problem was solved by tilting the crucible slightly toward the center of the casting wheel. This results in a gap between the wheel and nozzle that increases with increasing radius and the casting of uniform ribbon thickness. Thickness uniformity will be very important for motor manufacture in order to obtain the highest space factor possible and to reduce stresses in the core.

The important casting variables and their preferred values are listed below:

Composition	$Fe_{81.5}B_{14.5}Si_4$
Nozzle dimensions	.022 x 0.5-1.0 inches
Nozzle/wheel gap	.010" outside - .009" inside
Wheel material	Cu-1%Cr
Wheel finish	600 grit polish plus continuous wire brush conditioning
Ejection pressure	2.25 psi
Ejection temperature	1250°C
Surface velocity	65 ft/sec
Atmosphere	air

III.1.2 Property Assessment

The shape of the helical ribbon samples presents some unique problems for magnetic measurements. Special annealing and measurement fixtures were built to handle specimens of this shape.

Generally, as the method for casting helical ribbon improved so did the magnetic properties. In d.c. measurements coercive forces (H_c) of about 0.04 oersteds and flux densities at one oersted (B_1) of about 15 kilogauss were regularly achieved after annealing. In 60 Hz measurements at a peak flux of 14 kG losses of 0.13 watts per pound and excitation of 1.0 volt-amps per pound were achieved. These values are comparable to those achieved from straight ribbon casting. The properties of multiple turn samples were extremely sensitive to any stress on the samples during the anneal. Good properties were achieved only when the layers were carefully nested to provide exact registration between layers.

Several bonding compounds were evaluated. Compounds that cured to a hard or stiff state resulted in a stressed sample with poor magnetic properties. When an elastically compliant material was used for encapsulation, good properties could be maintained. Further work on bonding and minimizing stress is required in order to achieve an acceptable core.

III.1.3 Conductor Slot Casting

Cast, annealed and stacked helical ribbon could be utilized directly as the yoke of a motor stator and provide about 50-70% of the loss reduction potential of a complete amorphous metal stator core. In order to make the stator core completely from amorphous metal, conductor slots must be cut into the inside diameter of the helical ribbon. Direct punching would be possible but prohibitively expensive. Thus, a rapid, cheap method is needed to form the conductor slots if the full potential of amorphous metals is to be realized.

The approach that was taken to accomplish this was to explore the feasibility of directly casting the conductor slots. This was done by patterning the casting wheel with a low conductivity or non-wetting line pattern to produce a brittle region that could be readily broken away to form the slots. Three different methods for making the low quench-rate pattern were pursued. These were 1) an unfilled shallow grooved pattern, 2) a grooved pattern filled with glass or ceramic, and 3) a

grooved pattern filled with a low thermal conductivity metal.

The first method of unfilled shallow grooves was very successful in continuously producing slotted, helical ribbon. However, a small burr was always produced on the downstream edge of the slot. While these burrs were substantially less than a mil in height, they prevented the uniform stacking of the helix. Thus, this method was unacceptable.

Glass filled grooves solved the burr problem. The glass inserts, however, were unable to withstand the thermal shock of the casting and quickly fractured so that long casting runs were not possible. Plasma sprayed ceramic inserts also solved the burr problem and did not suffer from thermal shock. However, there was a gradual erosion of the insert so that only a few casting runs could be made before rework of the casting wheel was required.

III.1.4 Conductor Slot Forming

Four approaches were pursued to assess the feasibility of economically forming conductor slots on the inside diameter of the helical ribbon after casting. These included: 1) using a hot, resistance heated wire formed into the shape of a conductor slot and pressed onto the ribbon for a short time to create a crystallized, brittle outline along which the slot could be broken out, 2) using a stylus with electric current flowing through it into the ribbon to "draw" the embrittling pattern in the ribbon, 3) using a magnetically steered electron beam to form the pattern, and 4) using a heated die punch to punch the conductor slots without incurring excessive die wear.

All of these approaches worked to varying degrees. The hot wire method yielded a slot edge which was somewhat rougher than desirable. This drawback, however, could readily be improved to an acceptable level with further development work. The major deficiency of the hot wire method was inadequate speed for economic production. Rates of about four slots per second were achieved. Actual production rates would have to be about 400-1000 times faster. Further manufacturing development

could probably achieve a factor of 20 increase in speed, but it is doubtful that the additional factor of 20 could be accomplished.

The embrittled pattern created with the electric current carrying stylus was also capable of fracture and slot removal. Careful control of the operating parameters was required in order to achieve acceptable break-out without rough or cracked edges. The principal problem with this method was also inadequate speed for economical manufacturing. In this case, speed is limited by heating of the stylus tip to about 150 inches per minute. This is about a factor of 20 slower than the required velocity based on processing equivalent stack length with a high speed punch press on present motor lamination steel.

The third method of creating embrittled patterns was with a magnetically steered electron beam. This method is extremely rapid; the required speeds of 3000 inches per second were successfully achieved. Break-out of the patterns yielded acceptable edge quality. Development of ribbon handling equipment and rapid pattern break-out equipment would bring this method to production stage.

The fourth method evaluated did not rely on the creation of a brittle region for subsequent break-out. Rather, it was a method of hot die punching based on the fact that above a certain temperature (usually referred to as the glass softening temperature) the amorphous metal becomes very weak and can be cut easily without tool wear. To make this process work it is essential that the ribbon be heated quite rapidly and that after cutting it be cooled rapidly in order to avoid thermal structural relaxation that would interfere with subsequent stress relief annealing. A compound die was made of two pieces of brass which clamp the ribbon from both sides and through which passes a cylindrical steel punch. By preheating the steel punch and driving it through the die at a controlled rate, very little force was required to obtain a punch-out. Because of the poor dimensional tolerance in this die set and the high ductility of the amorphous ribbon in localized warm region, a deep-draw lip remained on the ribbon. This lip was removable with an abrasive belt. It is believed that with properly designed die tolerance the

punching could be achieved without forming the lip. This approach then shows considerable promise for die punching with long die life. However, it is unlikely that punching rates could equal or exceed those presently used with standard lamination steel. Thus, because of the thin gauge of the amorphous ribbon the economics of this approach remain a problem.

III.2 Detailed Results and Discussion

III.2.1 Helical Ribbon Casting

Figure 1 shows schematically the basic approach to helical ribbon casting. By casting on the side of a rotating casting substrate and using the appropriate process parameters, the cast product takes the shape of a helix. This shape is potentially ideal for use in motor stators. The simple helical shape without conductor slots could be used directly as the yoke of a motor stator. With conductor slots formed into the helix the entire stator core could be made.

During the preceding contract the feasibility of casting helical ribbon was established. On the present program the process was optimized particularly with regard to achieving optimum magnetic properties and uniform ribbon dimensions. The initial casting runs were done in vacuum in order to avoid problems associated with the air boundary layer on the moving casting substrate perturbing the molten metal liquid puddle. Very smooth ribbon was produced in vacuum, but the retention of the ribbon to the casting wheel was too short to achieve the quench rate required to obtain good magnetic properties.

In order to keep the ribbon on the wheel longer so that it quenched to a lower temperature, casting on this program was done in an air atmosphere. The casting equipment for these experiments is shown in figure 3. In air we found the ribbon tends to stick to the wheel too long. If this happens, the ribbon can stick a full revolution, come back under the casting nozzle, and ruin the casting trial.

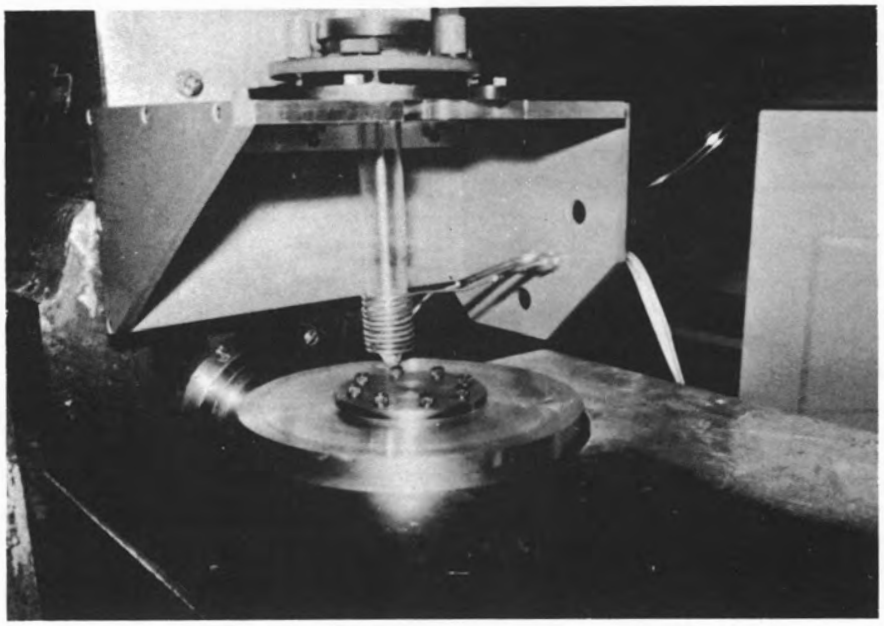

Figure 3. Air casting equipment

To solve this problem in casting straight ribbon, we have found that by constantly conditioning the wheel surface with a rotating fine wire brush the departure point of the ribbon can be controlled. Additionally, the surface conditioning from this rotating brush creates a steady state surface which gives a constant high quality ribbon surface.

With these basic casting methods and equipment in place 159 casting runs were run in air to debug the equipment and scope and optimize the important casting variables. The optimum conditions for the key variables are shown in section III.1.1. The general effect of variations in these variables is discussed below.

Increasing the nozzle to wheel gap, ejection pressure and nozzle opening, and decreasing the wheel speed either all simultaneously or individually makes thicker ribbons. Thus, there are many combinations of these four principle variables that yield the optimum thickness. However, all of the combinations that give this thickness do not give good quality ribbon.

There follows a discussion of the effect of each variable when the other variables are adjusted to maintain constant ribbon thickness.

Wheel Speed. High wheel speeds give the faster quench rates and consequently better magnetic properties. Increasing the speed beyond the optimum is limited by two effects. First, higher speeds cause a greater perturbation of the molten metal pool by the wheel air boundary layer which leads to larger and more air pockets on the bottom side of the ribbon. These, in turn, decrease the ribbon stacking factor and degrade the magnetic properties. Also, with increasing speed heat dissipation from the wheel becomes increasingly difficult since more heat per unit time is transferred to the wheel.

Ejection Pressure. Low ejection pressures cause a periodic fluctuation in the heel of the puddle which make the air pockets align along the width of the ribbon in a pattern referred to as "fish scale". Also, pressures both higher and lower than optimum result in rough edges on

the ribbon.

Nozzle Opening. Increasing the nozzle opening provides smoother ribbon and decreases thickness variation. The size of the opening is restricted by the limits of the other three compensating variables.

Nozzle to Wheel Gap. Smaller gaps require increasing precision in equipment tolerance to maintain uniform ribbon thickness.

The major differences between helical ribbon casting and straight ribbon casting are 1) because of the lower speed on the inside diameter compared to the outside diameter the crucible bottom should be sloped to increase the gap between the nozzle and wheel with distance away from the center of the wheel; 2) the cooling design for the wheel is much more difficult. Using presently developed cooling methods it is estimated that rotor inside dimensions of less than six inches would probably not be possible.

In this program the maximum width cast was one inch. The smallest inside diameter of one inch wide helix was 3-3/8 inches. The most material cast in a single run was 200 grams.

III.2.2 Property Assessment

Annealing and Measurement Methods

Magnetic properties were measured with a variety of developmental fixtures. The criteria on which these fixtures were developed was to maximize the through-put in annealing and measuring. In contrast to measuring straight samples, helical samples have the general shape of a torous which requires that each turn of the excitation or sensing coil thread through the center of the torous or that each turn of the helix thread the center of the coils. Since sample diameters and total core cross sectional area were known from the casting wheel diameter and melt sizes, calculations showed that a fixture split through the plane of the helix was impractical because of the required wire size and turn

density. An alternate fixture which would thread 20 turns simultaneously was built with the idea of reducing the winding work by a factor of 20. This fixture had male and female sockets on opposite ends, each wire incrementing one pin with start and finish leads attached to pins one and 21. After threading one end through the coil form 5 times, a total of 100 turns were in series on the sample. Comparative measurements made with this technique and precision wound excitation and pick-up coils gave inconsistent values varying by up to 30%. This discrepancy and variability was large enough to cause us to abandon the technique.

Some of the fixtures which finally evolved are shown in figure 4. The base of the coil form is aluminum of "U" shaped cross section with short legs. Over this an aluminum washer segment of 270° to 330° was placed. Pick-up coils were wound over the closed section of the coil form and excitation windings wound over the pick-up coil. Samples were then threaded through the opening. When more than 10 layers of sample were required, this fixture was abandoned in favor of hand-winding as insertion of multilayered samples become increasingly more difficult with an increasing number of layers.

The large ratio of pick-up coil cross-sectional area to sample cross-sectional area necessitated some means of air flux compensation. This was accomplished most conveniently by building a second fixture for flux voltage bucking. The bucking fixture had identical geometry but with access to the pick-up winding to allow turns to be added or removed to obtain balance. Balance was indicated by exciting both primaries in series and connecting the pick-up coils in series bucking. Turns count was adjusted to give minimum output with no sample in place.

To minimize handling, coils were wound with HML insulated copper so that a sample could be placed in a fixture in the as-cast condition, annealed and cooled under d.c. excitation and measured without having to remove the sample from the fixture. To prevent turns from shorting to

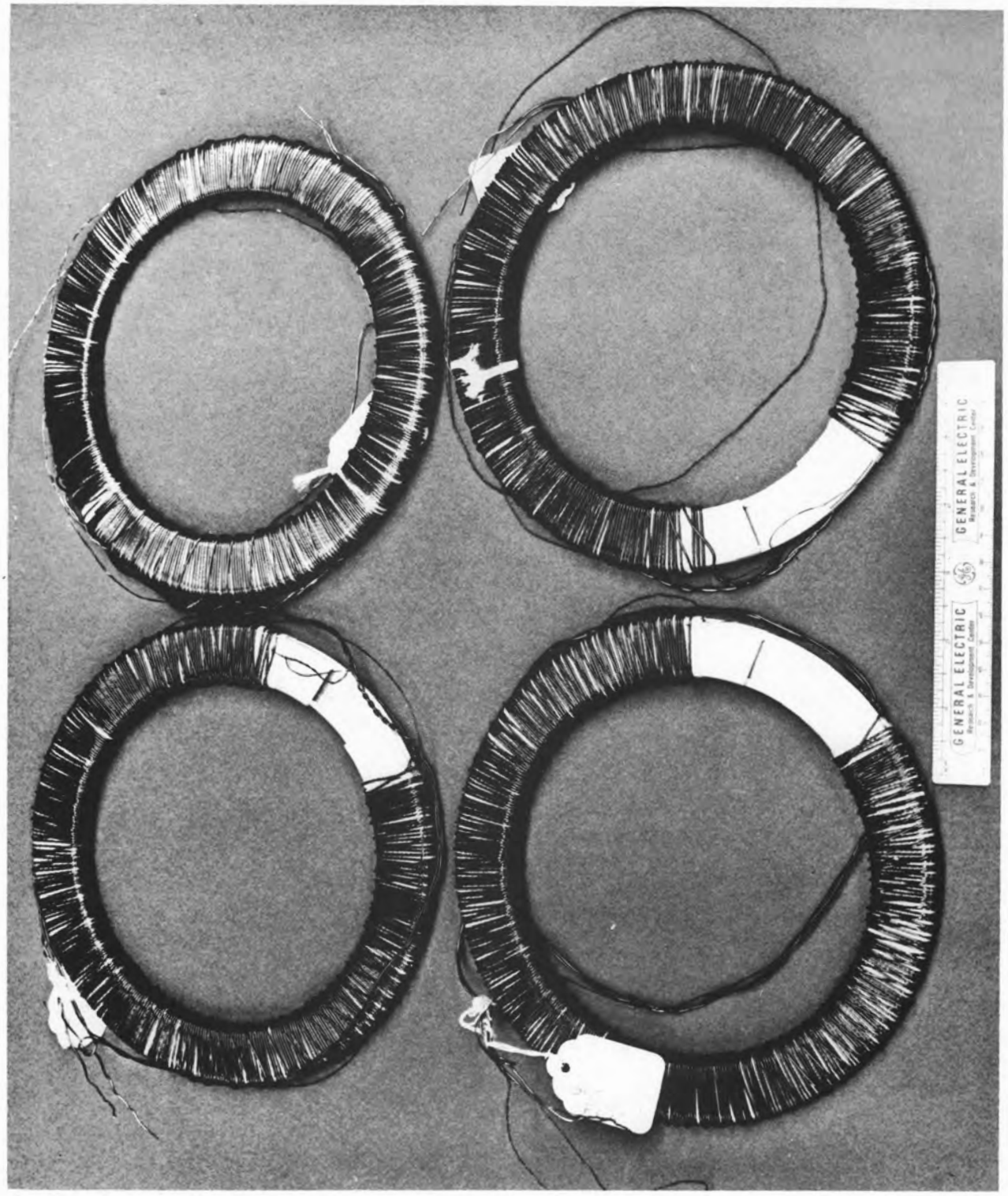

Figure 4. Fixtures for annealing and measuring d.c. properties

the coil form, all edges were rounded and KAPTON* insulation was used between layers and under the first layer. Based on work with straight ribbon casting, an anneal cycle of 345°C for 2 hours in N_2 with 25 oer d.c. field was chosen.

In general, hysteresis loops were drawn using a conventional set up of an integrating flux meter, bipolar power supply, current measuring resistor and chart recorder. Samples were sequentially excited through one oersted, ten oersted and fifty oersted hysteresis loops with the operator offsetting the zero position so that three loops could be viewed on one data page. Typical curves are shown in figure 5.

After experience was gained with multilayer samples, tests were made with sample length reduced to 1.1 turns. These samples were considerably easier to insert into a coil form and gave results in good agreement with multilayer samples.

Since d.c. magnetic properties of helically cast samples were found to be in reasonable agreement with straight cast material, the more significant a.c. properties were compared. Measuring a.c. properties in the aluminum fixtures originally designed for both annealing and d.c. measurements developed some problems. Phase shift between the excitation and pick-up signals was severe as observed on a.c. hysteresis loops. This phase shift is caused by significant eddy currents in the aluminum fixtures. To circumvent this problem a new measurement fixture was designed using Lexan** as the structural material, figure 6. Since this fixture would not withstand repeated anneal cycles, annealing and measuring were done in different fixtures. To prevent breakage of the embrittled sample during removal from the anneal fixture, it was desirable to work with 180° segments. It was recognized that a demagnetization factor would be evident and to determine this value d.c. curves were taken. These are shown in figure 7. The slope of the A curve in figure 7a shows a demagnetizing field of 0.7 oersted. This varies

* TRADE MARK DUPONT CORP.

** TRADEMARK GE CO.

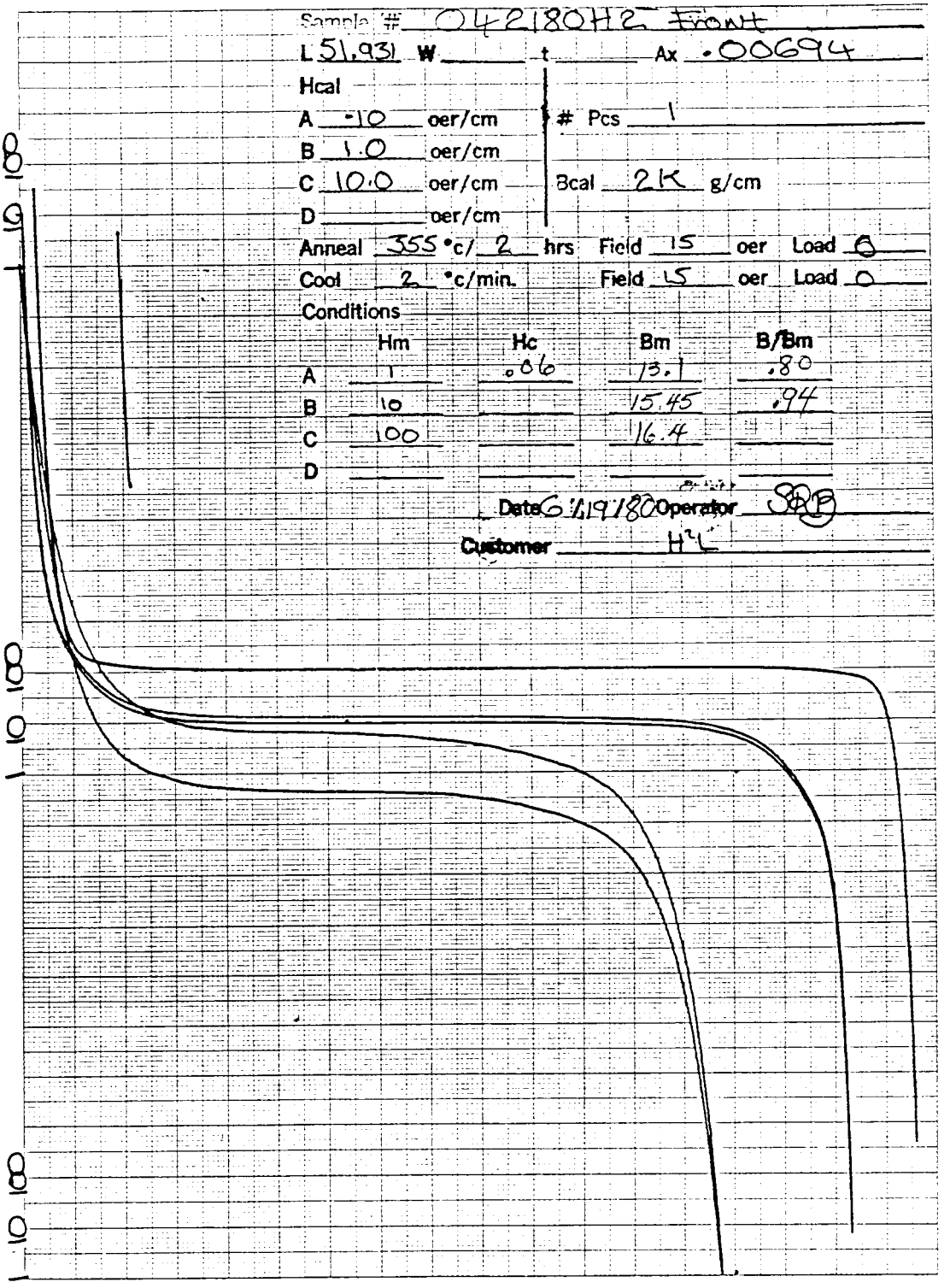

Figure 5. Typical d.c. hysteresis loops.

Figure 6. A.C. measurement fixture.

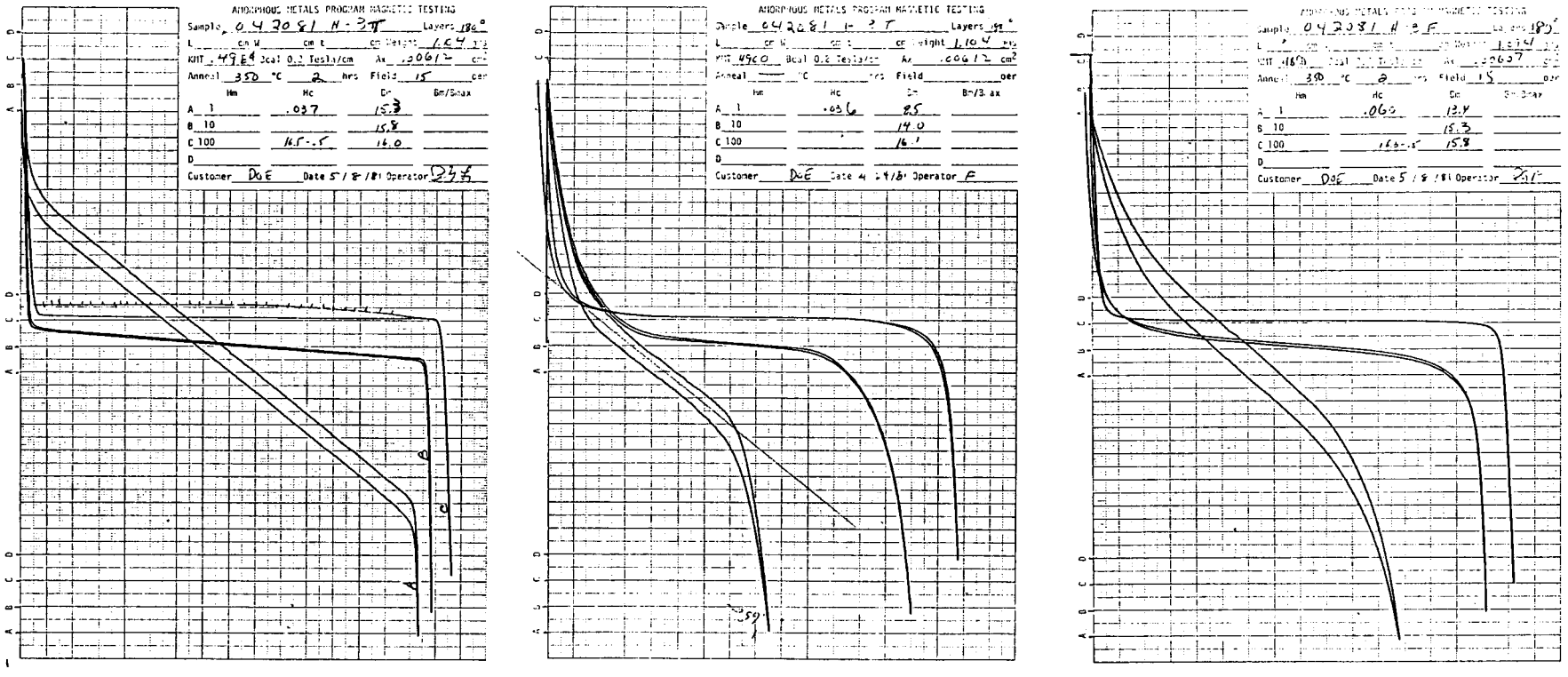

a. End of casting, annealed.

b. End of casting, unannealed.

c. Start of casting, annealed.

Figure 7. Effect of measuring 180° sample without a return flux path.

somewhat with samples of different widths and thicknesses. Since all samples measured in this part of the work were essentially the same dimensions, we have assumed this demagnetizing value to be a constant. This means that when an external field of one oersted was applied, the sample experienced only .3 oer.

The curves in figure 7 also show the small amount of unbalance between the pick-up coil and the bucking coil in the a.c. fixture. This value is calculated from the slope of the loop in the region between 50 and 100 oersted and has been evaluated at 5 gauss/oersted. A correction for this is made only when samples are driven over 10 oersted. Comparing figure 7a and 7c, the significant improvement in d.c. properties at the end of the 150 gram casting compared with the start is evident. Figure 7b is included to show the properties near the end of the casting in the unannealed state and to compare with figure 7a, after annealing.

A.C. measurements were made on many 180° sample segments and are tabulated in Table I. It will be noted that magnetic properties of helically cast ribbon segments compare favorably with straight cast ribbon. A.C. measurements were made using the circuit outlined in figure 8. Three voltage signals, $\dot{B}$, H and $\int\dot{B}$, were fed into a digital oscilloscope, a Norland 3001 which captures the three signals simultaneously. The voltages are sampled every 20 μsecond, digitized and stored in memory. A stored program is then called out to manipulate the data, incorporate calibration constants appropriate to the fixture and calculate maximum flux density, residual flux density, maximum drive field, coercive force, losses in watts/pound and exciting power in volt-amps/pound after the sample cross sectional area has been entered in the program. The calculated values are presented as hard copy. No corrections have been made for the demagnetizing field. Loss calculations are not affected by this but excitation power is presented approximately .5 volt-amps/# higher than true value.

TABLE I

D-C AND A-C PROPERTIES OF HELIX SAMPLES

		D-C				A-C			
						B_{max} = 14 kG			
						60Hz sine B			
Run Number	position*	H_c (oer)	B_1 (kG)	B_{10} (kG)	B_{SAT} (kG)	H_c (oer)	H_{max} (oer)	LOSS ($\frac{watts}{pound}$)	EXCITING POWER ($\frac{volt-amps}{pound}$)
58	20	.066	14.0	15.9	16.4				
61	20	.053	15.3	15.9	16.4	.029	.14	.078	.30
63	50	.052	15.5	16.4	16.4	.034	.22	.091	.43
64	50	.062	15.5	16.1	16.4	.032	.21	.089	.38
65	20	.054	14.7	16.1	16.4				
"	50	.046	15.1	16.1	16.4				
"	80	.068	13.2	15.7	16.4	.075	2.30	.129	4.23
66	20	.050	14.7	15.9	16.4				
"	50	.044	15.0	15.9	16.4				
"	20	.026	15.4	16.2	16.4				
67	20	.080	12.6	15.7	16.4				
"	50	.040	15.9	16.3	16.4				
"	80	.036	15.8	16.3	16.4				
68**	20	.068	13.9	15.6	16.4	.112	1.46	.171	1.38
"	50	.040	14.8	15.9	16.4	.101	.96	.170	.90
"	80	.054	14.3	15.8	16.4	.101	1.16	.167	1.05
69**	50	.050	15.1	16.3	16.4	.096	.81	.155	.79
72	20	.116	14.5	15.8	16.4				
"	80	.090	14.2	15.8	16.4				
75**	80	.050	15.1	16.1	16.4	.027	.18	.073	.37
92**	10	.056	15.0	16.3	16.4	.085	.89	.133	.813
"	30	.064	15.5	16.4	16.4	.102	.84	.164	.791
"	50	.058	15.5	16.3	16.4	.096	.71	.160	.701
"	70	.056	15.6	16.4	16.4	.101	.59	.160	.610
"	90	.064	15.6	16.4	16.4	.101	.62	.161	.614
94**	20	.055	15.0	16.1	16.4	.085	1.17	.136	1.15
"	50	.056	14.9	16.1	16.4				
"	80	.045	15.3	16.1	16.4				
95**	20	.060	15.1	16.1	16.4	.091	2.26	.156	1.55
"	80	.080	15.0	16.1	16.4	.107	1.86	.172	1.35
96**	50	.060	14.4	15.7	16.4	.091	1.17	.137	1.18
"	80	.070	12.7	15.9	16.4	.203	7.79	.220	1.60
97**	50	.048	14.7	15.5	16.4	.091	.91	.140	.86
"	80	.052	15.0	16.0	16.4	.091	.94	.145	.97
99**	20	.082	15.4	16.1	16.4	.118	2.01	.176	1.34
"	80	.065	15.1	16.1	16.4	.091	.74	.152	.76
100**	20	.064	15.0	16.1	16.4	.096	1.42	.148	1.29
"	80	.062	15.1	16.1	16.4	.091	.91	.151	.80
"	5					.130	2.00	.175	1.92
102	80	.056	15.7	16.2	16.4	.091	.53	.156	.61
104	20	.070	15.1	16.1	16.4				
122	20	.040	15.0	16.1	16.4	.147	4.57	.189	.43
"	80	.040	14.9	15.8	16.4	.113	2.89	.165	2.20
123	10	.060	12.9	15.2	16.4	.395	25.7	.201	21.9
"	80	.025	14.1	15.6	16.4	.107	4.31	.144	3.57
124	20	.050	14.1	16.0	16.4	.107	2.25	.144	1.86
"	80	.040	15.3	16.0	16.4	.085	1.05	.130	.99
125	20	.045	15.4	16.2	16.4	.135	4.36	.181	3.34
"	50	.038	15.4	16.2	16.4	.079	1.08	.129	.93
"	80	.032	14.5	15.8	16.4	.085	1.01	.125	1.06
128***	10	.038	14.4	16.2	16.4	.085	1.02	.117	1.01
"	25	.033	15.2	16.1	16.4	.073	.96	.126	.87
"	50	.027	15.3	16.2	16.4	.068	.64	.112	.73
"	70	.033	15.6	16.4	16.4	.073	.71	.118	.69
"	80	.029	15.4	16.2	16.4	.062	.59	.106	.63
"	90	.050	15.0	15.9	16.4	.090	1.02	.140	.82
129***	10	.050	13.1	15.6	15.8	.107	2.58	.149	2.18
"	80	.040	15.5	16.2	16.3	.079	.60	.131	.67
"	90	.042	15.2	16.1	16.2	.079	.62	.128	.64
133***	10	.060	13.4	15.3	15.8	.067	.93	.110	.98
"	80	.037	15.3	15.8	16.0	.056	.76	.097	.76

*All runs were about 100 layers in length. The position number is the percentage distance from the beginning to the end in the run where the sample was taken.

**Additional quenching provided by water spray on ribbon top 3/4" after casting nozzle.

***These runs containing 200 grams and produced about 200 layers.

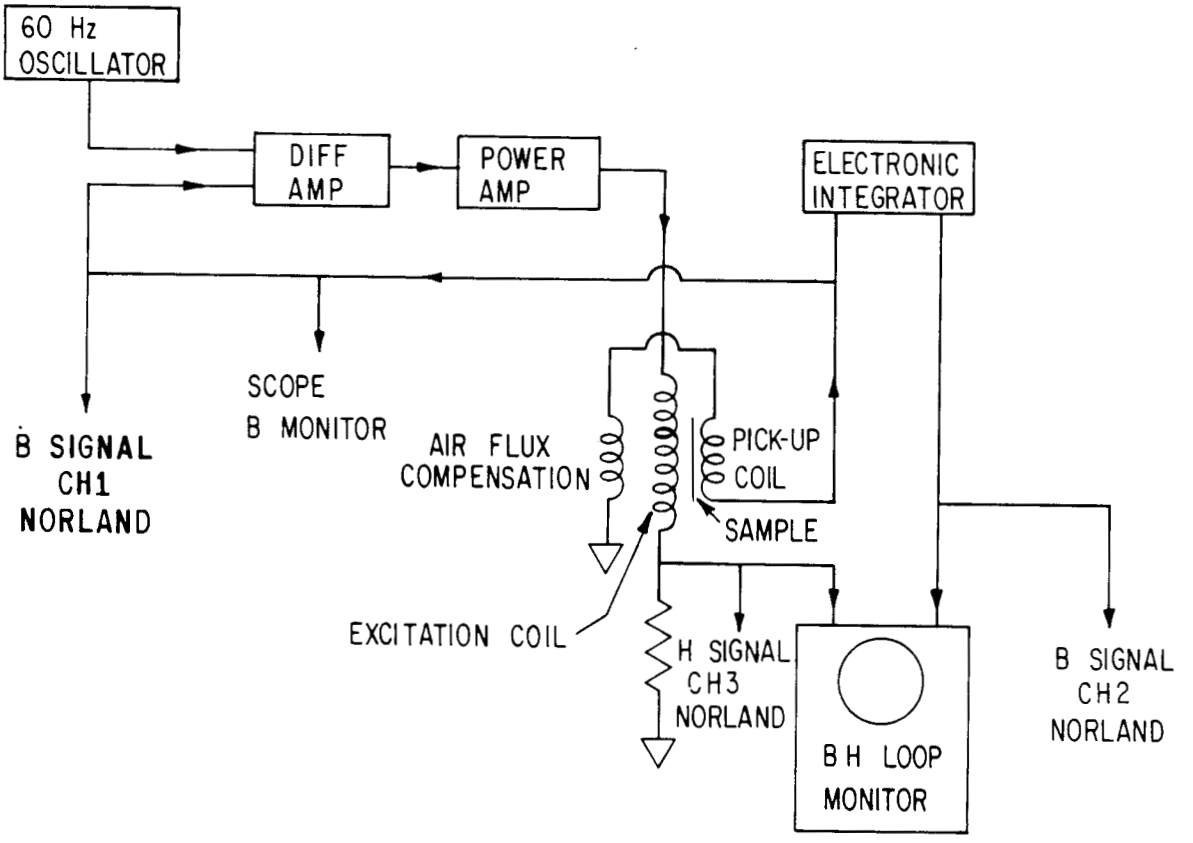

Figure 8. AC measurements--straight samples.

Properties of Multilayer Samples

In anticipation of experimentation with bonding techniques, samples with multiple layers were made, annealed and measured. To do this samples were loosely placed in a coil form and excitation and pick-up windings were manually wrapped around the torous. Values of exciting power measured on multilayer samples were significantly higher than for 180^0 segments of the same sample. Further investigation of this anomaly showed a significant variation in sample thickness around the circumference of the sample. The measurement technique was using the average cross sectional area of the helical stack to determine the flux density. This meant that through the thinnest region, flux densities were considerably higher than average requiring greater magneto motive force in this region. Although thicker segments of the sample required lower m.m.f. once excitation in one region exceeded the knee of the curve, the extreme nonlinearity of the incremental permeability manifested itself as high total excitation to maintain flux density constant in the sample.

Investigation of the casting system showed a slight wobble in the casting wheel such that the run out in the axial direction was approximately 0.0015". The product cast on this system showed a thickness varying between .00161" and .00189". The casting wheel was remachined on its arbor with axial run out reduced to less than 0.0005". Ribbon cast on this wheel showed thickness variation of ±0.00004" or 3% of gauge. Multilayer samples cast on this wheel and annealed with no physical constraints, i.e. loose in a slightly oversized coil form, showed excellent properties. This cyclic variation in thickness is far more critical in helical casting than in straight ribbon casting as alignment along the stack direction is guaranteed in helical casting but is highly unlikely to occur along the radial build of a wound core. If it did align for a few layers, it would advance around the periphery of the core because the length of turn of lamination is continually increasing with increasing build.

Effect of Stacking Pressure

Early work with amorphous metals applied to motors pointed to a potential problem associated with stacking and constraining motor lamination stacks with either axial or radial mechanical clamping or potting. As axial load was applied to a stack, permeability decreased markedly. To evaluate this effect on helically cast ribbon, a fixture was built as shown in figure 9. The fixture was designed to load samples to 30 psi by tightening 16 springs. Stainless steel springs, threaded rods and nuts in conjunction with Dural coil form, pressure plate and spider allowed the fixture to be used at temperatures up to 400°C. Both coil form and pressure plate were slotted in a continuously advancing spiral to allow the flux pick-up coil to nest closer to the sample and reduce the effect of excessive air flux. For every different sample tested the fixture had to be rewound.

A 10 layer sample was placed in the fixture. To guarantee that no pressure was established on the sample by winding pick-up and excitation coils, several strips of 0.005" thick stainless steel were placed around the periphery between the coil form and pressure plate. The strips were as long as the radial build of the coil form so that the winding load was born by these strips. These stainless steel strips were removed prior to annealing to minimize the sample perturbances after anneal but before measuring. D-C properties were obtained after anneal and at several loads up to 30 psi. The results are presented in figure 10. The precipitous decrease in B, with very light loads indicates a significant stress effect. The degradation in properties is mostly recoverable upon removal of the load. It should be noted that increasing the load from zero to 30 psi improved the packing factor from 0.76 to 0.88.

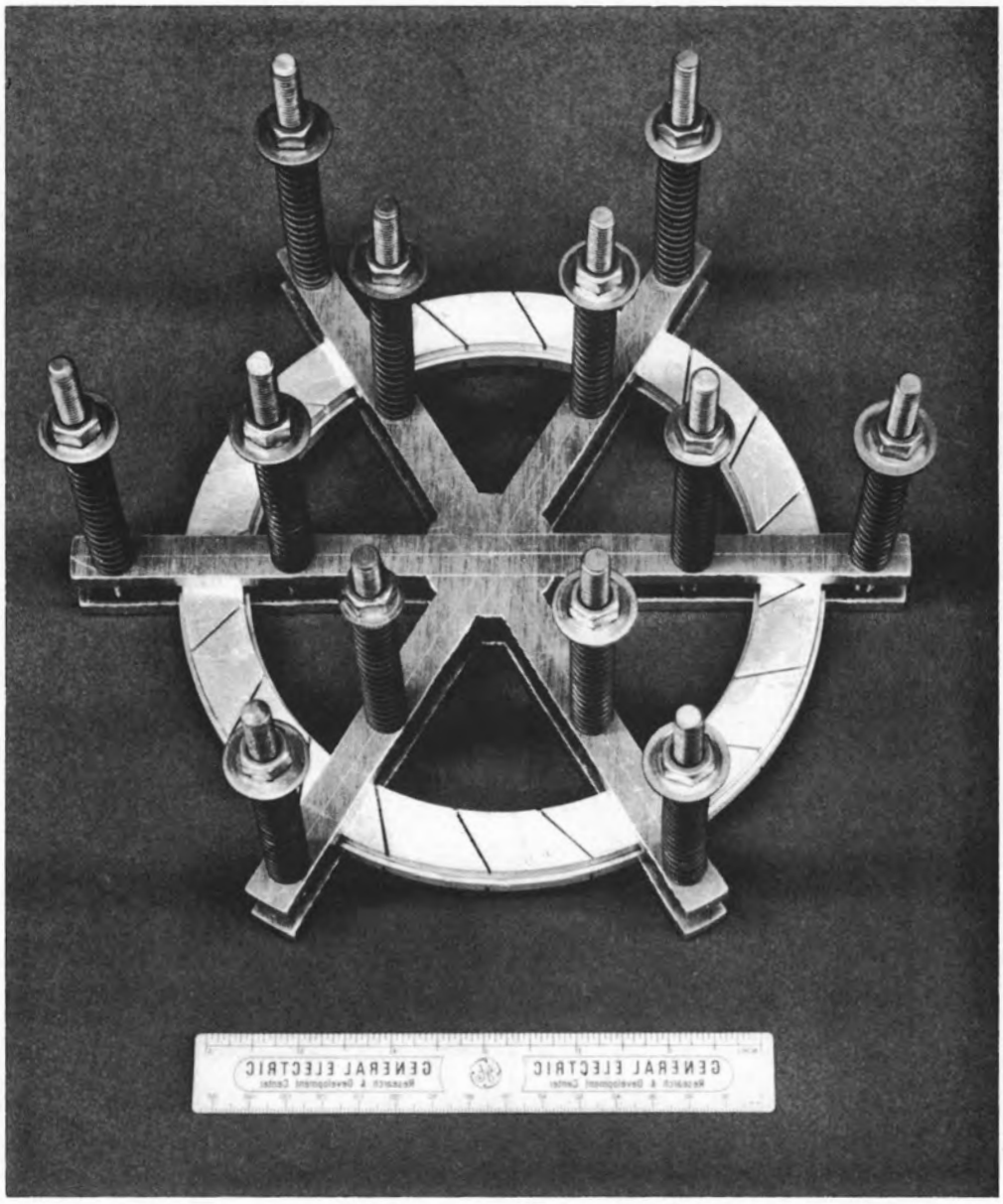

Figure 9. Fixture for annealing and measuring under axial load.

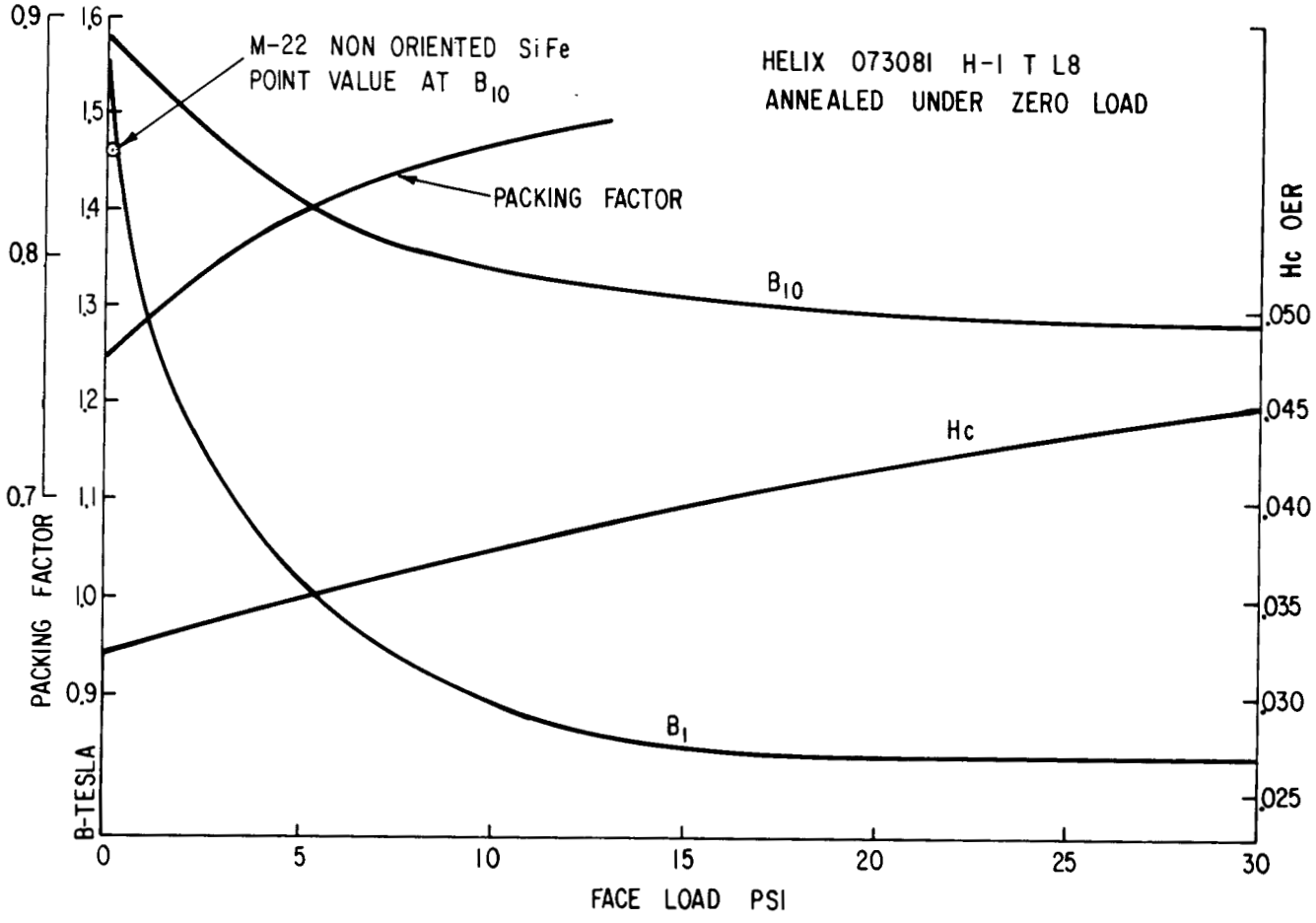

Figure 10. Effect of applying axial load to sample annealed under no load.

Annealing Under Load

The combination of improving packing factor with load and the sensitivity to axial load after anneal shown above suggests that if the sample is annealed under load, both properties may be improved. To this end a 10 turn sample from the same casting run and adjacent to the previous sample was placed in the axial loading fixture and wound with stainless steel shims in place as before. Prior to placing it in the annealing furnace, springs were tightened to load the sample with 30 psi. Upon removal from the furnace the d.c. magnetic properties were measured with disappointing results. As the load was removed, properties improved to near the value of the sample annealed and measured in the unloaded condition. As load was again increased to 30 psi, properties remained essentially constant, a very surprising result. The sample was allowed to remain under load for 5 days when properties were again checked. Magnetic values had degraded somewhat but not to the degree as after annealing and measuring under load. On repeated cycling without aging under load properties remained essentially constant but not at the highest level seen in samples from this run. The results are shown graphically in figure 11.

Few helical samples are geometrically flat in the as cast condition. This causes difficulty in determining precisely the as-cast diameter which is necessary to obtain precise fixtures for annealing. To obtain this measurement, samples were placed on polar coordinate paper between two glass plates. With a rotating and sliding motion the sample could be moved concentric with the polar coordinate center and flattened at the same time. A two layer sample improved the accuracy of measuring the flat diameter.

Even with an exact flat diameter, there may be cupping of the helix out of the casting plane. Such cupping would be removed during a flattening anneal but the material flow required to accomodate the flattening would generate a complicated strain induced anisotropy pattern in the sample and undoubtedly deteriorate the properties. Figure 12 shows the cupping pattern in a 10 layer sample which is properly aligned

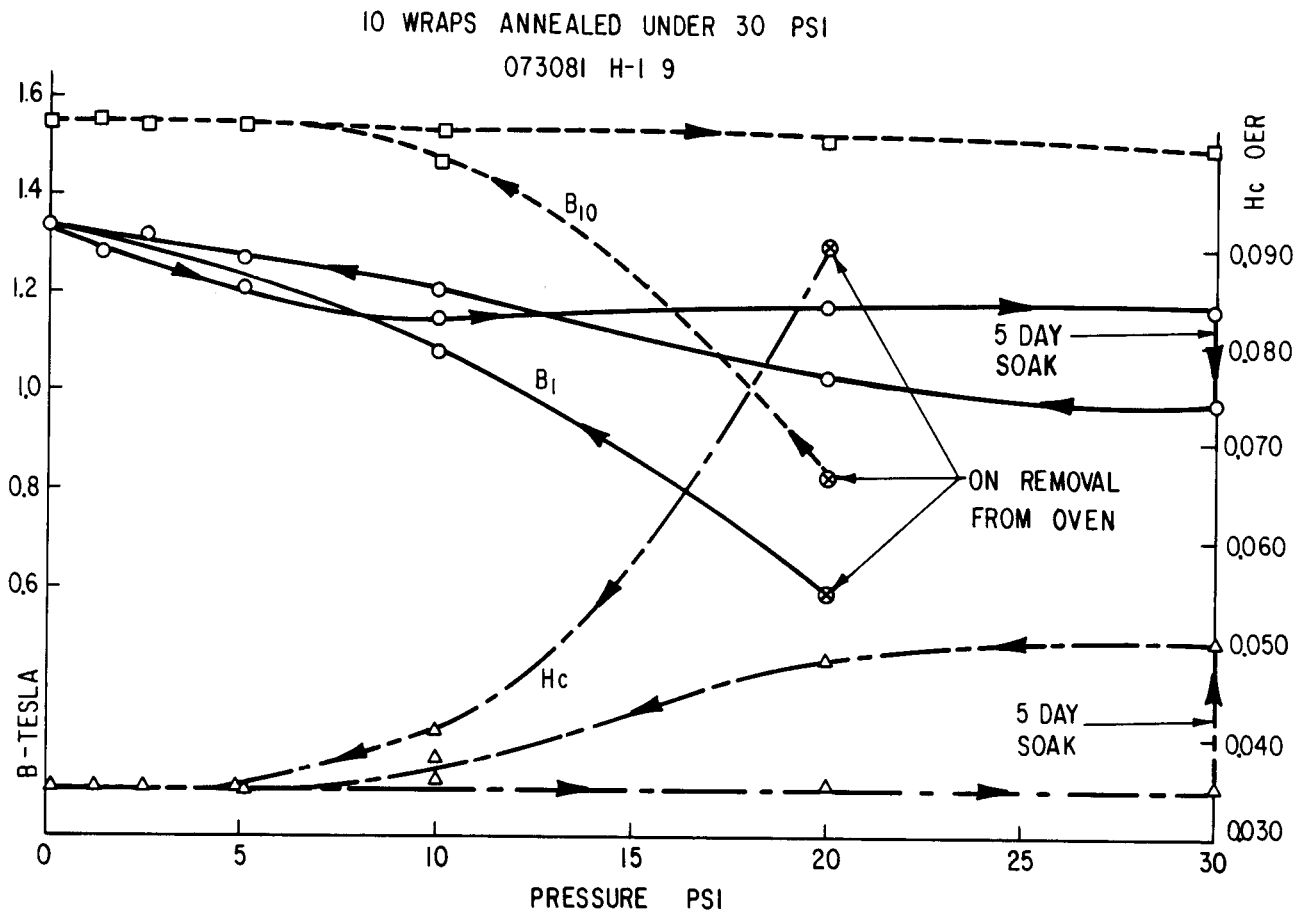

Figure 11. Sample annealed under axial load of 20 psi. (Springs relaxed from 30 psi during anneal.) Measurements taken at various loads.

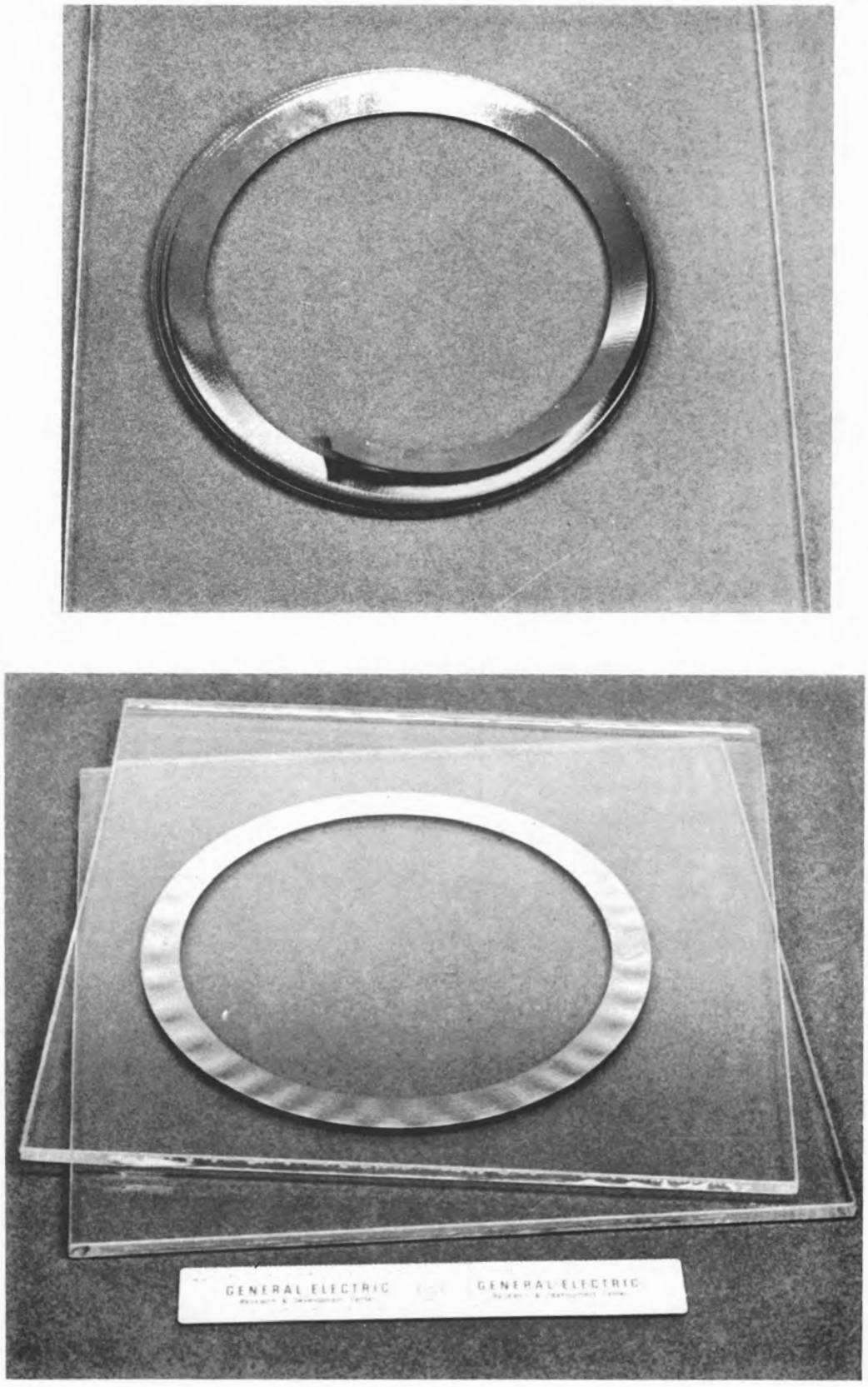

Figure 12. Ten layer sample before and after alignment.

between two layers of pyrex plate glass.

Annealing Under Flattening Load

Considerable effort was expended to evaluate the cause of degraded properties when annealed under a small flattening load. Table II shows d.c. properties obtained under various conditions of load. Also Table III lists a.c. properties obtained on the samples of Table II. Since a.c. properties did not consistently agree with d.c. properties, further measurements were made trying to minimize stress effects by mildly rapping the sample and remeasuring. When this was done several times a wide variation of properties, particularly exciting power were observed at all flux levels as shown in Table IV. Conclusions drawn from this work recognize the deleterious effect of heat flattening cupped ribbon similar to the effects reported on compacting amorphous metal flake (Final Report Contract DE-AC01-78ET29313). In addition, the strain sensitivity is ever present and its effect is amplified in helical geometries. It appears critical to have an alignment "key" to exactly nest each layer of helically cast ribbon. Minimizing stress and its negative effect are major obstacles to achieving a low loss core. This area needs more development.

Bonding

For any practical motor application it is necessary that stator laminations be bonded or mechanically held together and coupled to a non-rotating frame of reference. This coupling must be strong enough to withstand the torque which is developed in the motor. To determine the effect of encapsulating or bonding, a large number of rings 3/4" I.D. by 1" O.D. were chemically etched from an early production run of 2605SC material from Allied Corp. A number of core boxes were machined from lava to accept a stack of rings during anneal and subsequently during measurement of properties after bonding. Plastic coil forms were also used for measurement. Care was taken to make the core boxes stiff enough to prevent the windings from applying a load to the sample. The standard stack was either 1/16" or 1/8" high. A fixture was also built

TABLE II

D-C PROPERTIES UNDER VARIOUS CONDITIONS OF ANNEAL AND MEASUREMENT

Layers	Load Anneal	Fixture Anneal	Fixture Measure	H_c (oer)	B_1 (kG)	B_{10} (kG)	B_{30} (kG)	B_1/B_{10}
1	0	Loose	Loose	.042	15	16.1		.93
1	Wire Tension	Pressure	Pressure	.035				.97
1	Wire Tension	Press	Loose	.040	15.7	16.6		.95
2	0	Loose	Loose	.056	14.9	15.8	16.4	.94
2	Wire Tension	Press	Press	.035	13.6	16.1	16.8	.84
2	Wire Tension	Press	Loose	.035	15.4	16.5		.93
4	Wire Tension	Press	Press	.035	11.9	14.9	15.9	.86
4	Wire Tension	Press	Loose	.030	15.3	16.2		.94
8	0	Loose	Loose-Al	.031	14.9	16.0		.93
8	0	Loose	Loose Lexan	.040	13.3	16.0		.83
10	30 psi	30 psi Press	0 psi	.035	13.7	15.5	15.8	.88
10	0	Press	30 psi Press	.035	12.7	15.1	15.8	.84
10	0	Press	Press	.028	15.2	15.9		.96

TABLE III

A-C PROPERTIES OF MULTILAYER SAMPLES

			Loss (Watts/Pound)			Exciting Power (Volt-Amps/Pound)		
Layers	Anneal		12 kG	13 kG	14 kG	12 kG	13 kG	14 kG
2	Loose		.077	.092	.109	.239	.427	.886
4	Loose		.054	.068	.082	.096	.135	.273
2	Press		.063	.075	.090	.119	.176	.293
10	30 psi		.073	.087	.103	.310	.557	1.082
8	Loose		.085	.099	.114	.346	.596	1.094
10	Loose W/Cover		.061	.074	.092	.080	.120	.236
.014"	M-22	Si-Fe	0.9	1.07	1.26	1.96	3.00	5.00
.025"	M-22	Si-Fe	1.2	1.44	1.70	2.26	3.20	5.00

TABLE IV

A-C PROPERTIES RESEATING AND RETESTING SAMPLE 073081 H-1-TL4

B_{Max} (kG)	Test Number	B_R (kG)	H_{Max} (oer)	H_c (oer)	Loss (W/#)	Excitation (VA/#)
10	1	7.7	.23	.059	.067	.160
	2	8.3	.16	.054	.060	.113
	3	7.9	.18	.054	.060	.130
12	1	8.3	.61	.065	.094	.454
	2	9.0	.41	.060	.084	.307
	3	8.7	.46	.060	.085	.346
13	1	8.3	1.01	.070	.108	.783
	2	9.2	.73	.064	.099	.559
	3	8.8	.77	.63	.099	.596
14	1	8.3	1.80	.072	.125	1.45
	2	9.3	1.38	.064	.113	1.07
	3	8.6	1.37	.065	.114	1.09
	1	8.1	2.50	.072	.133	2.01
	2	9.2	2.03	.064	.122	1.60
	3	9.0	2.14	.068	.125	1.71

to facilitate removal of excess bonding material by applying axial pressure to the core stack before and during curing. Table V tabulates the results of work done both on this contract and some earlier work on the construction of the 1/3 h.p. segmented lamination motor, a project internally funded at General Electric.

The results of these efforts indicate that any material which applies a compressive stress on annealed material is detrimental to the magnetic properties. On the other hand, a material which merely encapsulates and remains compliant as did the Scotchgrip* material does not adversely affect properties. No testing has been done to determine the efficacy of either encapsulation or the use of Scotchgrip* through normal motor usage or life. In general the exciting power of a sample was more sensitive than losses to potting induced stress. This is shown in figure 13, where potting materials have not increased the losses beyond an acceptable value but exciting power values are approaching those for M-22 silicon steel whose properties are shown in Table III.

III.2.3 Conductor Slot Casting

The objective of this task was to establish the feasibility of directly casting conductor slots into the edge of an amorphous metal ribbon. The principle of the approach was to provide a parting line between the major portion of the ribbon, which would serve as the finished stator stack, and the ribbon cast in the conductor slot region, which would be removed and recycled into the melt. The parting line is made by making a pattern in the surface of the casting wheel which has a lower quench rate than the bulk of the casting wheel. The region in the ribbon that has the low quench rate should be significantly more brittle than the surrounding ribbon and should provide an easy parting line.

Three different methods for making the low quench-rate pattern were pursued. These were 1) an unfilled shallow grooved pattern, 2) a deep narrow grooved pattern either unfilled or filled with bonded glass or

* REG TRADEMARK 3M CO.

TABLE V

LOSSES WITH VARIOUS BONDING TREATMENTS

Sample	Treatment	Losses	
		10 kG	15 kG
1	Loose Annealed	.07 w/#	.15 w/#
2	Potted Lekton	.96	
601.3	Anneaed, Potted Lekton	.15	1.1
4	Annealed, Potted PEI	.32	>1.9
601.1	Potted, Cured PEI	.15	1.2
6	Annealed, Potted Epoxy	1.6	3.0
601.5	Annealed, Potted 11579-2 CA-25	.19	1.4
601.4	Potted 11579-1 CA-23	.38	2.2
5	Annealed, Potted Scotchgrip	.10	.82
7	Encapsulated Scotchgrip	.06	.28
1	Annealed Encapsulated Scotchgrip		.21
1	Retest		.23
601.7	Annealed Potted SCOTCHGRIP	.07	.39

All samples - 60 Rings 3/4" I.D. X 1" O.D.

All space factors ~ .8

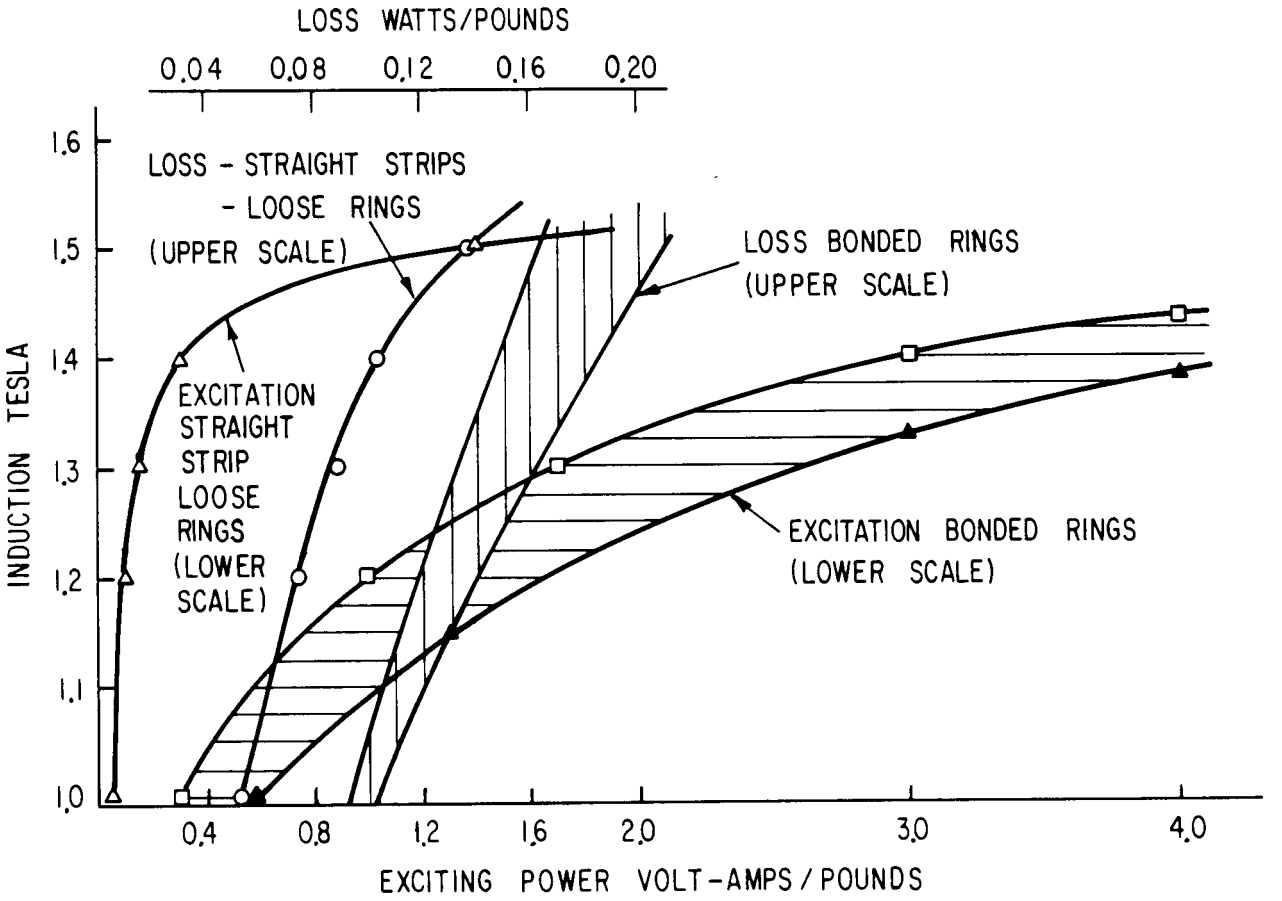

Figure 13. Effect of bonding sample rings with various agents.

ceramic, and 3) a pattern filled with a low thermal conductivity metal.

Shallow Grooved Patterns

The planar flow method for casting wide metallic tapes directly from the melt relies upon a very small (~10 mils) crucible-substrate surface spacing in order to assure laminar melt flow during casting. One advantage of this casting method over conventional chill block melt-spinning lies in the reduced sensitivity to fluid flow perturbations by surface asperities on the substrate. Initial experiments in the use of planar flow casting of patterned amorphous alloy tape were conducted by simply scribing the desired pattern with a sharp, 45° conical tool bit. Both laminar melt flow and the presence of a melt perturbation attenuating "ceiling" were effective in forming a patterned tape without accompanying molten alloy ball spraying.

A variety of grooves which outlined rectangular cut-outs on the side of the ribbon were scribed into the casting surface. The depths of the various grooves were 1, 3, 5, and 7 mils. The surface was then polished to remove the ridge of displaced metal along the sides of the grooves.

Several casting runs of straight ribbon were made on this patterned wheel. All the groove lines were reproduced in the cast ribbon. Most of the 7 mil groove cut-outs separated during casting and others could be removed by flexing the ribbon. All of the shallower groove cut-outs remained attached. The embrittlement at the groove demarcation lines decreased with decreasing depth (or width) of the groove until almost no embrittlement was observed from the 1 mil grooves.

This open groove slot casting technique was applied to the casting of helical ribbon as follows. A copper wheel was constructed with open grooves machined into the casting surface to several different depths (5, 7, 10, and 12 mils). A 60° engraving tool was used rather than the 45° conical tool bit. Thus, these grooves also had a triangular cross-section but, unlike the previous grooves, their width was slightly

greater than their depth. The grooves were cut to form several series of rectangular cut-outs on the inside diameter of the cast helical ribbon.

Casting on this wheel produced a continuous helix of ductile ribbon. The effect of the various groove dimensions is shown in the series of photographs in figure 14. As expected, the cut-out definition increases with increasing groove dimensions. For the 1.3 mil thick ribbon shown here, casting over grooves greater than 7 mils deep actually produces voids on the radial lines. On the circumferential grooves the molten alloy did flow slightly into the groove forming a ridge on the underside of the ribbon. The size of this ridge obviously increases for deeper (and wider) grooves.

Many of these rectangular cut-outs separated during casting although most remained attached. The highest incidence of separation during casting was for the leading cut-out of any given series (~3 inches of smooth ribbon separated each series). Manual separation of the remaining cut-outs was easily accomplished without fracturing the adjoining ribbon. However, the ridge under the circumferential line retained some ductility and did not always break by simple bending. Usually, after cut-out separation all or part of this ridge remained attached to the ribbon. The presence of this burr on the border of the cast slot is the most severe problem associated with slot casting over open grooves. When the helix is stacked, the ridge prevents the individual layers from lying flat and thus prevents the high packing density necessary for good magnetic properties.

Figure 15 shows the entire helical ribbon with all of the slots removed. Figure 16 shows how well the layers of the ribbon register on top of each other. The effect of the high ridge at the slots on the stacking factor is readily apparent in figure 17 where the stack factor in the slot region is less than one-half that achieved in the non-slot regions.

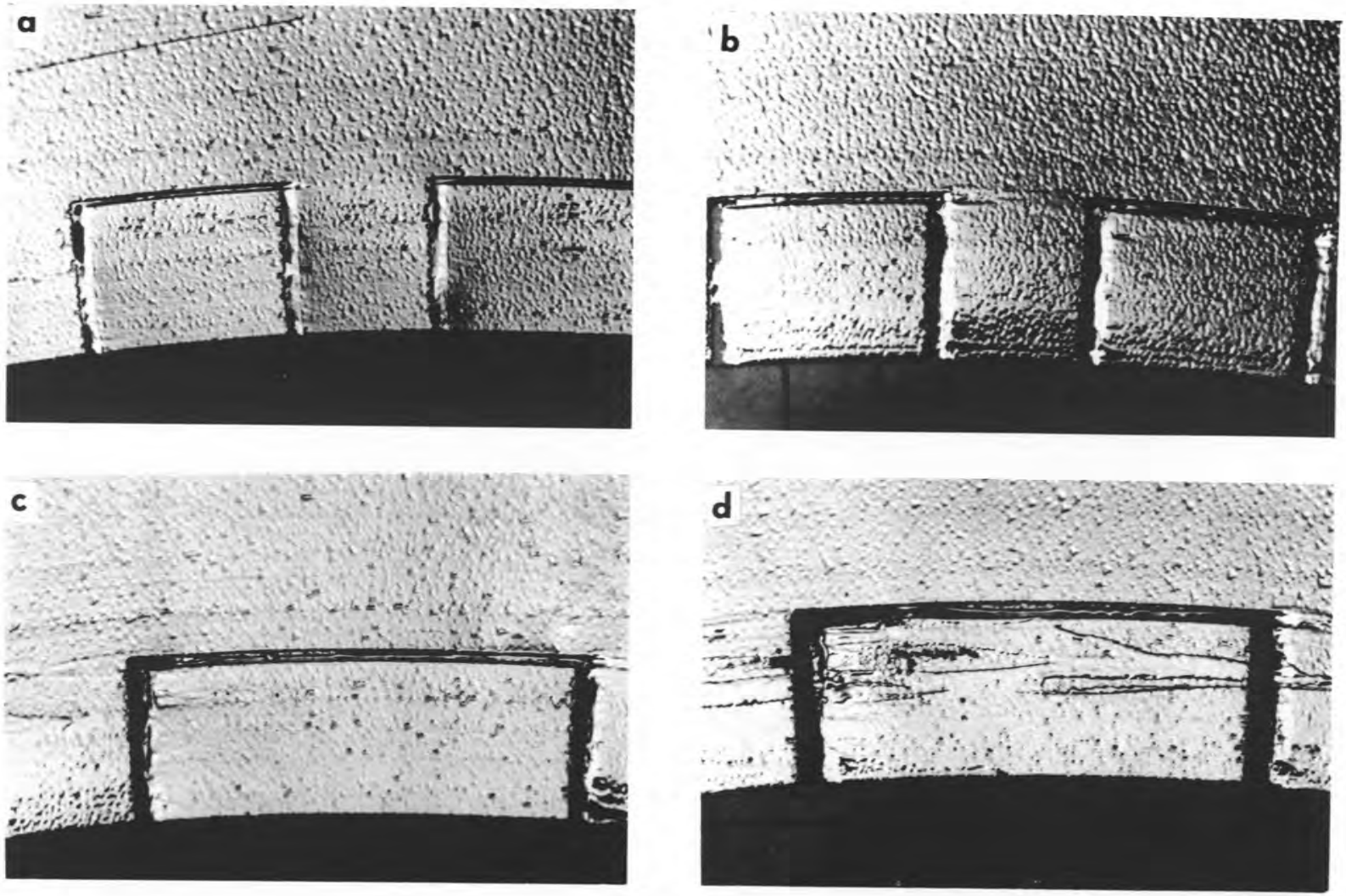

Fig. 14. Top surface of helical slotted ribbon showing effect of groove depth on cut-out definition. Photos show 1.3 mil thick ribbon cast over a) 5 mil, b) 7 mil, c) 10 mil, and d) 12 mil deep grooves. (5X)

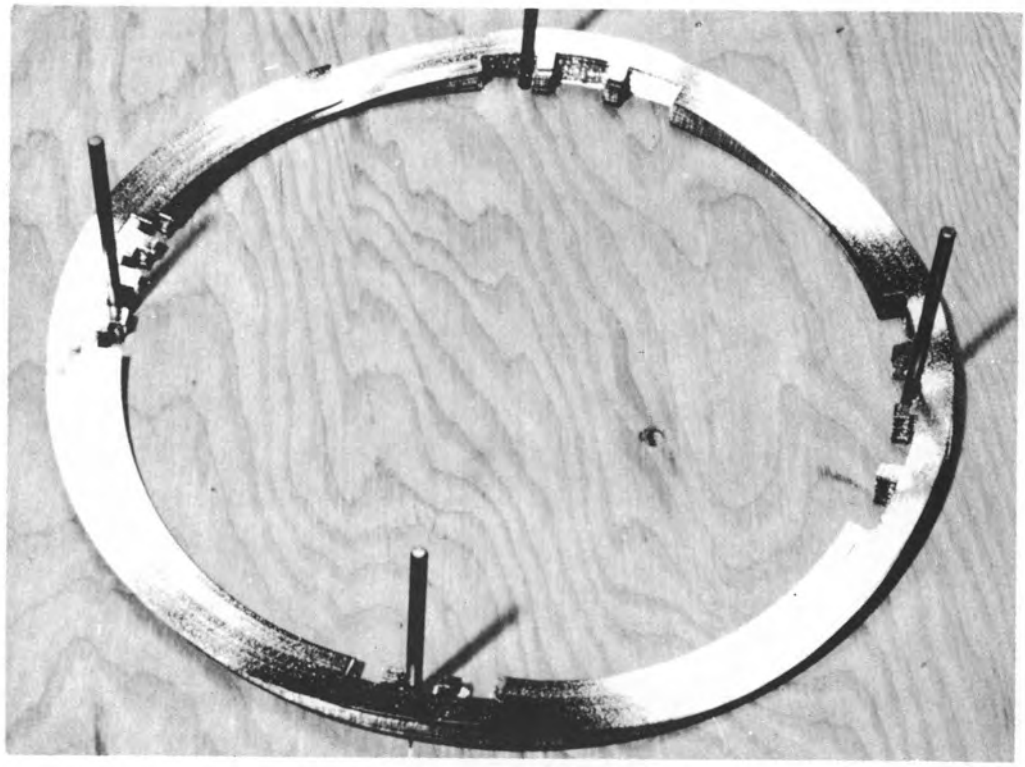

Fig. 15. Helical ribbon cast over unfilled shallow groove pattern.

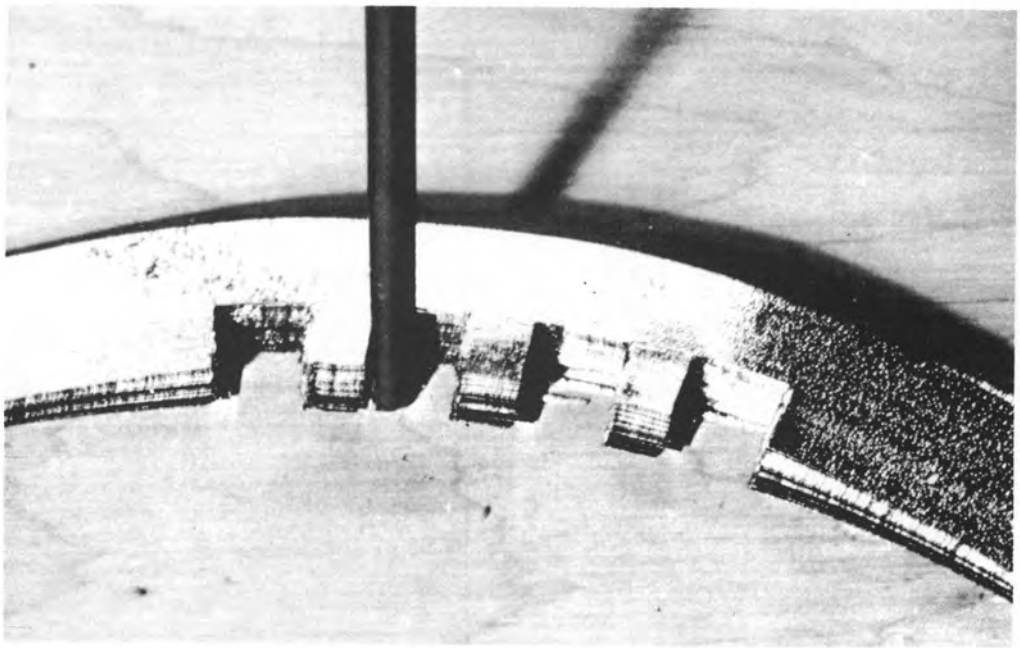

Fig. 16. Detail of slot registry.

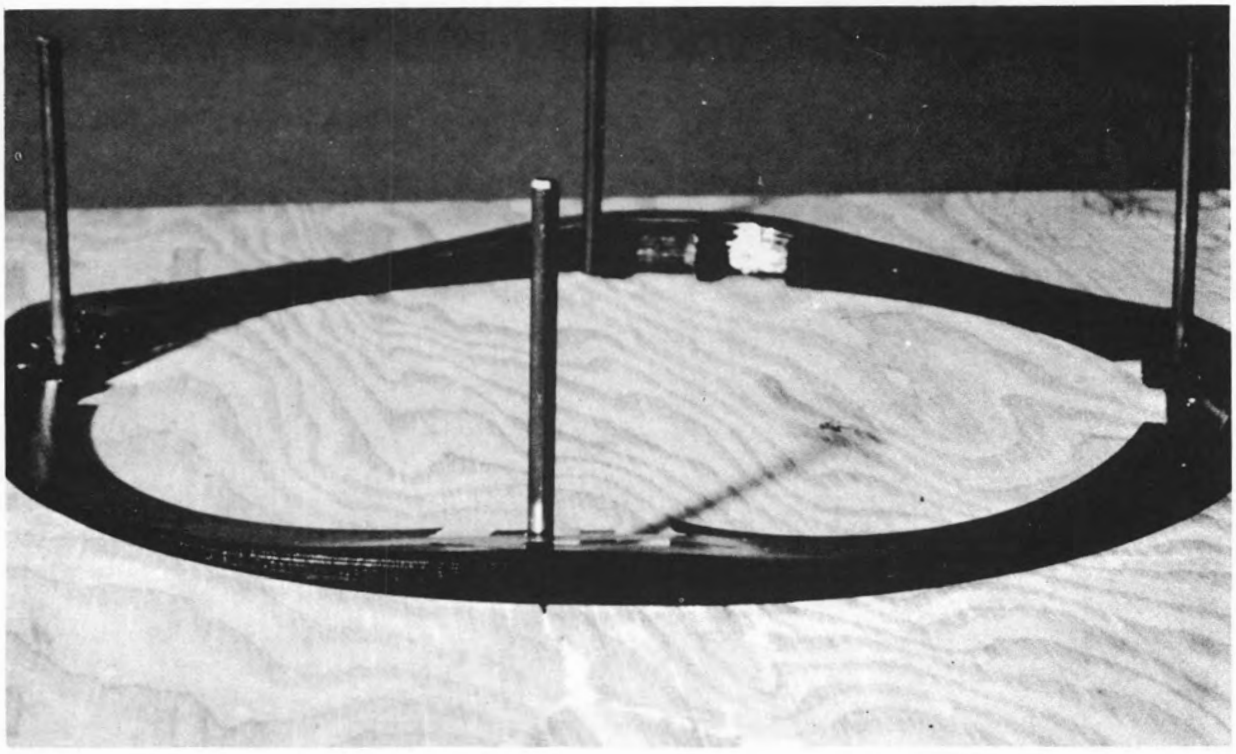

Figure 17. Reduced stacking factor due to high burr at edge of slots.

Another less serious drawback to open groove casting was also observed. That is the deterioration of the substrate grooves. In the casting of straight ribbon it has been found that the casting surface must be continually renewed during extended runs through the use of a conditioning wheel. This is usually a stainless steel wire brush. Such a brush was used during these helical slot casting runs. Even on these short casting runs the wire brush has smeared the copper on the edges of the radial grooves. The loss of edge definition is especially bad on the trailing edge. Most of the subsequent casting wheels were made of Cu-1%Cr which is much harder than copper and did not suffer the damage experienced by the copper wheel.

An actual motor lamination obviously will not have rectangular conductor slots like the cut-outs which have just been described. Thus, the casting of such a lamination will not encounter transverse and longitudinal lines but instead some smooth, continuous line defining the shape of the desired slot. To more closely model this actual case, a casting wheel was constructed with more realistic cut-out shapes. This wheel was machined from a Cu-1%Cr forging. The cut-out shapes were machined into the casting surface with the 60° engraving tool and a numerically controlled end mill. The grooves were cut 8, 11, and 15 mils deep.

Casting on this wheel was generally successful. About 60 revolutions of a helix could be cast with a 100 gm charge. Figure 18 shows one revolution of such a helix with the actual conductor slot cut-outs. This ribbon is 1.5 mils thick and 6 inches in diameter. All the cut-outs separated very easily. In fact, most of them fell out during casting. Not surprisingly, the incidence of cut-out separation during casting was slightly greater at the 11 and 15 mil grooves. As previously observed, casting over these 60° grooves produced voids above the grooves which are roughly perpendicular to the casting direction. Thus, cut-out separation usually consisted of breaking a short segment on the round end of the slot. This was generally much easier than separation along the end of a rectangular cut-out. Since the groove is never parallel to the casting direction, the molten alloy does not establish a

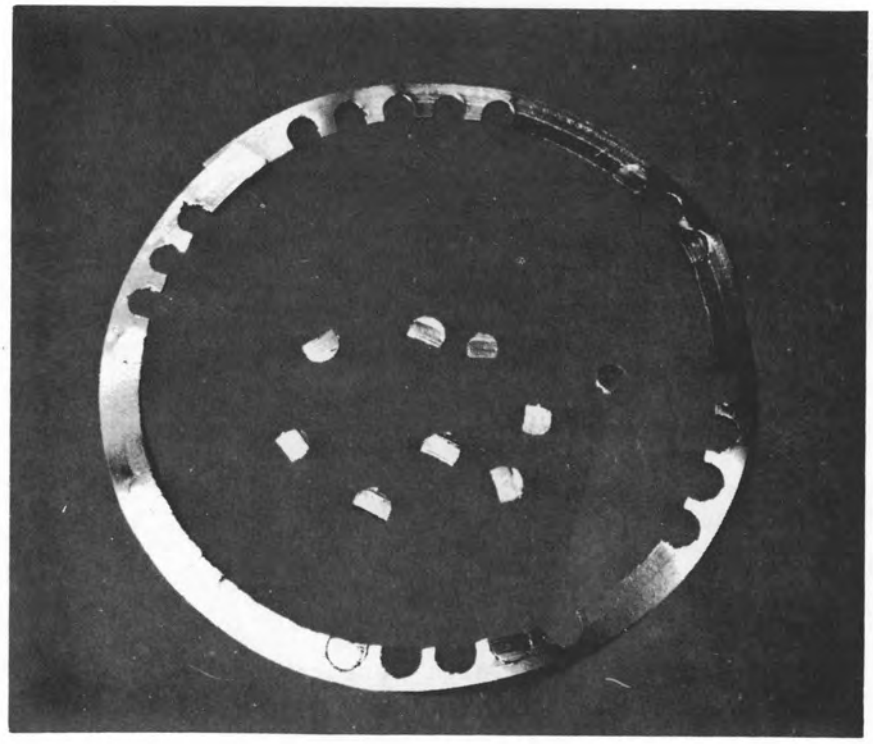

Figure 18. One revolution cast over open groove. Ribbon is 1.5 mils thick. The series of 3, 4 and 5 cut-outs had groove depths of 8, 11 and 15 mils, respectively.

smooth flow into the groove and the resultant ribbon line is somewhat thinner. A section through this round cut-out line is shown in figure 19.

The mechanism for the casting of voids along the transverse 60° grooves can be deduced from the ribbon cross-section in figure 20. The stream of molten alloy is broken as it falls into the passing groove. Since the flow rate must remain constant excess metal collects in the bottom of the groove. This forms a lip of material along the back side of groove which is out of the plane of the ribbon. This void formation was not observed in the 45° scribed grooves used in the straight ribbon casting experiments. This is probably due to a combination of factors. The 60° grooves are 40% wider for any given groove depth. Additionally, the 60° helical casting grooves used depths up to 15 mils while none of the 45° straight ribbon grooves were deeper than 7 mils. Thus, the helical cut-out grooves were significantly wider. As the groove width increases, the surface tension of the melt becomes less able to support the melt puddle across the groove opening. Above some width, the continuity of the cast product is disrupted. Contributing to this effect, the helical ribbon was cast with a substrate surface speed of 65 ft/sec while the water cooled straight ribbon was cast at 48 ft/sec. This additional speed makes it more difficult to cast on the leeward side of the groove. When the melt drops into the wider grooves, it misses the downhill side and leaves a void. The relative contribution of these two factors is not known.

Since this lip of excess material always forms on the downstream side of the groove, it will remain on one side of the slot after cut-out removal. Close examination of the bottom series of slots in figure 21 reveals the left slot border to be very smooth and flat while the right side border has a rough ridge of material which was cast into the groove. Again, the existence of this ridge is unacceptable because it prevents high density packing of this helix.

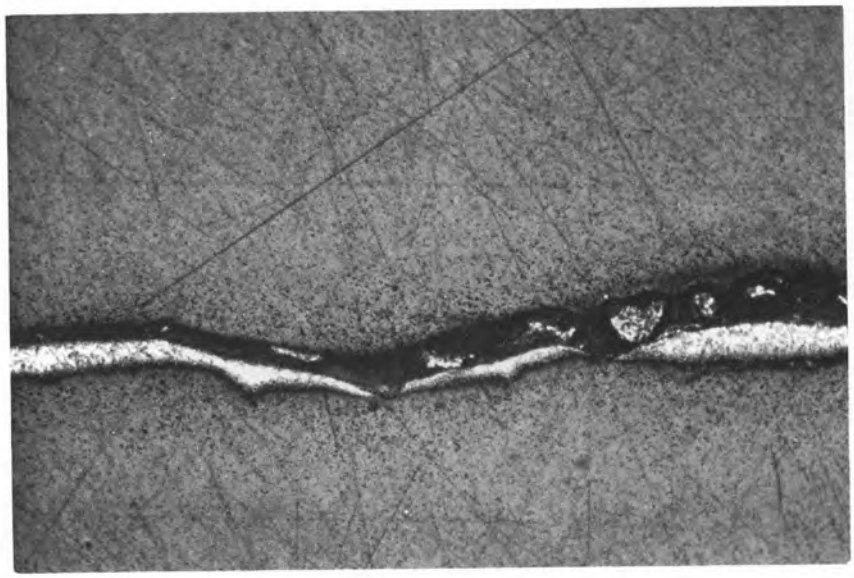

Figure 19. Cross section of helical ribbon cast over an 8 mil deep groove parallel to casting direction. (125X)

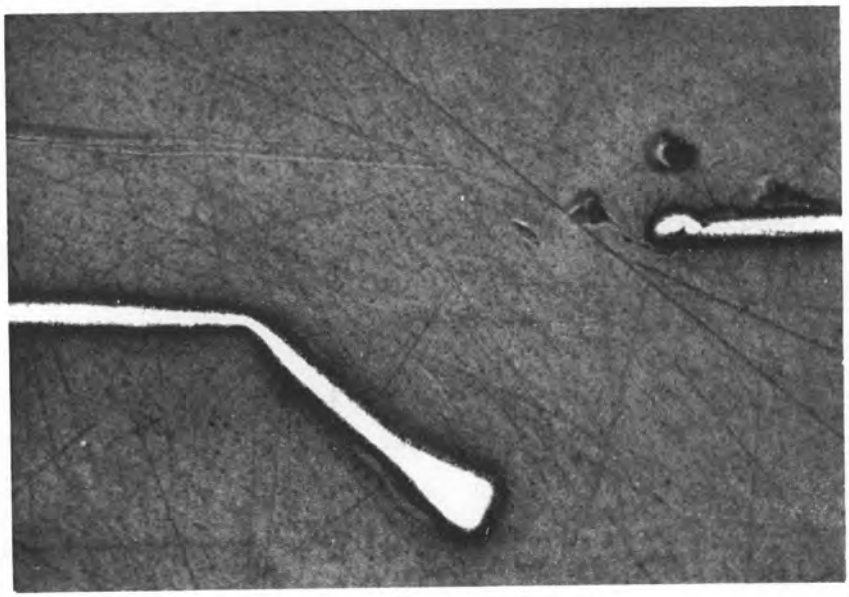

Figure 20. Cross section of a helical ribbon cast over an 8 mil deep radial groove. Casting direction is to the right. (125X)

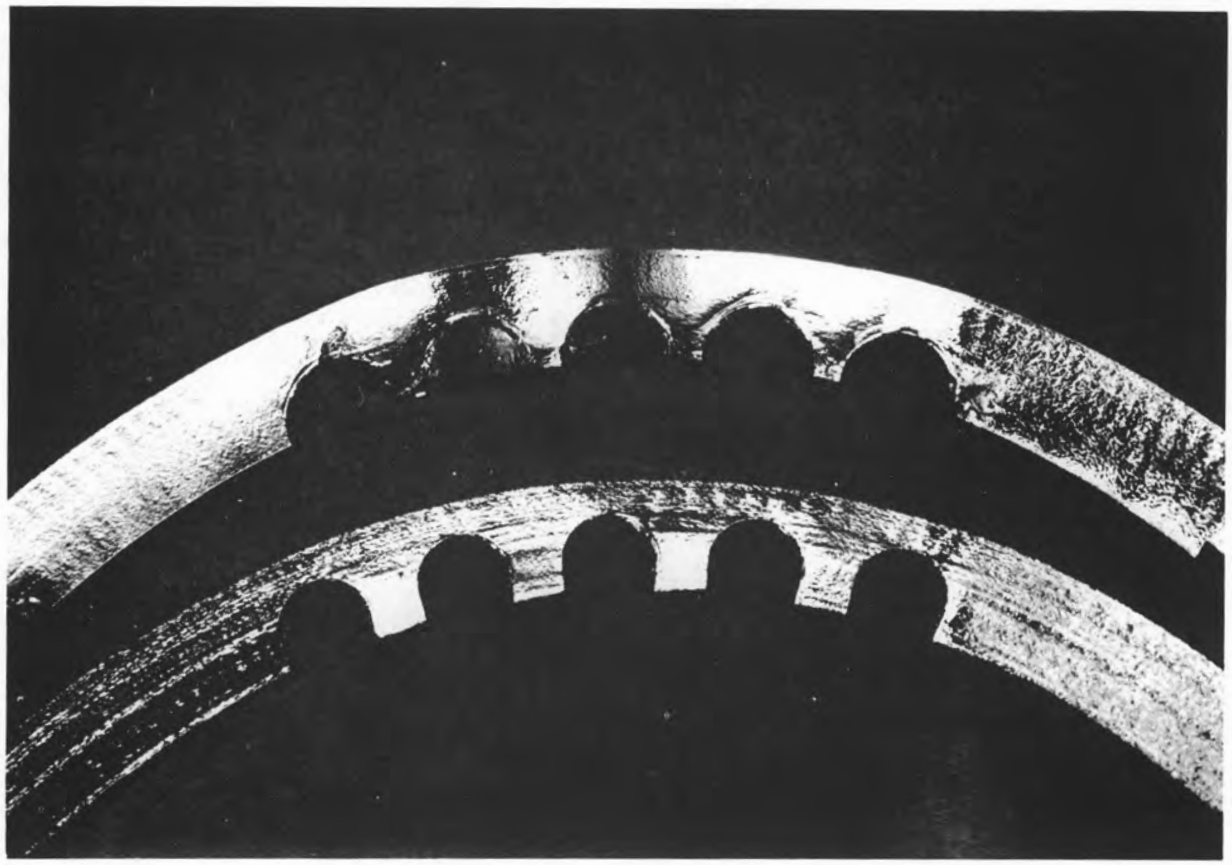

Figure 21. Effect of ribbon thickness on slots cast over 15 mil deep grooves. Top ribbons 1.9 mils thick, bottom ribbon is 1.5 mils thick. Note burr along right side of slots in bottom ribbon. (1.5X)

The effect of ribbon thickness on cut-out formation is also illustrated in figure 21. The top helix has an average thickness of 1.9 mils while the bottom helix is only 1.5 mils thick. The increased metal flow rate of the thick ribbon is seen to introduce significant melt turbulence around the cut-outs and the adjacent ribbon surface is disrupted by the formation of ripples. These ripples are accompanied by brittle, blue oxidized regions on the underside of the ribbon. Although the smooth sections of this ribbon are ductile on bending, the area near the slots has become mildly embrittled by the heat of the thick turbulent regions around the cut-outs. Even though cut-out separation remains very easy, care must now be taken to avoid cracking the remaining ribbons. This adjacent ribbon embrittlement was not a problem with the 1.5 mil thick ribbon.

Deep Open Grooved Patterns

In order to try to eliminate the burr cast on the downstream edge of the slot, a wheel was made with deep, straight-sided, open narrow grooves. These grooves were made by electrodischarge machining. In two casting trials molten metal penetrated and stuck in the grooves.

In order to try to prevent this penetration, the wheel was modified to supply a high pressure gas within the grooves. Holes were drilled under each slot tip from the bottom side of the wheel until they connected with each EDM groove. A stationary manifold beneath the wheel fed inert gas through these holes to bleed through the EDM groove. During the casting run this gas would be used to support the molten puddle under the crucible. With adjustment of the gas pressure the molten metal would neither flow into the EDM groove nor be blown away.

The gas supply manifold was positioned under the wheel so that gas would be supplied to a groove starting about 30° of rotation before the crucible position and continuing until the groove had passed 15° beyond the crucible.

A 100 gram casting run was made with this arrangement with almost all the metal made into ribbon before the crucible broke. A high-speed movie of the run showed that while the air knife that is used to remove the ribbon from the wheel was successful in removing the ribbon, it did not always remove the separated pieces of ribbon from the conductor slot region. Just before the crucible broke, the ribbon broke at one of the slots as it passed by the air knife. The ribbon that was on the wheel passed by the air knife, passed under the crucible and received a second molten layer. This continued until the ribbon was thick enough to come in contact with and break the crucible.

The ribbon quality was very good with virtually all of the slot pieces separated from the main ribbon during the casting. A small burr was present on the downstream side of the slot and some voids were noted emanating from the EDM grooves at the very top of the slot at the position of the gas feed hole. This may have been due to an uneven pressure in the groove since the gas was fed through one small hole to each groove.

A modification was made to the wheel to increase the depth of the gas feed holes so that an increased flow of gas could be supplied, the gas supply pressure was increased from 20 psi of the previous run to 40 psi, and two air knives were used to remove the ribbon. Casting with these parameters also led to sticking of the ribbon to the grooves after several revolutions of casting.

We conclude that open grooves 0.015" wide even with a backing gas pressure are not suitable for casting ribbon. Surface tension of the molten metal is not sufficient to prevent its penetration into the groove. It is estimated that the grooves would have to be less than 0.004" wide to prevent penetration.

Metal Filled Groove Patterns

In order to avoid the penetration of the molten metal into the grooves a series of casting wheels were made with a variety of low conductivity metal inserts in the grooves. Three different approaches were taken: filling the grooves with various braze alloys; bonding solid metal strips into the grooves; and filling the grooves with a high temperature, low conductivity nickel-base alloy with low pressure plasma spray.

Since wheel construction was relatively simple, the first experiments were done with braze filled grooves. Ten and 15 mil wide grooves were cut into a thin OFHC copper wheel by EDM. The selected braze alloys were allowed to flow into the grooves by hydrogen furnace brazing for 6 minutes at 1900°F. Although thermal conductivity data for braze alloys is somewhat scarce, it was found that their conductivity generally decreases with increasing melting temperature. Obviously then, the optimum choices were restricted by the melting point of copper. The alloys used were AM1770A, AMI936, and Nicrobraz 50 (Ni-base alloys) and AMI935 (a Cu-base alloy). After furnace brazing, the excess material was ground off to expose the filled grooves. All the nickel base alloys resulted in distinct lines on the wheel surface. Because of a higher diffusivity the copper base alloy left only a diffuse blotch on the surface.

The durability of the braze alloy lines appears to be very sensitive to their composition. The condition of these lines after casting is shown in figure 22. Both the AMI936 and the Nicrobraz 50 suffered severe surface cracking and spalling. Cracking along the center of the line and "bulging" of the braze alloy indicate that differences in thermal expansion contribute to this problem. The surface of the AMI770, however, exhibited virtually no degradation from contact with the molten alloy.

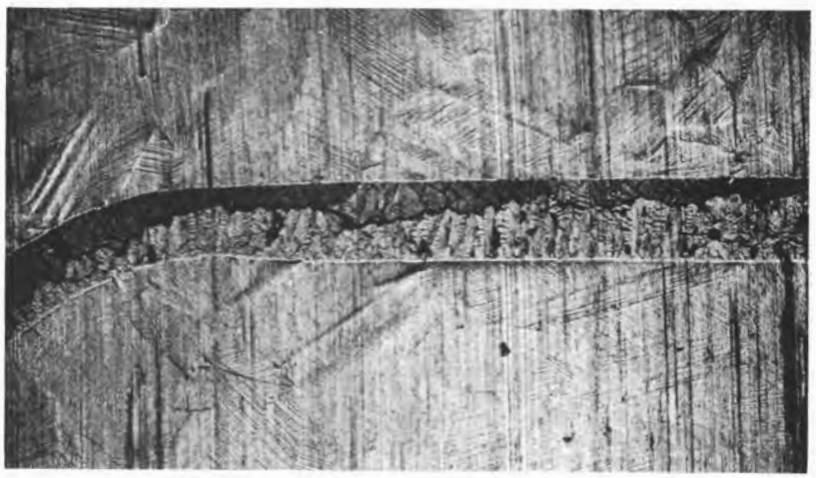

a) AMI 936

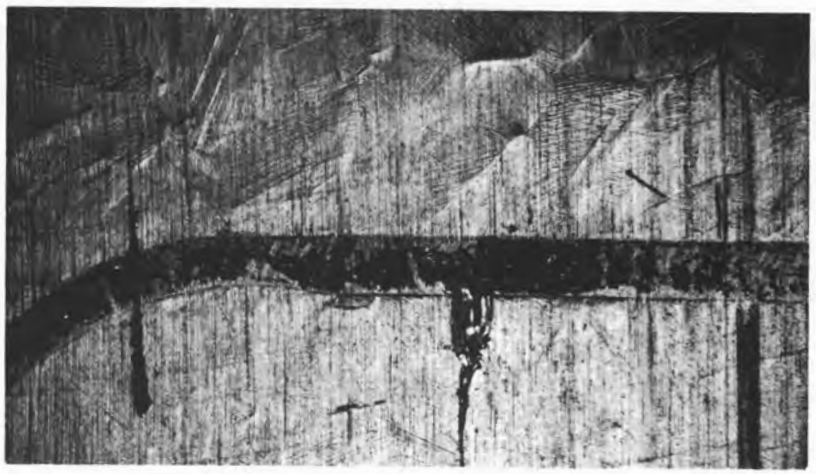

b) Nicrobraze 50

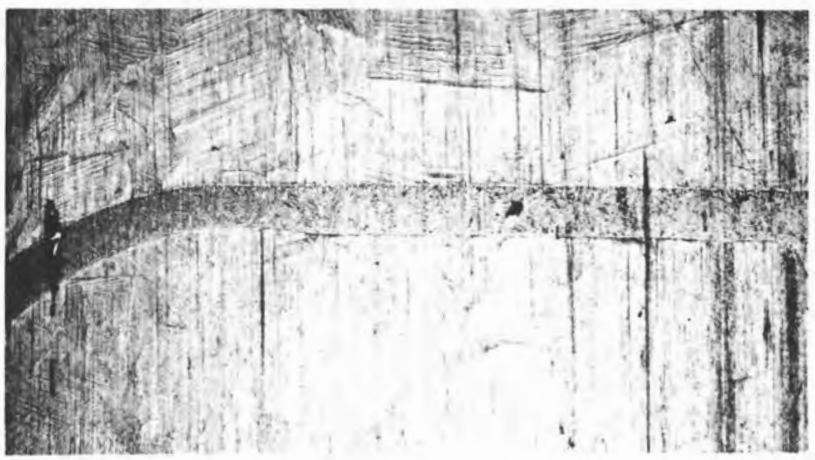

c) AMI 770A

Figure 22. Effect of one casting run on braze alloy inserts.

The section of the successfully cast helix did have visible lines on the surface which reproduced the lines of nickel base alloys on the wheel. However, there was no indication of embrittlement or tendency for separation along these lines. The blotch of copper base alloy had essentially no effect on the cast product. The braze alloys do not provide a sufficiently low quench rate to achieve embrittlement.

The method of metal inserts was originally tested in an attempt to produce amorphous metal flake. This attempt consisted of casting on a small copper wheel with several 304 stainless steel inserts. These were mechanically staked in, diffusion bonded and machined to a smooth surface for casting. Local ribbon embrittlement from this wheel was only moderately successful. The stainless steel lines were reproduced on the ribbon and fracture occurred preferentially on these lines after a few bend cycles.

This insert method was applied to helical slot casting using several easily available refractory metals. Molybdenum, tantalum and niobium sheet was inserted into the usual EDM cut-out grooves. The surface of the inserted metal and the adjacent copper was heavily deformed with a hammer and machined smooth. Optically, this formed a high integrity metal-copper interface. No gaps or separations were visible.

The casting response to all three metals was very similar. The lines were again reproduced very clearly in the cast product. The lower thermal conductivity of the insert did cause a drop in the melt puddle solidification front making the lines visible on the ribbon where the top surface dipped accordingly. The ribbon did not, however, show any marked tendency for embrittlement or separation at these lines.

Closer examination of the wheel-side surface of the ribbon revealed that the insert affected the air pocketing response of the melt puddle. Air pockets tended to be nucleated at the copper-metal interfaces. This was observed for all three filler metals as shown in figure 23a, b, and c. Large air pockets were nucleated at the first interface. An air pocket free zone then formed behind these initial large air pockets

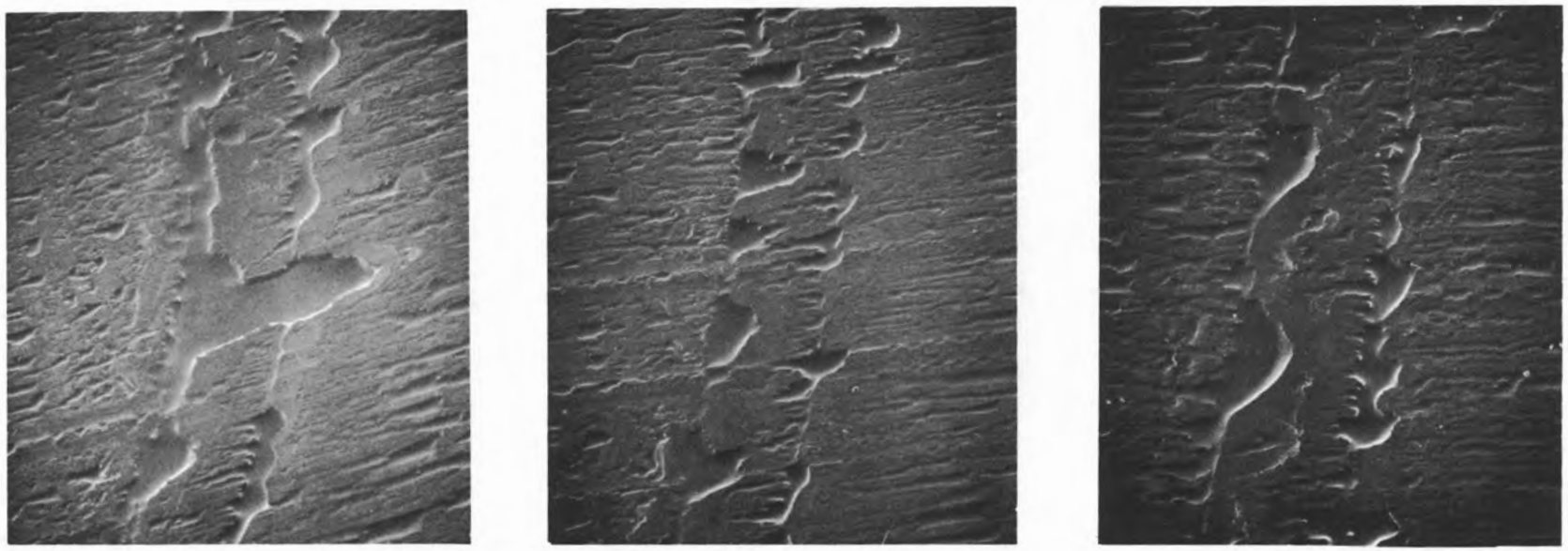

a b c

Figure 23. SEM micrographs of the air pocket structure formed on ribbons cast over inserts of a) molybdenum, b) tantalum, and c) niobium. Casting direction is to the left. (65X)

roughly following their contour. Heavy air pocketing was then again initiated at the second interface. The reason for this interface air pocket nucleation is due to slight interfacial separation at higher temperatures. (The coefficients of expansion for the three filler metals are only about one third of that for copper.) This limited interfacial air pocketing did not appear to contribute significantly to ribbon embrittlement along the cut-out lines. All of the cut-outs remained intact after casting and could not be easily removed.

A second wheel was made of thick Cu-1%Cr with EDM grooves of four widths: 0.005, 0.010, 0.015 and 0.020 inches. These grooves were filled with 304 stainless steel, Nichrome, Hastalloy X, Nickel 200, Inconel 718 and Kovas in order to give inserts of varying thermal conductivity and wettability.

Five casting runs were made on this wheel. Ribbon from each run did replicate the inserts, figure 24. It was not possible to break out the slots along the patterned line. Careful metallographic examination of the ribbon cross-section over the groove patterns revealed that no crystallization had taken place. Thus, the quench rate was too fast to achieve localized embrittlement.

After the fifth casting run on this wheel it was noted that many of the inserts in the 0.015" and 0.020" wide grooves had begun to separate from the wheel. Close examination of the ribbon from the fifth run showed that molten metal had begun to penetrate into the gaps between the wheel and the inserts even though these gaps were less than 0.002" wide.

The third metal groove filling technique investigated was that of plasma spray. The use of this technique should allow the filling of intricate cut-out patterns with high temperature, unworkable alloys. This idea was tested using Rene 80 as the plasma sprayed filler metal. This high temperature nickel base alloy was chosen for its very low thermal conductivity and previous experience in its spraying parameters.

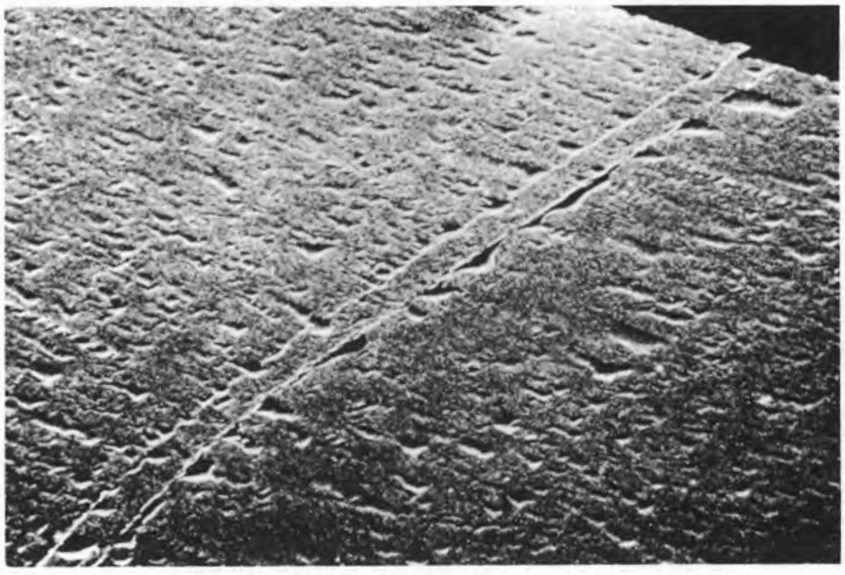

Figure 24. Ribbon cast over metal insert. Insert width was 0.010".

Optimally any metal filled grooves would be relatively deep. This would allow many remachinings of the casting surface thereby extending the wheel life. Unfortunately, the plasma spray method was found to be subject to very severe limitations in the geometries of grooves which can be filled. The groove filling capacity was tested on small copper test blocks machined with grooves of various geometries. The blocks were chemically etched clean and heated to ~600°C in the spraying apparatus. As is standard practice, the surface was further cleaned by reverse arc sputtering to ensure a good plasma bond. It was then plasma sprayed with Rene 80 using multiple passes sufficient to fill the grooves.

The degree of filling obtained for each groove was revealed by metallographic cross sections of the sprayed grooves. Several of these sections are shown in figure 25. The aspect ratio (depth:width) of the grooves was found to be very important in determining the degree of filling. The groove in figure 25a has a nominal aspect ratio of 10:10 (mils) and is completely filled by the plasma spray. Some large porosity, over and above the porosity of the sprayed layer, begins to appear along the sides of the groove as the depth is increased (15:10) in figure 25b. Increasing the depth further (20:10) as in figure 25c prevents complete filling of the groove. A large void is formed after the groove is about 75% full. Plasma droplets collect on the edges of the surface coating, and it grows inward closing off access to the groove before filling is complete.

This filling problem is probably inherent to the plasma spray process and cannot be cured by changes in the apparatus or spray parameters. The use of spray collimators would not help significantly because the problem is not caused by divergence of the plasma spray. For comparison, figure 25d shows a section of a groove near the edge of the test block where the spray impacts the groove at some oblique angle. The voids are principally on the leeward side of the groove. Figure 25c has a symmetrical void distribution so the spray of plasma droplets must be essentially vertical. An attempt was made to circumvent this filling problem by using a two-step spraying process (i.e., fill grooves half

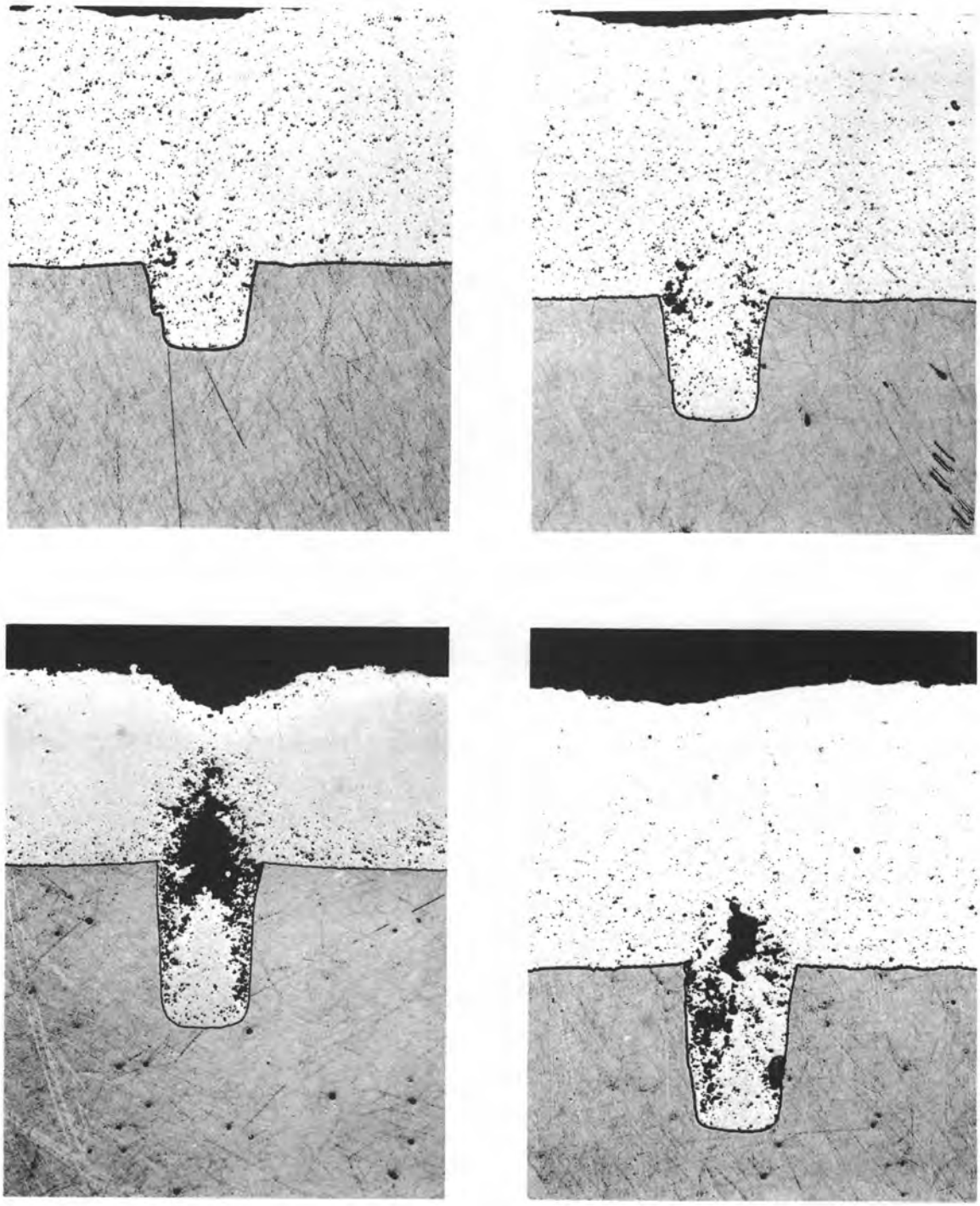

Fig. 25. Metallographic sections of copper grooves plasma sprayed with Rene 80. Groove dimensions are (depth X width in mils) a) 10 X 10 b) 15 X 10 c) 20 X 10 (oblique spraying angle). (50X)

way, grind off surface coat then spray with second coat). This was unsuccessful because the second coat of Rene 80 would not bond to itself.

A 1 inch thick OFHC Cu-1%Cr slot casting wheel was constructed using this plasma spray process. EDM grooves 15 and 20 mils wide were cut 25 mils deep. These were sprayed with Rene 80 and surface ground. The resulting surface was generally good. Only a few voids were visible. To eliminate the chance of molten alloy sticking, the crucible was positioned so that the cast ribbon would miss these voids. The usual helical casting parameters were used resulting in good ductile ribbon 0.0015" thick.

During casting, most of the Rene 80 insulator lines pulled away from the copper leaving a gap at the interface. One area of this interface separation is shown in figure 26. Typically, this separation occurred at all interfaces exposed to the melt. Figure 26 shows that this separation is not restricted to the directly exposed areas but extends beyond the boundary of the ribbon. This damage is due to thermal expansion differences between the wheel and the filler metal. Figures 25b and 25c show that zones of less dense material occur along the sides of the grooves. Deformation from thermal stresses is concentrated in these weak zones leaving a gap along the interface. This interface separation was not observed with the metal inserts which have coefficients of thermal expansion similar to Rene 80. The reason for this apparent discrepancy lies in the residual stress states imposed by the two filling techniques. The insert method leaves the filler metal in residual compression from the surface deformation while the plasma sprayed metal is in residual tension. Although the expansion coefficient for Rene 80 is less than that for copper it is being cooled down from a much higher temperature. The Rene 80 in the final groove has cooled down from its melting temperature while the copper has only cooled from some intermediate temperature. The greater temperature difference of the cooling Rene 80 more than compensates for its smaller coefficient so that it undergoes more shrinkage and is left in tension at room temperature. Heating the wheel again during casting increases

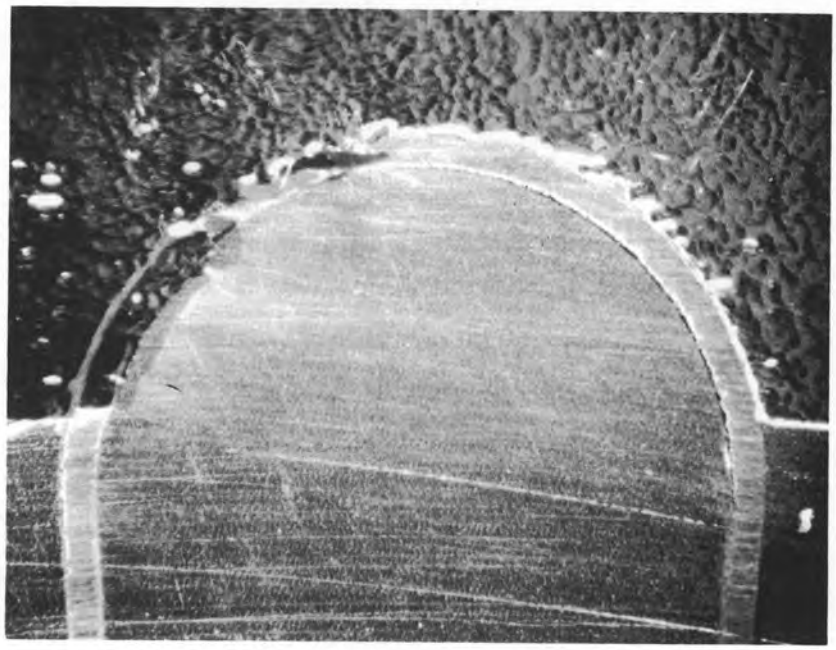

Figure 26. Helical ribbon slot superimposed over the corresponding plasma sprayed Rene 80 insert. The wheel-insert interface separation is seen to extend beyond the ribbon edge. Slot separation is seen to follow the interface lines. (11X)

these tensile stresses causing separation. Clearly, the strain temperature response of Rene 80 and copper should be the same on cooling as on heating and yet the separation did not occur when the wheel was cooled from the spraying temperature. This is due to the physical constraints imposed by the deposited surface layer of Rene 80 during the initial cooling. After the surface coating is ground off, this constraint no longer exists. Thus separation is free to occur when the temperature is raised again during casting.

The local embrittlement of the ribbon cast over these Rene 80 lines was the most pronounced of any of the metal filled grooves tested. However, the cut-out separation was not as easy here as in the glass insulator (to be discussed later in this section) or open groove case. All of the cut-outs remained intact after casting and, unlike the glass and open groove cut-outs, these could not be easily removed. Instead, these cut-outs required substantial flexing before there was sufficient cracking to allow removal. This flexing often propagated cracks into the remaining ribbon before the cut-out could be removed. Cracks were most easily formed on reverse bending (i.e., with the wheel-side surface on the outside).

Although the embrittlement response casting over Rene 80 is better than the other metals tested, not all of this improvement can be attributed to the decreased thermal conductivity. On the top surface of the ribbon the cut-out boundary appears to be two separate lines; one above each copper-metal interface. Cracking and cut-out separation generally occurs along these lines. This can be seen in figure 26 in which the cast ribbon is superimposed over the corresponding filled groove. Separation has occurred along both the inside and outside interface lines. The trace of one of these lines visible on the top surface of the ribbon can be seen in this figure on the remaining cut-out segment. Since separation always occurs along these interface lines, the ribbon embrittlement was not sensitive to the width of the Rene 80 insulator line.

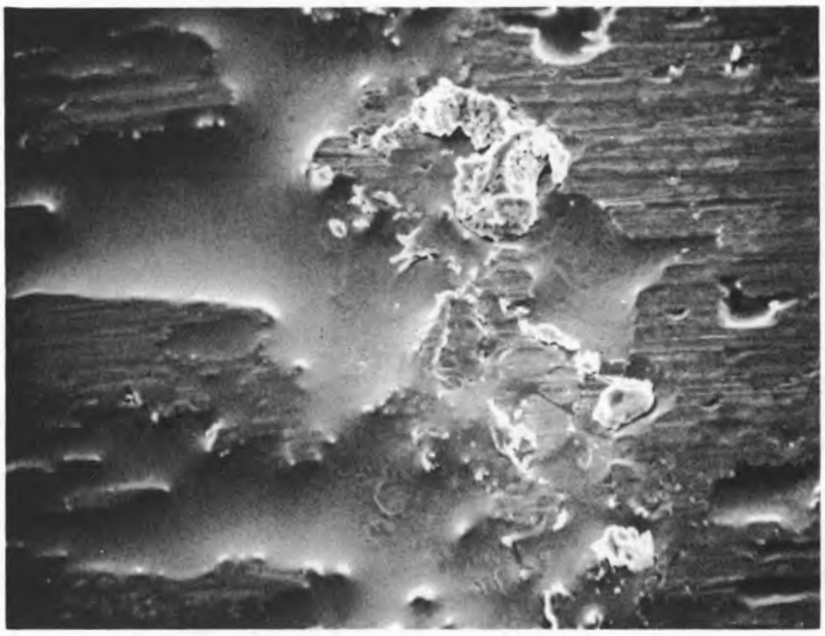

Figure 27. SEM micrograph of Rene 80 plasma sprayed particles embedded in the ribbon directly above the interface line. (600X)

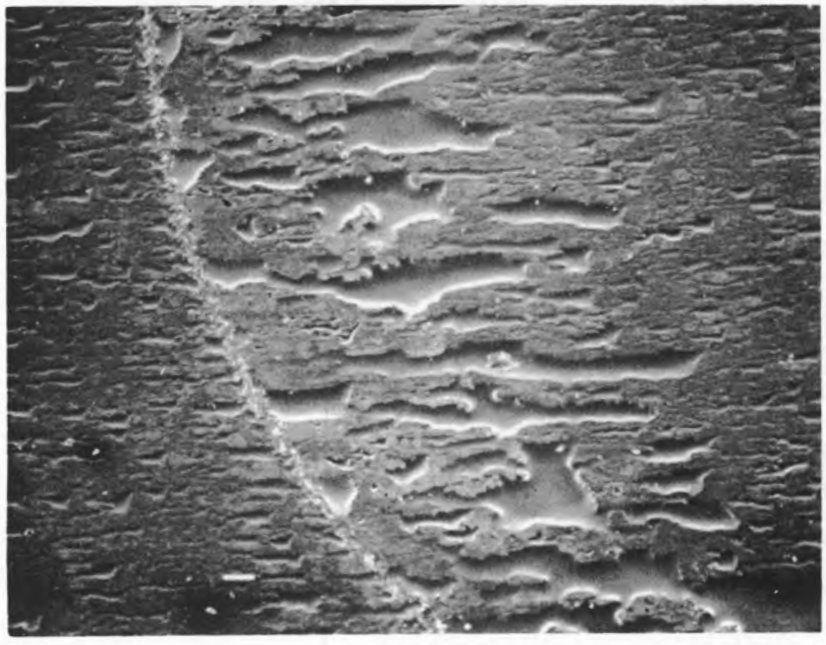

Figure 28. SEM micrograph of air pocket structure formed over Rene 80 insert. Note string of embedded particles at interface line. (45X)

Figure 27 reveals why cut-out separation occurs preferentially along the interface lines. This is a high magnification micrograph of an area on the underside of the ribbon which was cast directly above the copper-metal interface gap. The interface line on the ribbon is seen to consist of a string of embedded particles. Energy dispersive X-ray analysis confirms that these particles are Rene 80. The solidifying ribbon has extracted poorly bonded plasma particles from the low density area along the side of the filled grooves where the interfacial gap has formed. The presence of these angular particles in the ribbon help to confine crack initiation to this interface line. This particle crack initiation phenomenon is obviously not useful for cut-out separation during extended runs. Thus, the successful use of plasma spray as a groove filling technique for other insulator materials is dependent on the avoidance of the low density, poorly bonded regions along the sides of the grooves. It may be necessary to use even shallower grooves and slightly inclined groove sides.

The air pocketing behavior on the wheel-side surface of this ribbon is similar to that of ribbon cast over the other metal inserts. Air pockets formed over the Rene 80 did not, however, nucleate predominantly as the copper-metal interfaces. Although many are interface nucleated, more air pockets are formed directly above the filler metal. A typical air pocket structure is shown in figure 28. The occurrence of interface air pocketing has some dependence on the extent of copper-metal separation in the casting wheel. Larger gaps nucleated more air pockets especially on the second interface where the air pockets are being formed above a copper substrate.

Figure 29 shows some available data on thermal conductivities for materials used in this investigation. The actual conductivity of the enameling glass used was not known. However, all glass conductivities available were found to be in the same range. The conductivities of some common typical glasses are plotted here to show that range. The conductivities of the braze alloys are on the same order as the refractory metals.

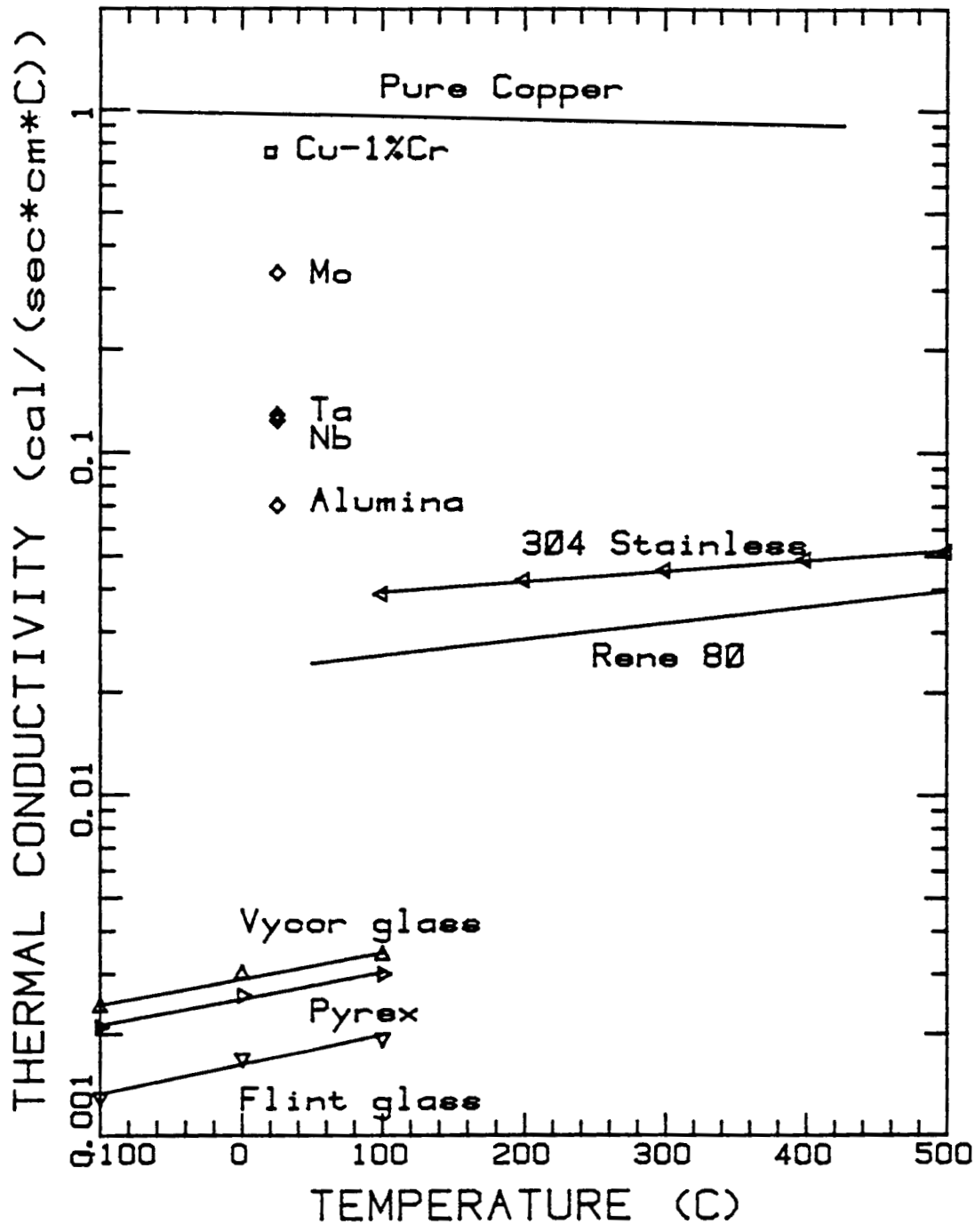

Figure 29. Available thermal conductivity data for groove insert materials.

It has been found that the ribbon embrittlement and cut-out separation resulting from these groove filler materials follow a trend of improving with decreasing thermal conductivity. However, thermal conductivity has not been shown to always be the dominating factor in determining the ease of cut-out separation. Other insulator characteristics such as surface topography and wetting angle can make significant contributions.

Glass Filled Groove Patterns

In order to achieve a slower quench rate in the patterned regions glass was chosen as a filler material because of its low thermal conductivity and non-wetting characteristics. Enameling the glass to the copper, however, was plagued with the formation of gas bubbles in the glass. These bubbles, when intersecting the casting surface, were found to be deleterious to the casting of amorphous flake because they acted as sticking sites for the molten alloy. Splashing, wraparound and/or broken crucibles was the general result.

Thirteen different glasses were tried with a variety of firing schedules to find those compositions and conditions at which the gas bubbles would be minimized. The best results were obtained with Pemco I413 frit glass fired at 700°C for short times. For this enameling procedure the filled slots generally contained only small and infrequent bubbles. Thus, I413 was the glass used for all casting experiments.

Filling the slots in the copper substrate was accomplished by suspending -120 mesh glass in methanol (30 v/o solids) and spraying this slip onto the surface. The slip was then heaped over each groove with a spatula and fired at 700°C. Unless the slip was piled up over each groove, there was insufficient material available for filling it. Instead, a deep meniscus would form in the groove and the exposed copper on the corners of the groove would become heavily oxidized.

To determine the filling capabilities of various groove geometries a small copper test plate was prepared. Parallel sawcuts of several different depths and widths were cut into this place. It was then enameled with I413 and surface ground to reveal the filled grooves. Although surface grinding did introduce a small amount of glass chipping, it was a satisfactory method of removing the glass.

Figures 30a, b, and c are photographs normal to the surface of the copper showing some typical bubble concentrations for the indicated geometries. The occurrence of surface porosity appeared to have some

dependence on the geometry of the groove. Most of the bubbles were concentrated near the bottom of the groove as shown in figure 31. The bubble frequency did not appear to be a very strong function of the groove width. The maximum bubble diameter was, however, limited to the width of the groove.

The use of a stainless steel conditioning wheel was previously found to be very detrimental to the integrity of an open groove on the casting surface. To see the effect of such a conditioning wheel on the glass filled grooves, the above mentioned test plate was subjected to a spinning stainless steel wire brush for approximately one minute. The glass was unaffected, but a small amount of copper did smear over the glass at the first copper glass interface. Although this limited smearing was judged to be relatively harmless, much larger disruptions occurred whenever a bubble was adjacent to the second glass-copper interface. Here, the situation is the same as the open groove. Behind each bubble the copper edge is locally smeared away as shown in figure 32 destroying the integrity of the line. Thus, in addition to the molten alloy sticking problem, large bubble formation must be avoided to maintain the integrity of the insert.

Four series of cut-out grooves were machined into the casting surface of a Cu-1%Cr wheel by EDM. The grooves were cut to two different widths to determine the optimum width of the resulting insert. Those widths were: 0.015" and 0.020". The groove width of any given cut-out could be distinguished on the cast product by the number of cut-outs in the series. All grooves were cut to a depth of 0.025". After enameling and surface grinding this wheel the condition of the glass surface was generally very good. Figure 33 shows the surface of a 20 mil wide groove after grinding. Surface bubbles were rare and those present were usually very small. This wheel is shown in figure 34. The glass surface was greatly improved over previous attempts. The average bubble size and frequency had been significantly reduced.

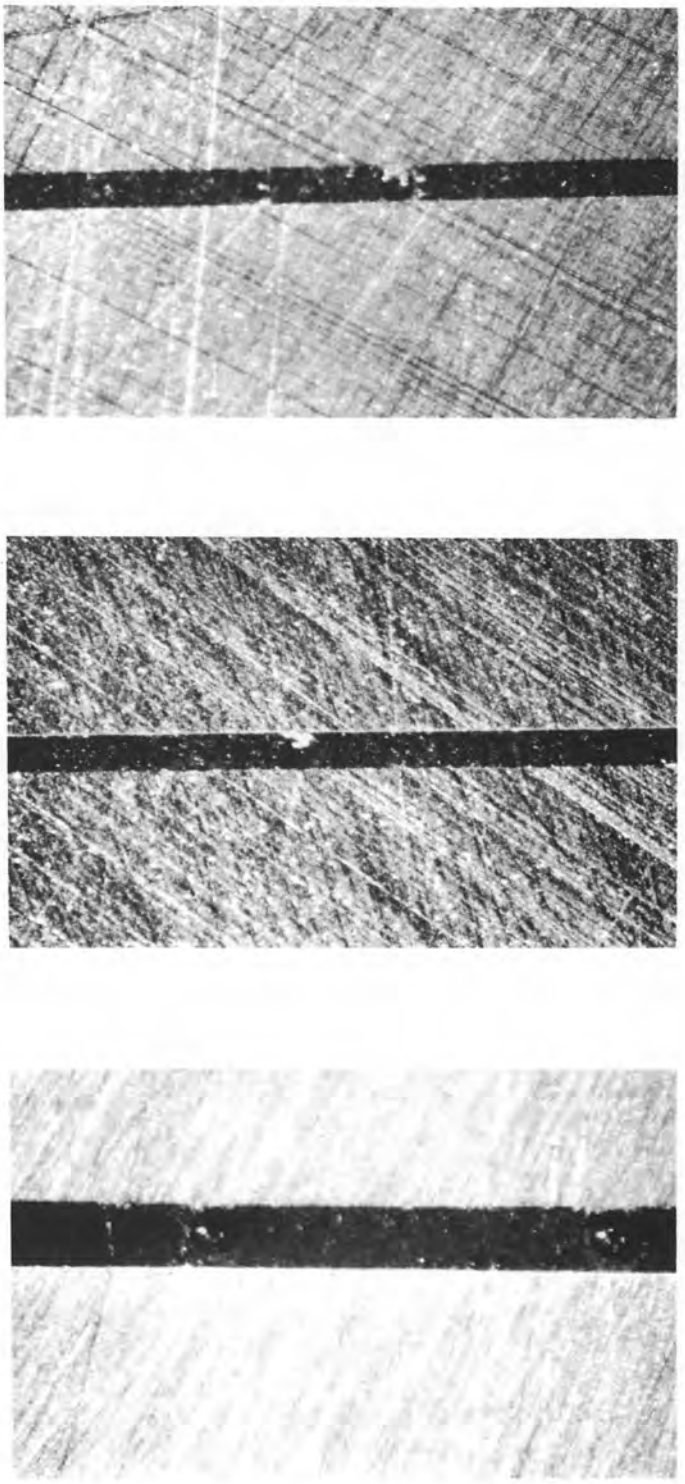

Fig. 30. View of top surface of glass filled grooves after surface grinding showing typical bubble structures. Groove dimensions (width X depth in mils) are a) 6 X 20 c) 10 X 20.

a) Slot ∿.008" x .020" deep

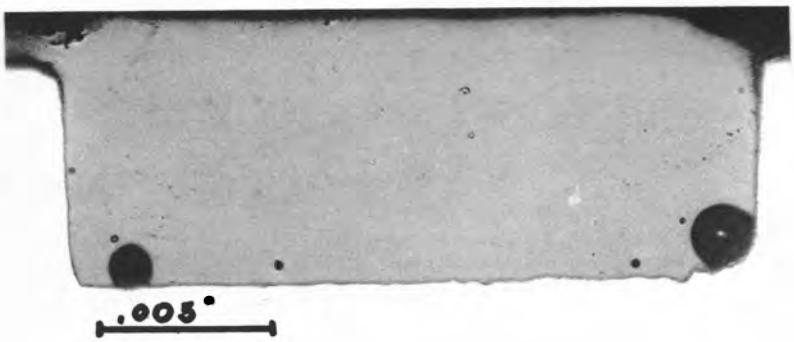

c) Slot ∿.008" x .010" deep

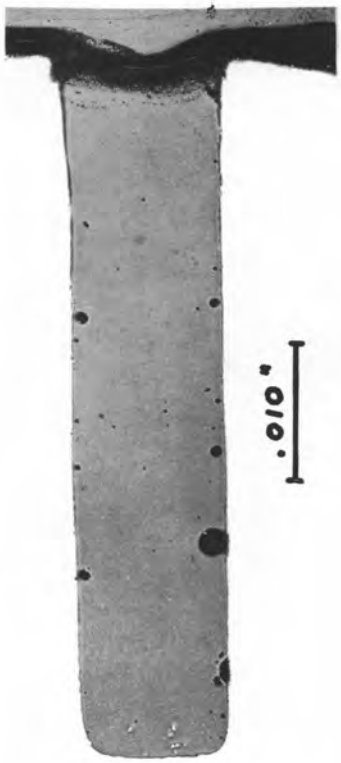

d) Slot ∿.010" x .050" deep

Fig. 31. Photomicrographs of metallographic cross-sections showing slots in copper plates filled with I413 glass applied by firing at 700°C for 6 min. Fifty mil deep slot in (d) required two applications of enamel for complete filling. Glass in all slots contains only small and infrequent bubbles. (a-c (200X), d (81X)).

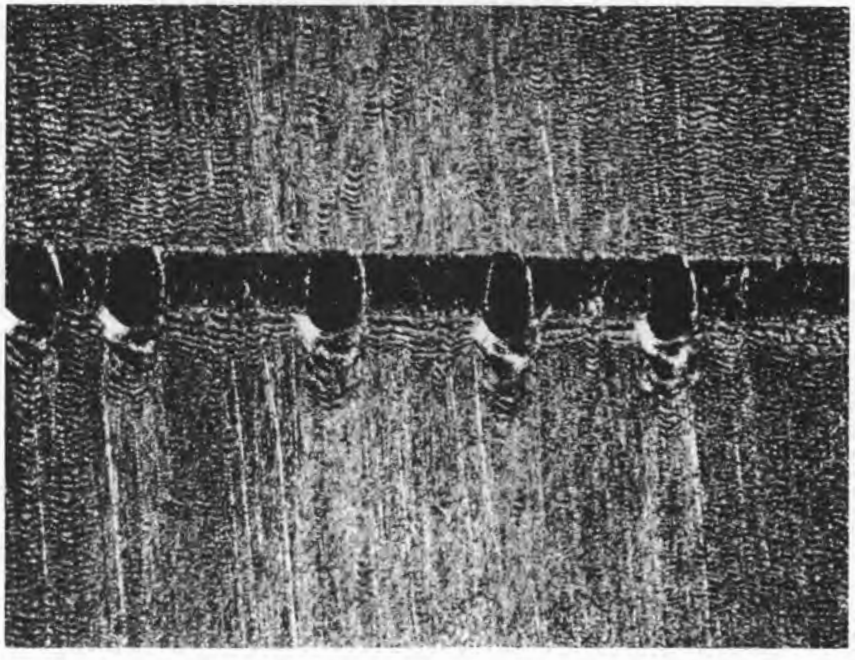

Fig. 32. Surface bubbles on a glass insulator line after exposure to a stainless steel wire brush.

Figure 33. Surface of glass insert before casting. (20X)

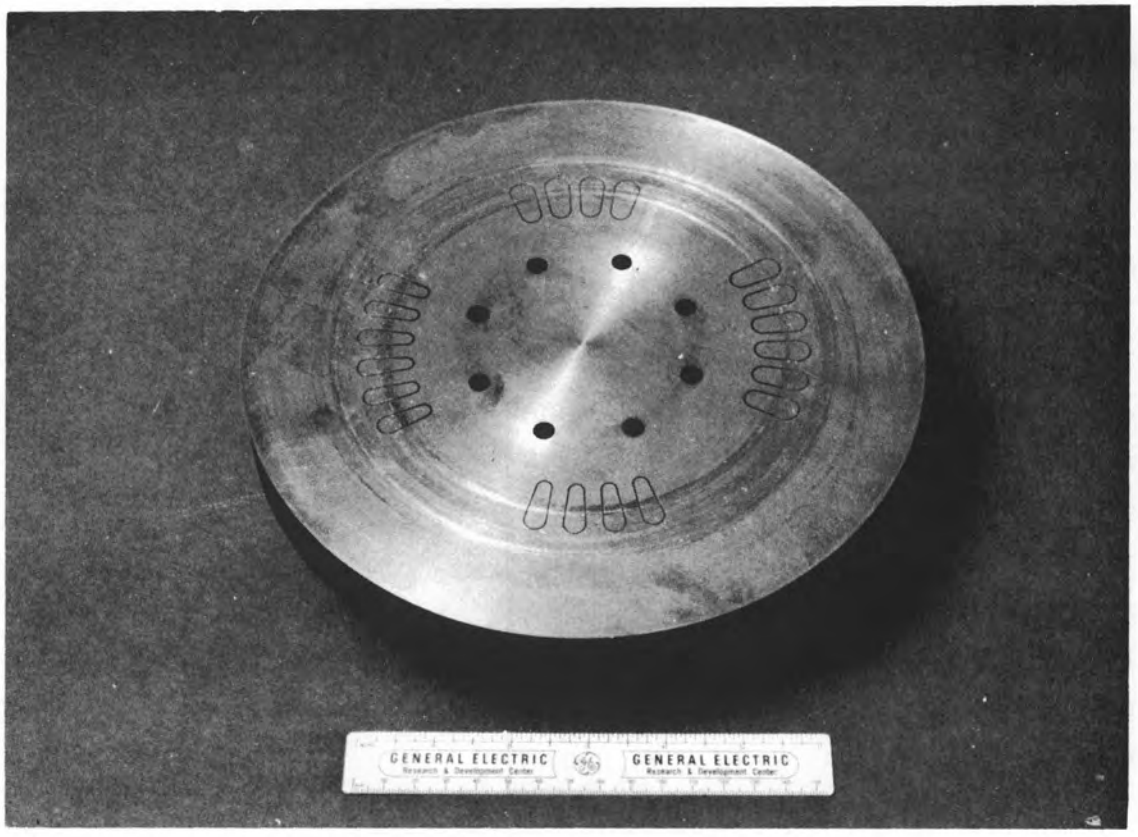

Figure 34. Casting wheel with glass filled grooves.

After casting ~30 turns of good helical ribbon, solidified metal stuck to one of the glass inserts dragging the cast ribbon past the high pressure air jets and under the casting nozzle. This situation is shown in the high-speed movie frame of figure 35. The specific cut-out identified as the sticking site in this movie is shown in figure 36 after the casting run. Comparing these two figures the cause of the sticking is seen to be a large open bubble in the glass. This bubble completely spans the width of the 20 mil groove. Obviously, large bubbles like these must be eliminated for any casting run on glass insulator lines to be successful.

Also visible in figure 36 is the typical deterioration of the glass insert observed in all grooves after casting. The oblique illumination of this photo reveals that glass was removed from the surface of the insert leaving a shallow groove. Closer inspection of the remaining glass reveals sharp angular surfaces indicating that it had undergone extensive cracking before being pulled out. There was no evidence of glass melting. The cracking of the glass was only observed where the glass was directly under the cast ribbon. It stops abruptly at the inside edge of the ribbon. Assuming that the high conductivity of the copper ensures a shallow temperature gradient across the surface, a large area beyond the actual ribbon contact area will reach high temperatures. Since the cracking stops at the edge of the ribbon, it cannot be caused by the strains of differential thermal expansion between the copper and the glass. Instead, it is caused by thermal shock. The glass, being a very poor thermal conductor, supports a steep temperature gradient beneath the molten alloy contact area. The resulting subsurface tensile stresses cause extensive cracking in the glass.

By comparing the warping of the thin copper test coupons enameled with the candidate glasses a qualitative comparison of thermal expansion coefficients is possible. While several of the glasses warped the copper coupons the Pemco I413 coupon showed very little warping or cracking. Thus, its coefficient is on the order of that for copper ($16.6 \times 10^{-6}/^{\circ}C$). The use of a glass with a much smaller coefficient of expansion will significantly reduce the tensile stresses associated with

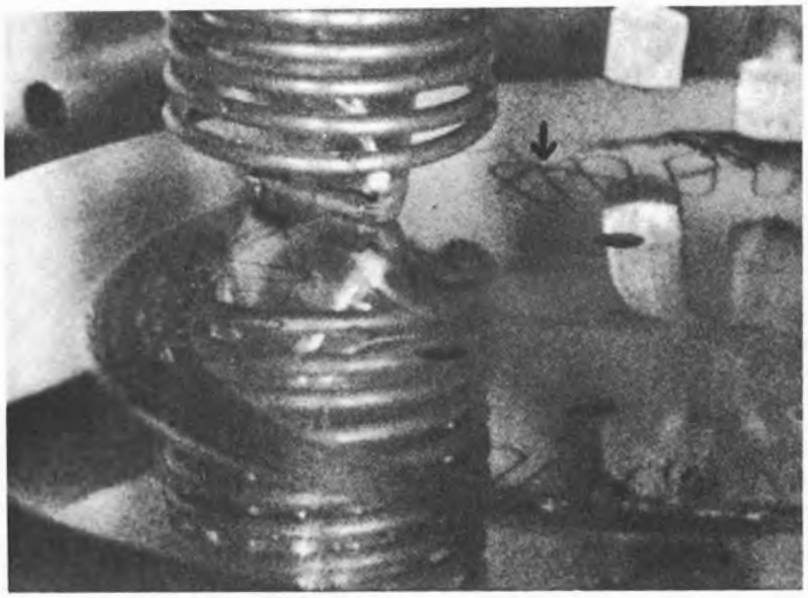

Figure 35. High-speed movie frame of casting over glass inserts. Arrow indicates where ribbon stuck to air bubble in the insert.

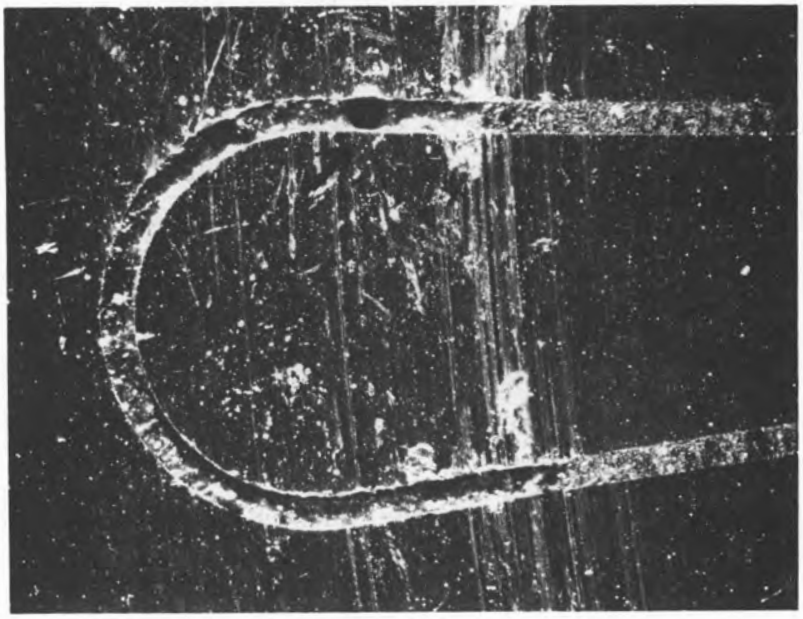

Figure 36. Glass insert with arrow showing air bubble where ribbon stuck.

the thermal gradient and may prevent the cracking. Incidentally, enameling of a copper groove with such a glass will greatly increase the residual compressive stresses on the glass thereby increasing its mechanical stability. If the cracking problem is alleviated, however, the melting point of the glass may become a more crucial consideration. Although no melting was observed on the present casting wheels if the glass stays intact in the groove, its surface will probably reach temperatures very near that of the melt (1250°C). This is much higher than the melting point of the glass.

Figures 37 and 38 illustrate how the glass is removed from the copper wheel during a casting run. As the surface cracks in the glass open up, they are filled with molten alloy which solidifies there. The ribbon is then pulled off and the process repeats. Figure 37 shows the underside of a ribbon along the cut-out boundary line where the solidifying melt has replicated the surface cracks in the glass. The thin, feathery projections are metal which had frozen in the cracks. When the cracking becomes so extensive that chunks of glass break free, they are pulled out by the solidified metal. Figure 38, a lower magnification of this area, shows one such piece of glass being held to the underside of the ribbon by the thin tongues of solidified metal.

Although the durability of I413 frit glass has been demonstrated to be unsatisfactory, its embrittling performance was encouraging. On the section of good helical ribbon cast before the crucible broke the glass inserts caused local embrittlement and easy cut-out removal. In fact, many of the cut-outs separated during casting. Figure 39 shows one revolution of the helix cast on the thick glass-filled wheel.

The outline of the cut-outs on the ribbon show very little increase in thickness above that of the adjacent smooth ribbon. Micrometer thickness measurements on the embrittled line generally range from 0.0 to 0.0001" thicker than the adjacent ribbon. This small thickness increase is probably due to casting over sections of glass pull-out and not due to the actual embrittlement mechanism. Because of the virtual absence of any ridge on the cut-out border this helix stacks very well.

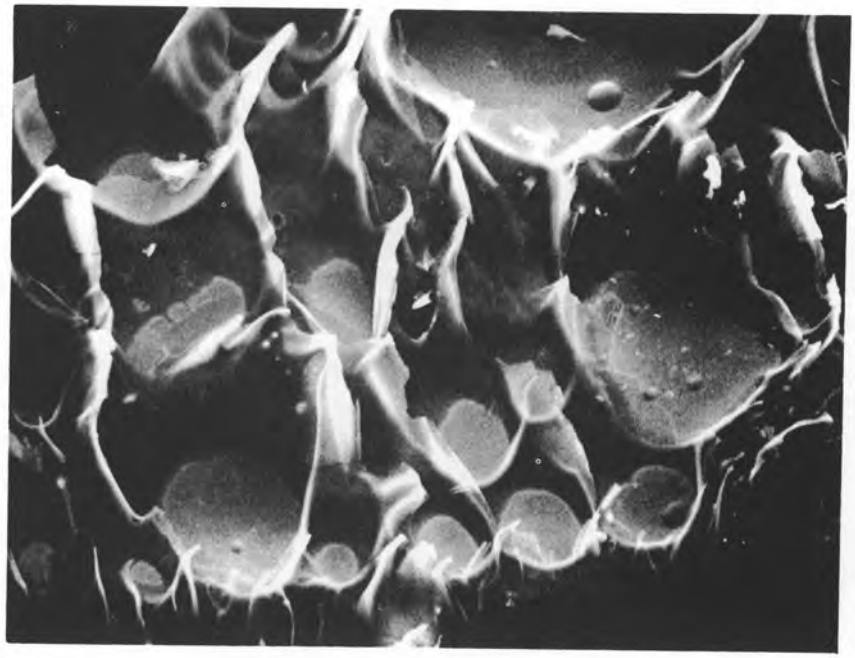

Fig. 37. SEM micrograph of ribbon showing replication of cracks in glass insert. (300X)

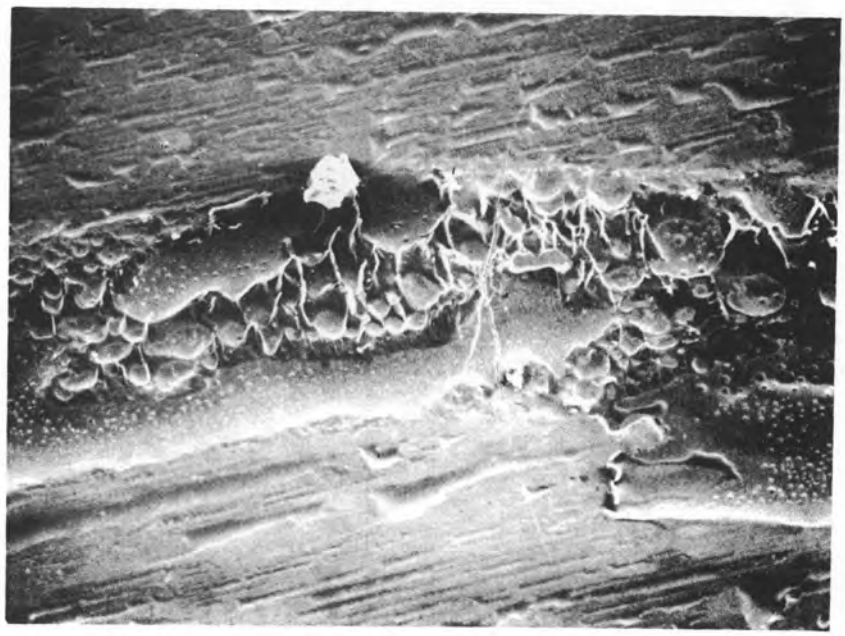

Fig. 38. Lower magnification of Figure 37 showing a piece of glass which was pulled out of the groove. (60X)

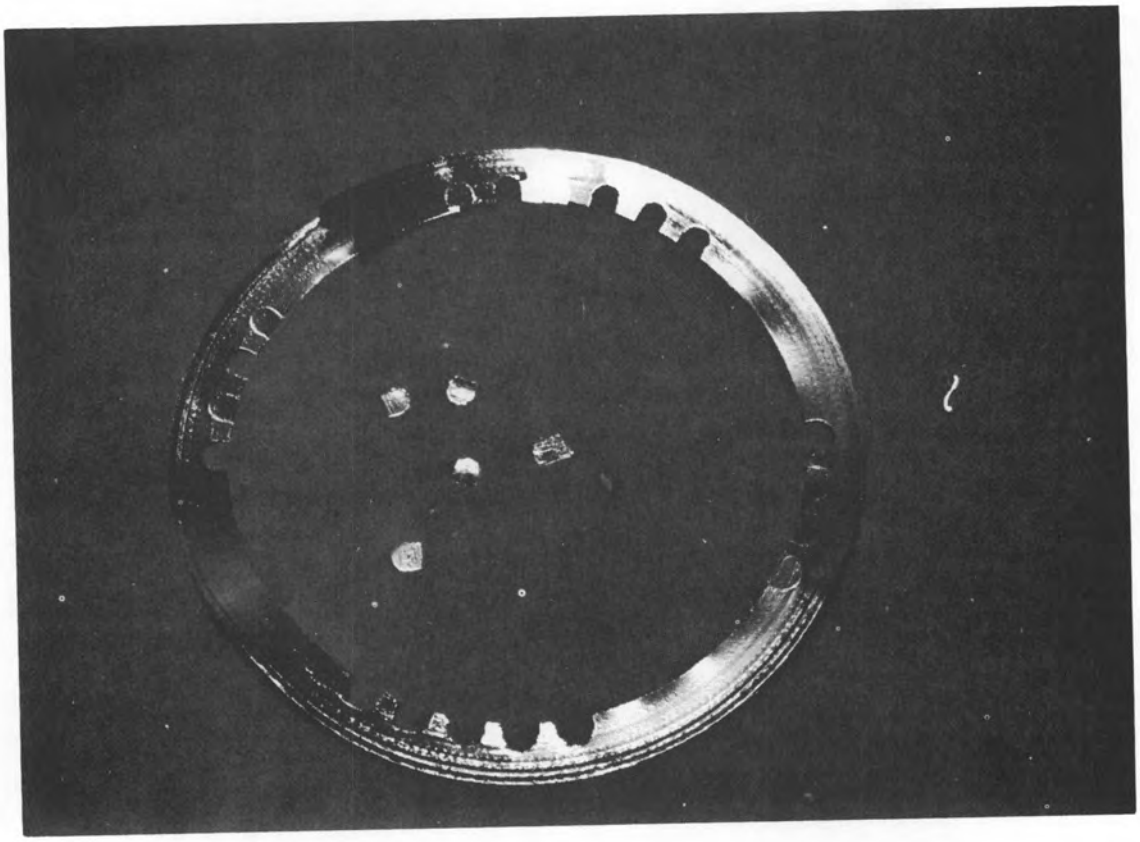

Figure 39. One revolution of ribbon cast over 15 and 20 mil wide glass inserts. Ribbon is 2.4 mils thick.

The embrittling mechanism over a glass insert is some combination of the low thermal conductivity and a phenomenon of amorphous ribbon casting known as air pocketing. Typically, the casting of smooth ribbon is subject to the formation of air pockets on the wheel-side surface of the ribbon wherever the liquid metal does not sufficiently wet the casting wheel surface. The upstream surface of the liquid melt puddle forms some equilibrium contact angle θ with the casting wheel dependent on the wetting characteristics of the wheel material. Whenever this angle is decreased below some critical angle θ^* (whether by melt puddle fluctuation, higher local air pressure or wheel surface defects), air penetrates into the melt-wheel interface forming an air pocket. Using this criterion for air pocket formation, the glass insert will introduce another possible mechanism for reducing the contact angle below the critical angle. This is schematically illustrated in figure 40. The wetting of the glass by the melt may be such that the equilibrium melt-glass contact angle is less than the critical angle for air pocket formation. Thus, no local perturbations are necessary. Large air pockets are formed whenever the melt contacts the glass surface. Figure 41 shows the underside of a ribbon cast over a glass insert. The random air pocketing from melt puddle fluctuations and wheel surface defects are visible over most of the surface. The surface cast directly above the glass, however, consists predominantly of very large air pockets. They generally start and end abruptly at the copper-glass interfaces.

These air pockets contribute significantly to the local embrittlement of the ribbon cast above the glass insert. The introduction of a layer of air between the melt and casting wheel results in a region of poor interfacial heat transfer. This locally retards solidification and causes a dip in the solidification front. Thus, the ribbon above the air pocket becomes thinned from both the top and bottom surfaces. It is these thin regions of slow quench rate which form the locally embrittled line. A high magnification view of this area in figure 42 shows that cracks initiating in these embrittled lines are somewhat erratic. Thus, on a small scale the cut-out edge is fairly jagged. The cracking is, however, generally well confined to the width of the line so the cut-out is still well defined.

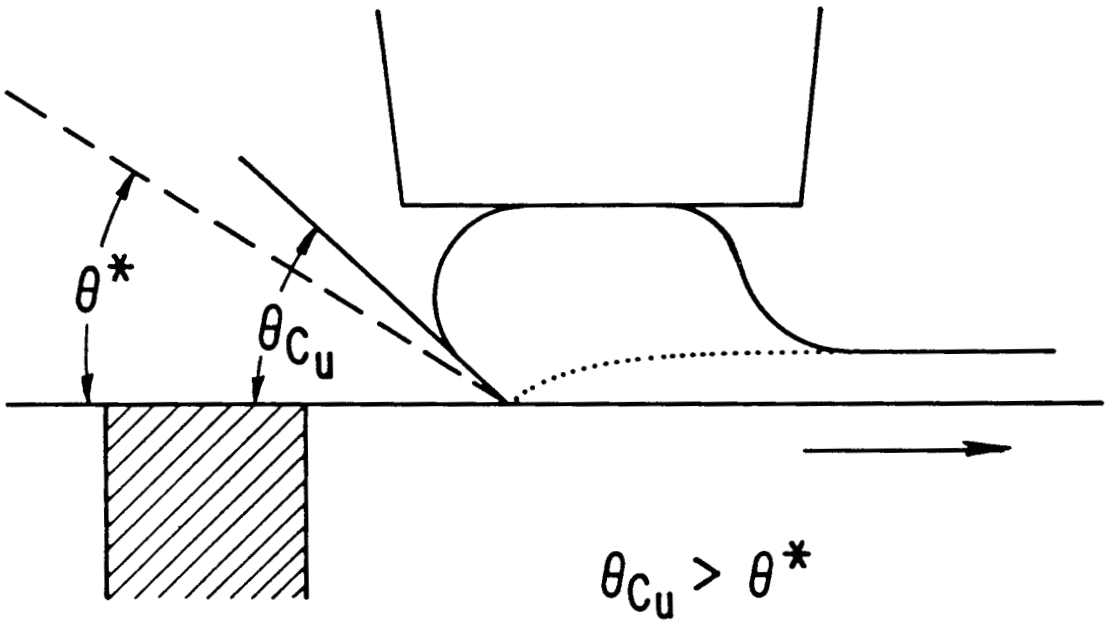

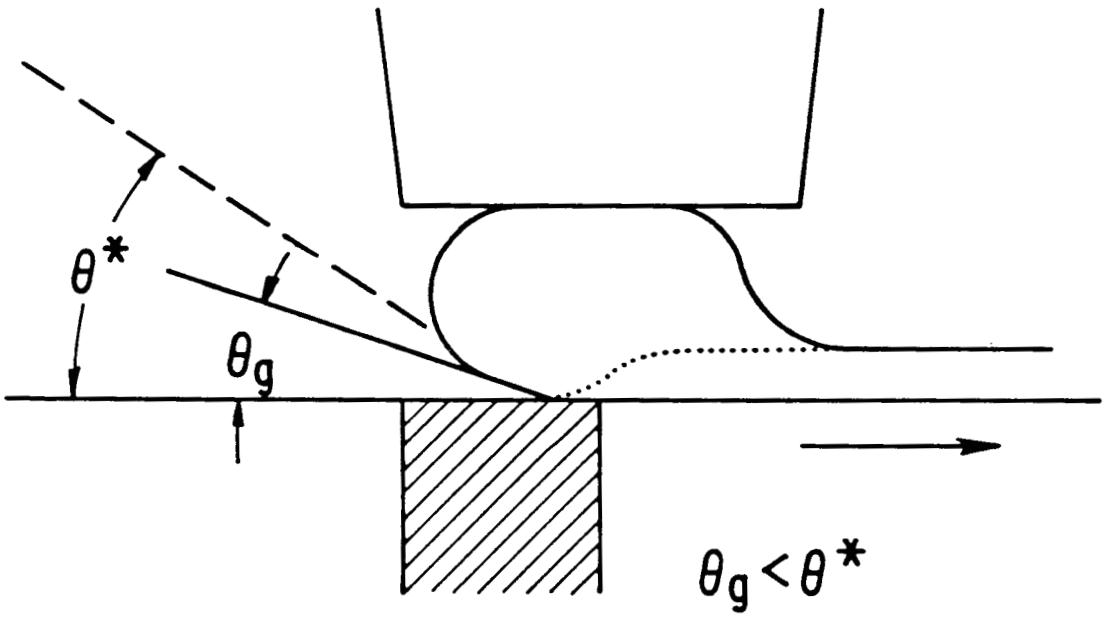

Figure 40. Schematic representation of the equilibrium wetting angle for copper and glass. θ* is the critical angle for air pocket formation.

Also visible in figure 42 is a phenomenon which has not been observed in "conventional" air pocketing. That is the presence of small beads on the surface of the air pockets. Further magnification in figure 43 shows these more clearly. Evidently the non-wetting glass surface and the slow solidification rate allow the melt time to bead up on the surface before solidifying. These beads are formed only in air pockets which have been initiated on the glass surface. In figure 42 it can be seen that there are no beads in the air pockets formed before reaching the glass line (on the right side). Curiously though, the beads can be present in air pockets solidified over the copper after the glass line has passed as long as the pocket is connected to a glass formed air pocket. Air pockets formed immediately after the glass line but which are not connected did not form the beads.

Although air pocketing is beneficial to the embrittling process it also limits the permissible width of the glass insert. Large air pocket "streamers" can form after the embrittled line and disrupt the integrity of the ribbon if the glass insulator is too wide. Figure 44 shows a series of cut-outs where the glass line is slightly too wide. Air pockets trailing after the embrittled line are so large that they penetrate through the thickness of ribbon leaving elongated voids. Obviously then, the maximum permissible width (to cast without voids) is dependent on the thickness of the ribbon being cast. A thicker ribbon is more tolerant of a wide glass insert. This thickness effect is illustrated by figure 45 which shows a direct comparison between two ribbons of different thickness cast over 20 mil glass inserts. The thicker ribbon (0.0024" thick) casts very well over the 20 mil glass. The ribbon remains intact between well-defined cut-outs. The casting of the thinner ribbon (0.0015") however, is totally disrupted by the 20 mil glass insert. This disruption is caused by extremely large trailing voids which link up between adjacent lines obliterating the whole series of cut-outs. The ribbon in figure 44, a borderline case, is 0.0014" thick and was cast over a 15 mil glass insert. Thus, for the casting parameters used, the maximum permissible glass line width appears to be limited to roughly 10X the thickness of the ribbon being cast. From a practical standpoint, this limits the line width to about 15 mils as the

Figure 41. SEM micrograph of ribbon cast over glass insert. (20X)

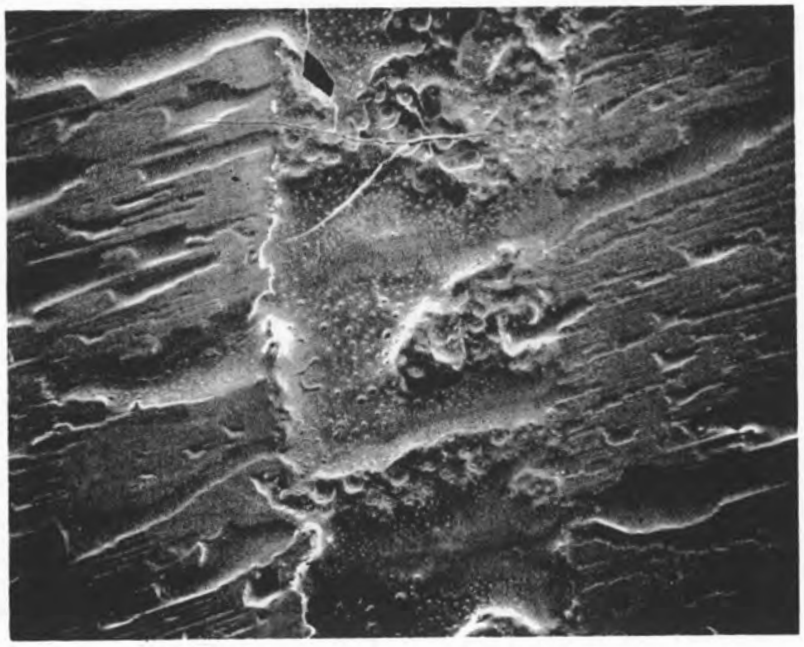

Figure 42. Higher magnification of figure 41 showing details of air pocket formation. (60X)

Figure 43. Higher magnification of figure 42 showing beads which formed in the air pockets above the glass inserts. (300X)

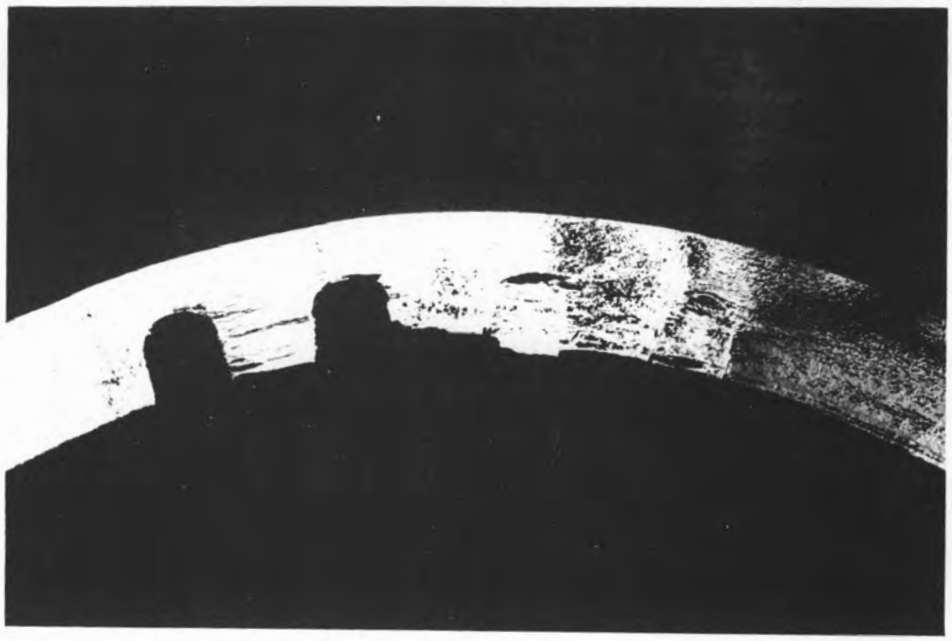

Figure 44. Series of slots cast over 15 mil glass inserts. Ribbon is 1.4 mils thick. Casting direction is counterclockwise.

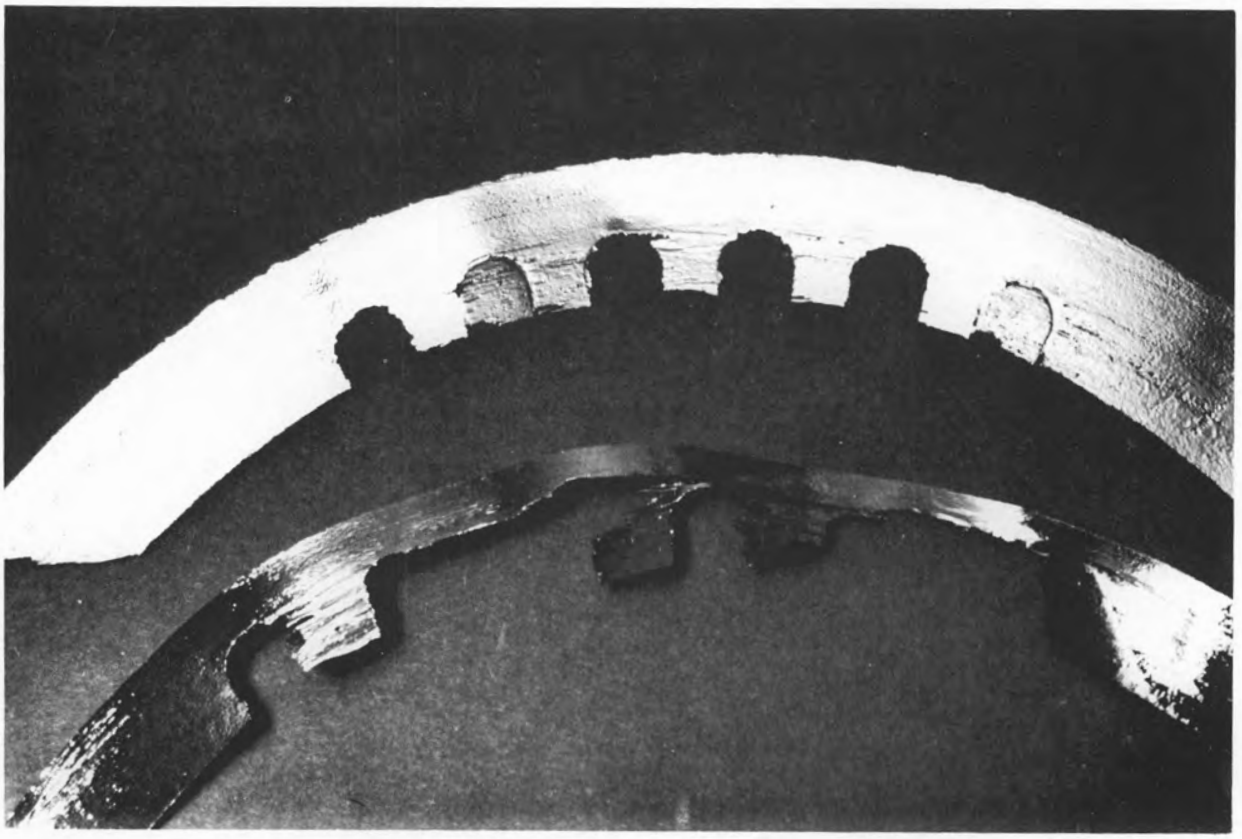

Figure 45. Two ribbons cast over 20 mil wide glass inserts. The top ribbon is 2.4 mils thick and the bottom ribbon is 1.5 mils thick. (1.5X)

thicker ribbons tend to be brittle and have poor magnetic properties.

Beyond filling slots with conventional glasses, past experience indicated the possibility of using a glass filled thick film paste such as those commonly used for insulating crossovers and capacitor dielectrics for silk screened electronic circuit components. A selection of these materials was obtained as shown in Table VI.

The material as received was too thick to force into narrow slots. Pine oil was added until the material was thin enough to be conveniently worked into the slots. Several copper blocks were machined with slots .005, 0.010, 0.015, and 0.020 inches wide as test samples for evaluating slot fill. A continuous mesh belt furnace with three controllable temperature zones and variable atmospheres was used to generate the time-temperature-atmosphere cycle recommended by the paste manufacturer.

Slots were filled in several different ways to obtain the best fill possible. A single fill with a surface wipe gave extremely porous fill. The volatilizing of the vehicle and the shrink on sintering both contributed to the porosity. The most successful fill resulted from a fill schedule which consisted of squeezing paste into the slots and wiping the slot as clean as possible with a razor blade. The sample was then sent through the furnace with the approximate time cycle recommended by the manufacturer but with the temperature increased 50°C above the recommended valve. Our intent is to have the glass flow and reduce its surface tension to fill voids. This is, of course, contrary to the originally designed use of the material. The above fill cycle was repeated 14 times after which the sample was sectioned and polished as shown in figure 46. As seen from this figure although the glass bonded reasonably well to the walls and bottom of the slot and some sections are free from large voids, there are regions with unacceptably large voids. Although limited effort was expended on this technique of slot filling, it is felt that the rigorous requirements for long life under high erosion conditions and thermal cycling will not be met by these low temperature glass materials.

TABLE VI

THICK FILM PASTES USED TO FILL COUPON SLOTS

Manufacturer	Type	Fire Temp °C	Use
Electroscience Laboratory	4608C	900 ± 100	Dielectric Coating
Thick Film Systems Inc	1129RCB	600 ± 25	Cross Over Insulation
Thick Film Systems Inc	1123RCB	530 ± 30	Cross Over Insulation
Thick Film Systems Inc	1125RCB	600 ± 40	Cross Over Insulation
Thick Film Systems Inc	1141	490 ± 30	Hermetic Seal
E.I. Dupont	8190	875 ± 25	Cross Over Insulation

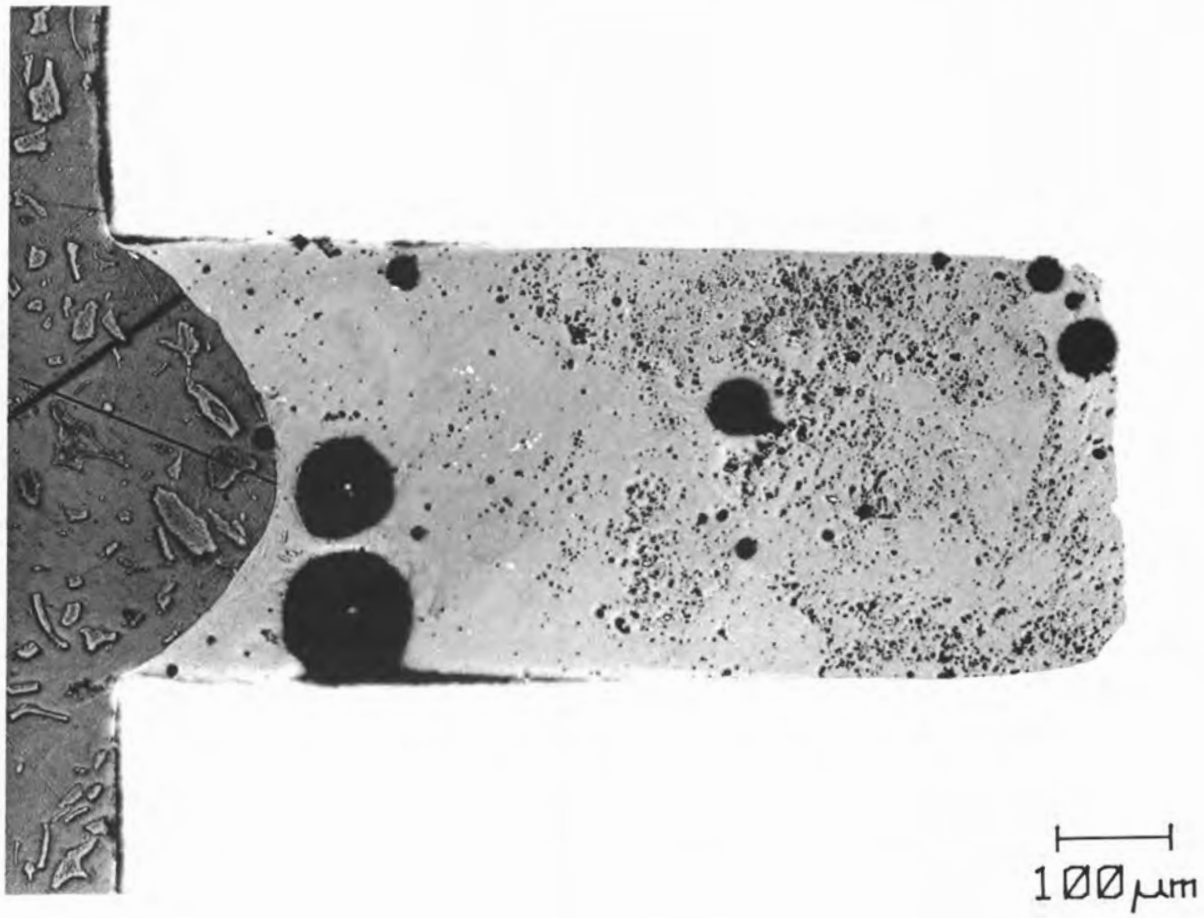

Figure 46. Section through fired "thick film" glass insert.

Ceramic Filled Groove Patterns

In order to try to avoid the thermal shock failure of the glass inserts it was decided to try a partially dense ceramic. Yttria stabilized zirconia has been developed as a thermal barrier coating for gas turbine blades. When properly applied by plasma spray, it has the characteristics of very low thermal conductivity and good resistance to thermal shock. These are the two important properties for its use as a thermal barrier coating, and they are two of the properties required for solving the problem of groove inserts.

A test plate with grooves 0.020" wide and 0.025" deep was plasma sprayed with zirconia-8% yttria powder. The grooves were uniformly filled and contained about 25% finely dispersed porosity. A casting wheel containing groove defining conductor slots was sprayed with the same conditions. The wheel was surface ground to remove the excess ceramic. The surface of the ceramic appeared rough with spherical ceramic particles bonded securely together. The grinding tended to smear the metal alloy over the edge of the ceramic filled groove.

A full 100 gram melt charge was successfully cast on this wheel using the preferred casting parameters. No sticking of the ribbon occurred. Approximately 60% of the slots separated from the ribbon during the casting and the rest were extremely easy to remove by flexing the ribbon. The fracture line between the ribbon and the break-outs stayed entirely within the 0.020" width defined by the ceramic insert.

Figure 47 shows the bottom of the ribbon in the region of a ceramic insert. The wetting of the molten metal to the ceramic is so minimal that over 80% of the area of the ribbon in this area was noncontacting to the substrate during solidification. The resulting slow quenching has left the ribbon very brittle in this region. Figure 47 shows a partial fracture in this brittle region.

This ribbon had no burr at the slot edges and it stacked very well. This casting run was the best achieved in the program.

The wheel was lightly repolished and a second casting run was successfully made. The quality of this ribbon and its slot cut-outs was extremely good—essentially identical to the previous run.

Examination of the wheel after the first run revealed some erosion of the ceramic insert surface. During the second run this erosion continued. Figure 48 shows a typical ceramic filled groove after the second casting run. The scratch marks on the wheel on the downstream side of the insert are due to abrasion from ceramic particles which have eroded out of the grooves. Figure 49 shows a higher magnification of the insert. A profilometer tracing over this insert showed an average depression below the level of the copper of 0.0001" and a depth of the valley at the downstream ceramic/copper interface of 0.0004".

Additional casting runs on this wheel also gave generally good results. However, the inserts continued their gradual erosion and a slight burr began to appear on the downstream side of the slots where the molten metal penetrated the deepening valley at the copper/ceramic interface.

Thus, while the ribbon product with cast conductor slot was excellent and the durability of this wheel with ceramic inserts was significantly better than that with glass inserts, it is concluded that the long term durability is inadequate for economical large scale production.

III.2.4 Conductor Slot Forming

Four approaches were pursued to assess the feasibility of economically forming conductor slots on the inside diameter of the helical ribbon after casting. These included: 1) using a hot, resistance heated wire formed into the shape of a conductor slot and pressed onto the ribbon for a short time to create a crystallized, brittle outline along

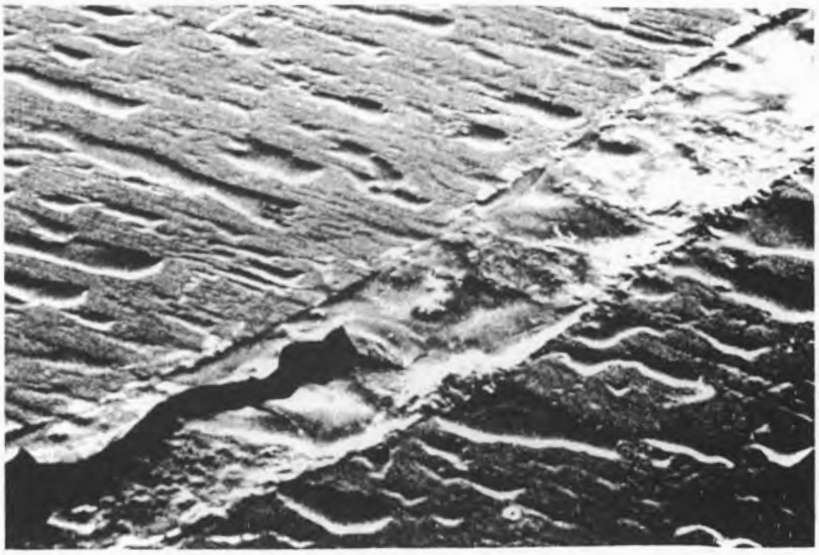

Figure 47. Ribbon cast over plasma sprayed ceramic insert. Insert width is 0.020".

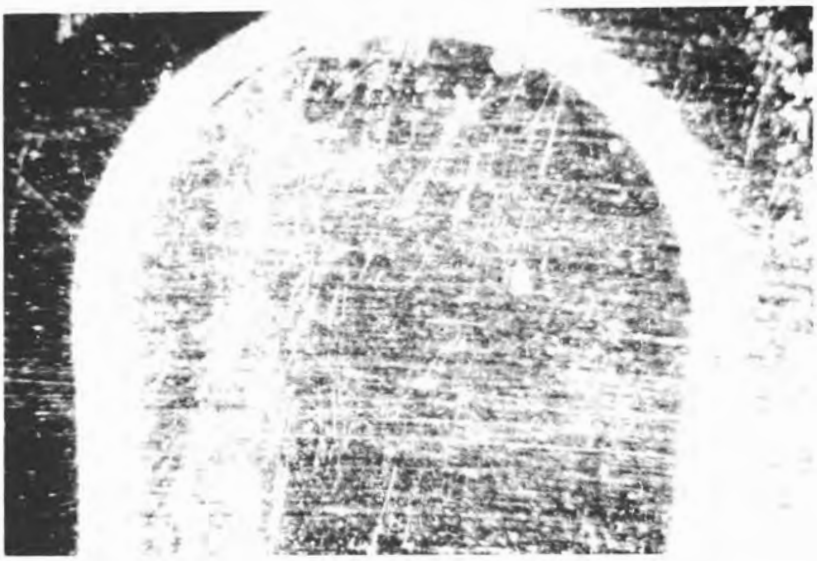

Figure 48. Wheel with ceramic insert after casting showing erosion.

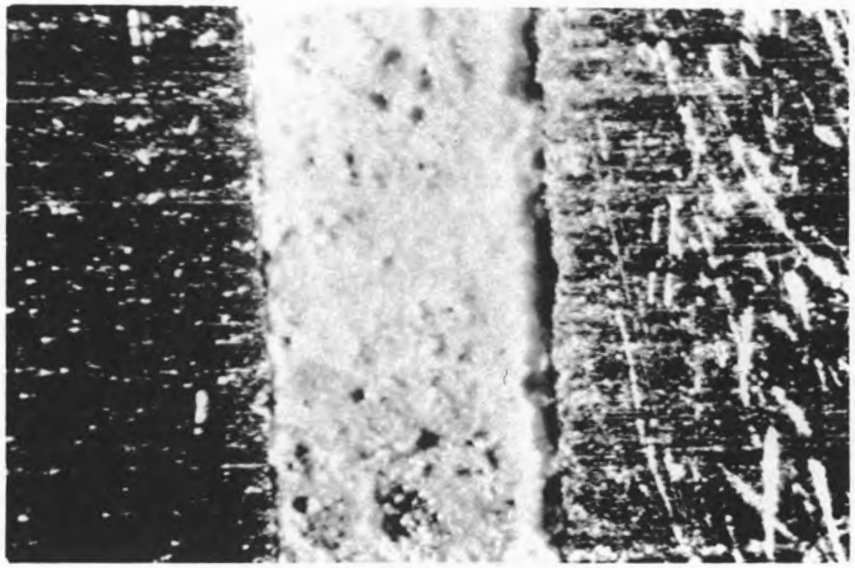

Figure 49. High Magnification of ceramic insert erosion.

which the slot could be broken out, 2) using a stylus with electric current flowing through it into the ribbon to "draw" the embrittling pattern in the ribbon, 3) using a magnetically steered electron beam to form the pattern, and 4) using a heated die punch to punch the conductor slots without incurring excessive die wear.

Hot Wire Forming

In this method a .025" diameter nichrome wire was bent into the shape of a conductor slot and heated with an electric current to about 800°C. Using a ceramic push rod this was pushed against the ribbon (being on a ceramic plate) for varying times up to one second and with varying pressures. These qualitative tests showed that an embrittled pattern could be made and broken out from the ribbon; however, the edge of the cut-out was quite rough.

Based on these results this method was mechanized for further tests with better control of the parameters. The hot wire was flexibly positioned about 3/32" above the ceramic base plate. The push rod was placed in a slip collar above the hot wire and driven down with a motor driven cam. The pressure was controllable with springs in the drive linkage and the time of contact controlled by the motor speed. Another cam on the motor advanced the ribbon forward under the hot wire in the time interval between impressions.

Using this mechanism it was found that fairly good embrittled patterns could be made. A second mechanism of a large diameter soft rubber roller running against a small diameter hard rubber roller was used to run the imprinted ribbon through and remove the slots with the flexing action provided by the rollers.

Both pieces of equipment were run at speeds up to four slots per second. As the speed increased, the quality of the slot edges improved. However, increasing the speed further was limited by the cooling effect on the hot wire; more current had to be provided to the wire to keep it hot enough to accomplish the embrittlement. But as this was done, the

frequency of wire failure increased. Also, as the process continued there was an increasing tendency for the wire to stick to the ribbon and cause a failure. Exhaustive solutions to these problems were not explored and it is quite possible that further work could solve them. However, currently the method is limited by life of the hot wire, and, in the long term it is unlikely that economical speed can be achieved.

I^2R Stylus Heating

During early work in bonding amorphous metal, spot welding consecutive layers was done. On occasion the spot welds would break out cleanly leaving a hole in the material. This observation led to the idea of embrittlement of lines by Joule heating in controlled areas of the ribbon.

Initial experiments were carried out by placing a strip of amorphous metal on a copper plate to which one terminal of a low voltage, current limited power source was attached. The other terminal was connected to various metallic probes and the probes were manually drawn across the amorphous metal. Due to the relatively high resistivity of amorphous metal, current was constrained to a narrow region in the width of the strip. With sufficient current, limited contact area and limited velocity, the contact region was heated and became embrittled. Since the embrittled region could not support bending stresses, the region would break away when moderate bending stresses were applied. Early work showed that the phenomena was relatively insensitive to stylus or probe material as well as the polarity of the current.

In an attempt to quantify the embrittling process, an x-y recorder was modified so that smooth, constant and measurable velocities of the stylus could be obtained. A stylus holder was built with insulating material and mounted in place of the pen holder. A finely stranded #12 wire was attached to the stylus and mounted 5 feet above the center of the recorder. This minimized the constraining effect of the lead wire. The paper support plate of the recorder was replaced by a plate of 1/8" copper electrically isolated from all other hardware but electrically

connected to one terminal of the power supply. Initially a stainless steel stylus 1/4" diameter was machined to a 0.005" radius tip with an included angle of 75°.

A range of currents to 20 amps were used at speeds from .5 in/sec to 4 in/sec. A Talley-surf profilometer was used to measure the profile of the tracks. This equipment repeatedly gave depth of track to be of the order of half the thickness of the material and widths of ten times the material thickness. These are in contradiction to what was observed optically and in the scanning electron microscope. Figure 50 shows an SEM photo of a 20 amp current line indicating negligible line depth and width less than twice the amorphous metal thickness (0.0015"). Further analysis of the Talley-surf curves indicated that we were observing a strained heat effected zone which caused a slight deformation under the stylus. This in turn caused the material to lift on each side of the stylus. When the stylus was traversed over amorphous metal with no current flowing, no deformation was observed. This indicates that significant heating to a temperature above the glass softening temperature occurs to some distance on either side of the crystallized line under the stylus. The pressure from the small radius tip is then enough to cause the material to deform.

When the material was separated along the desired line, many transverse cracks were observed to emanate from the parting crack. This is shown in figure 51. Microscopic observation indicated the contact line was not uniform in width. It appeared as if (in an exaggerated sense) the line consisted of a series of tear drops connected head to tip.

Since the power supply was operated in a constant current mode, it was obvious that the current density through the amorphous metal varied considerably due to the changing contact area. This changing area is partly caused by surface topology. Current density is the significant parameter in determining heat input and it is concluded that different amounts of heat were applied along the line which undoubtedly caused differential stresses, varying embrittlement and the transverse cracks.

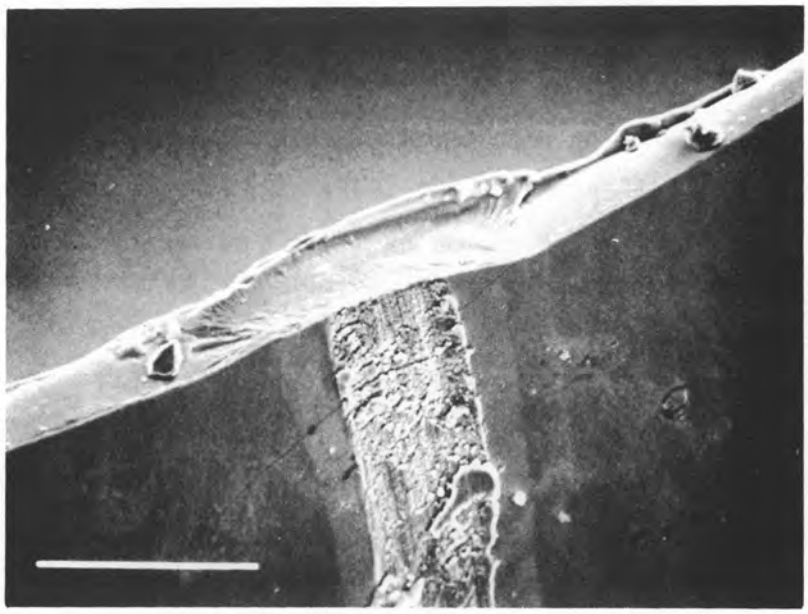

Figure 50. SEM cross section of strip scribed with 20 amp stylus. (320X)

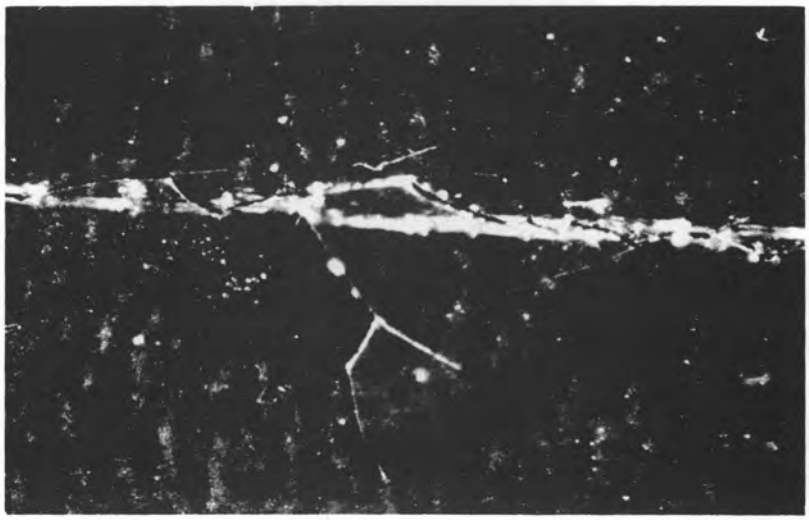

Figure 51. Material broken along crystallized line showing characteristic transverse cracks. (10X)

To minimize the effect of surface topology and the accompanying changing contact area, a new stylus was made, also of stainless steel but with a flat face 0.024" in diameter. Tests performed with this stylus did not show the differential stress as the ribbon remained flat at currents up to 15 amps. All of the above tests were done at a relatively slow stylus speed of one inch per second. Up to about 7 amps there was no significant embrittlement line on the ribbon. From about 10 to 15 amps excellent results were achieved. First, unlike the case of the small rounded stylus, the ribbon stayed perfectly flat with no deformation. Under bending the ribbon broke fairly easily along the lines with only occasional side branches. It was found that, by tracing over the line with a ball-point pen while the ribbon lay on a somewhat pliable pad, the ribbon easily broke along the embrittled line with no side cracking. The best results were achieved by forming the embrittled line with the stylus on the wheel side of the ribbon and tracing over the line from the opposite side of the ribbon. Tracing the line on the stylus side gave poorer results. Tracing lines which were generated by a fine point stylus caused severe transverse cracking and developed a very jagged edge. At 20 amps current there was unacceptable surface melting and arcing. With a tungsten stylus the same effects were observed at lower currents. The lower current requirements were probably due to the fact that the tungsten stylus was hotter. When the material was parted, the edge had an average roughness of about ±0.010". This is felt to be acceptable for motor punchings. Examination of the heated region made at increasing currents and constant stylus speed shows a distinct change in the features of the line above 15 amps. Below that current the contact zone is discontinuous. The density of contact spots was high and cracking of the line was accomplished with few side cracks. It is felt that a better <u>average</u> heating is accomplished in the region contacted by the stylus when the contact area is large enough to be nearly constant at any position.

Above 15 amps the contact area changed from discontinuous islands to a narrow continuous line. Separating this material was similar to separation of material heated with a more pointed stylus, i.e. many side cracks. It is felt that this change in pattern is caused by channeling

of the current due to the reduction in resistivity of the material on crystallization. As current is increased the whole area under the flat stylus heats to the crystallization temperature. One small region crystallizes first causing the resistivity in that region to decrease and since the system is driven from a constant current source, the crystallized region receives more current while adjacent regions receive less current. This decrease in current keeps the adjacent regions from heating more and they remain amorphous. During the crystallization of the small region, two things happen simultaneously. The higher current causes the crystallization to accelerate which gives off the stored heat of fusion causing more heating which increases the ductility of the material to improve the contact with the stylus. The current is thereby channeled to the region of the good contact. The second is the increase in current density caused by the reduction in resistivity.

The "window" for acceptable embrittlement with the x-y recorder table and a non-cooled stylus was from 8 to 16 amps through a flat 0.024" diameter stylus at speeds from 0.5"/sec to 4 in/sec. At speeds above this the stylus did not remain in good contact (bounce occurred). With a constant current power supply any bounce causes arcing which rapidly deteriorates the stylus contact area and forces an end to a test. Since break-outs were successfully achieved at low speeds, it was then necessary to evaluate components of the system which would be limiting in competing with punching 0.018" laminations for motor construction. Even under the assumption of computer controlled stylus position, several aspects of I^2R heating present severe engineering problems but the one felt to be most limiting is the heating of the stylus itself.

Experiments were done with 0.024" tungsten and stainless steel wire as well as a 1/4" dia. rod which was tapered to a point and ground back to a 0.024" flat. The 0.024" wires heated excessively at currents over 25 amps ($J = 55$ K amps/in^2), and the tip of the larger rod would rapidly wear to a larger area. Detailed calculations based on heating the volume under the stylus to 700°C, the temperature considered necessary for crystallization with the assumed thermal environment and speed, indicate a realistic maximum stylus speed of 150 in/second. This

velocity is a factor of 20 lower than the equivalent velocity of a high speed punch press based on cutting equivalent stack lengths of finished punchings.

Electron Beam Heating

To increase the speed of forming slots in helical ribbon over that obtainable from direct I^2R heating we investigated the use of electron beams. With reasonable deflection systems we could attain acceptable beam velocities of over 3000 in/sec which are then equivalent to high speed punching 0.020" thick material. Additionally, stylus bounce and arcing are nonexistent. Electron beam energy is the product of the accelerating voltage and current as long as the gage of material is thick enough to prevent the electrons from passing through. With low current and high voltage, energy densities to crystallize or melt tracks at 3000 in/sec are easily achievable.

Experiments were done in a new electron beam welder with a 7.5 kW, 150 kv system of state of the art design. This equipment was used in all e-beam embrittling as energy could be controlled and moderate deflection velocities were available. Initial work was done by physically moving the sample on an x-y traverse table in the e-beam vacuum chamber. All samples were held in place on a copper plate with masking tape. The geometry was such that low thermal contact between the ribbon and the copper plate was achieved. Poor contact is desirable to minimize heat loss and reduce energy requirements. This is another advantage of the electron beam system compared with I^2R stylus heating which, because of the high currents, required good electrical contact to the current sink with attendant good thermal contact and high heat loss.

At the low velocities of sample travel, a considerable amount of warpage of the sample was observed along with a wide heat affected zone. At these velocities, thermal conductivity was sufficient to spread the heat over a large area before any region reached the crystallization temperature. Writing at 1"/sec with beam energies of 3.5, 5 and 7 watts is shown in figure 52. Attempts to break these ribbons along the e-beam

line resulted in significant side cracking because of the large width of the embrittled region. Thus, we significantly increased the beam velocity and the beam energy which greatly reduced warpage and gave a well defined, narrow heat affected zone. Figure 53 shows the results of increasing the beam velocity by modulating the beam with a sinusoidal wave in x while the table moves linear in y to 10 in/sec with an increase of power to 72 watts. Two things are evident—i.e., the velocity is still too slow to eliminate the warpage and the pattern chosen allows an excessive heat buildup as the beam over-writes at the extremes of its deflection.

For crystallization, there is a time-temperature window in which one must operate. There is also a minimum temperature below which crystallization will not take place in a reasonable time period. Sample EB30 was run to try to place a lower bound on this window in units of energy and time. Writing was done with 0.1, 0.5 and 1 joule/inch of line. Nothing was observed either on the surface of the sample or by sectioning, metallographically polishing and etching with energy density of .1 joule/inch. At .5 joule/inch surface damage was visible and sectioning showed a small region where crystallization had been accomplished. Figure 54 shows these two samples. It had been determined earlier that the electron beam heating effects were almost independent of which side the beam entered so all samples were written on the wheel side as visual observations were more easily done on this side. Figure 54 also shows the comparison of writing speed at constant energy per unit length of beam travel. Here we have experimentally confirmed the idea that crystallization is more efficient at higher writing speeds with the same energy per unit line length. Under these conditions less heat conducts laterally and the heat of fusion is rapidly released aiding the heating process.

To obtain higher writing speeds in a controlled fashion and allow multiple samples for each system pump down, a programmable arbitrary waveform generator was borrowed. In operation, two 11 inch long samples were taped to the two outer edges of a copper plate. Adjacent to the copper plate but at the same vertical distance from the splash plate, a

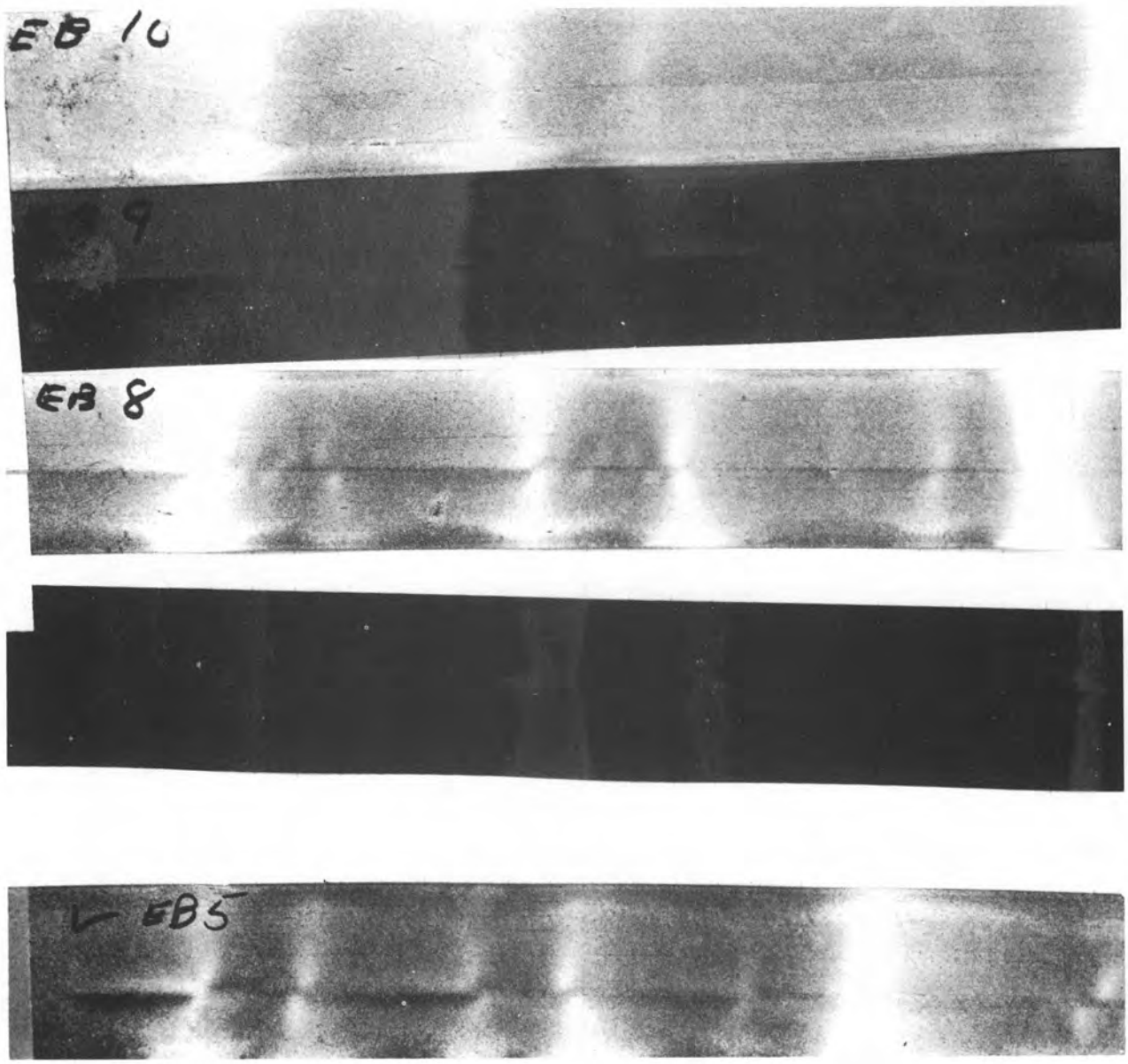

Figure 52. Samples marked with electron beam at one inch per second.

Sample	Side Up	Watts
10	Wheel	3.5
9	Air	3.5
8	Wheel	5.0
7	Air	5.0
5	Wheel	7.0

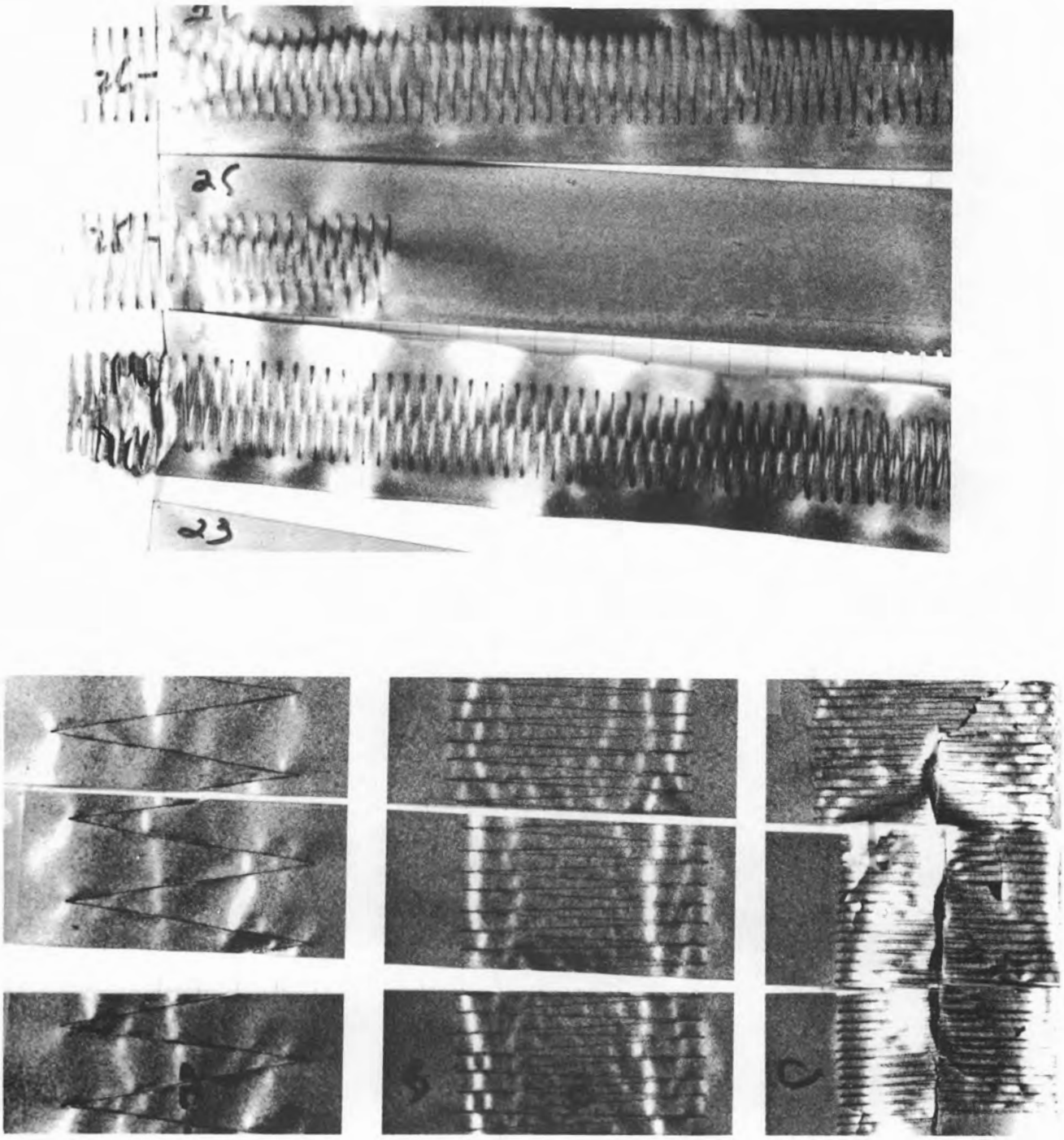

Figure 53. Sawtooth beam modulation.

Sample	24	25	26	A	B	C
Power (watts)	72	36	36	40	80	160
Speed (inches/sec)	10	10	10	20	80	160

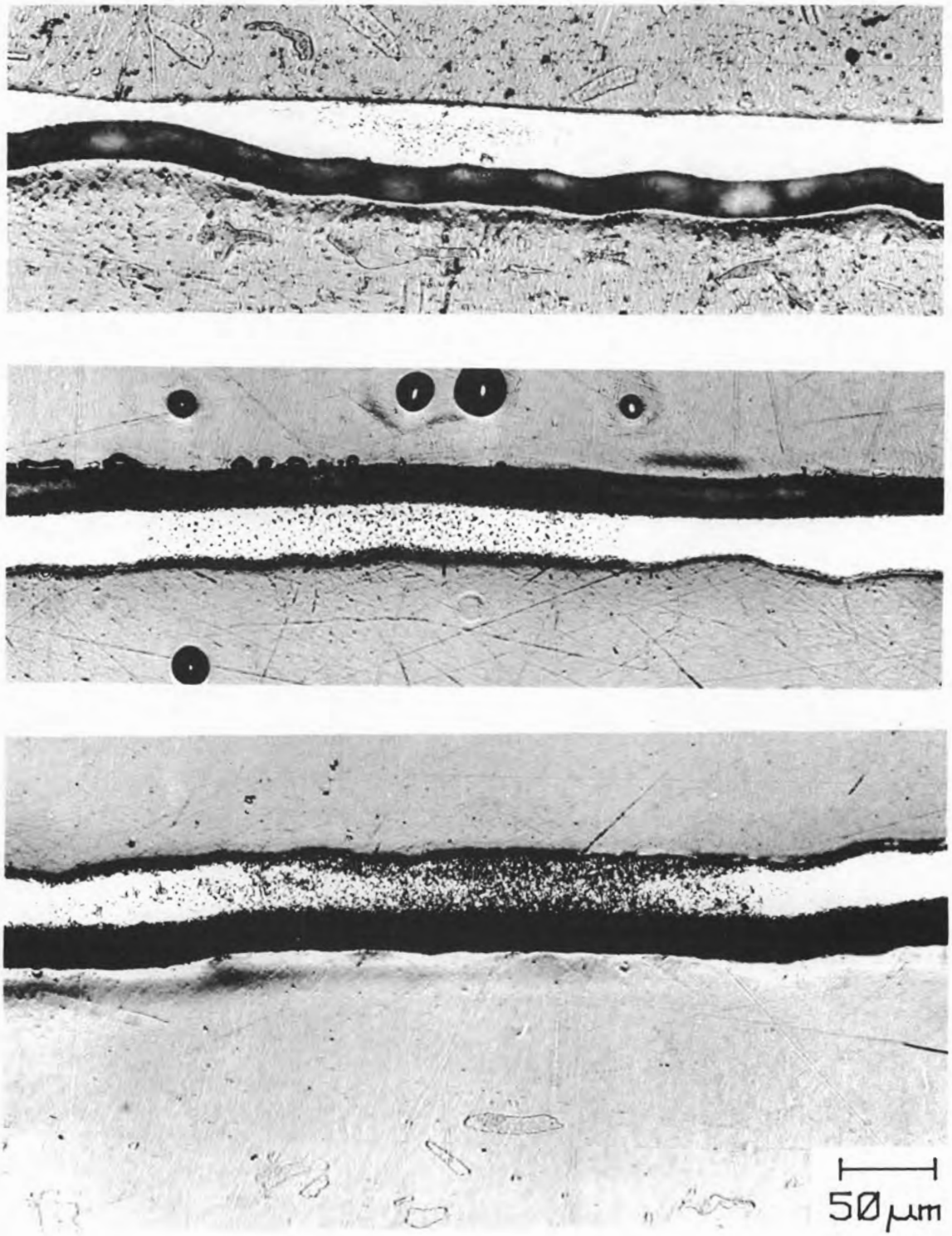

Figure 54. Cross section micrographs of electron beam traces. (Linear horizontal white area is the ribbon. The dark line parallel to the ribbon is a void between ribbon and metallographic mount.

Sample	a	b	c
Energy (joule/inch)	.5	1.0	1.0
Beam speed (inch/sec)	40	40	160

tungsten target was placed to allow focusing the beam at the proper plane. The wave form generator was set up to deflect the beam on to the sample in the y direction with a linear ramp upon manual trigger command. The table which carried the samples was driven in the x direction at about 10 inches per minute. The beam was located 1/4 inch off the edge of the sample and kept on. As the table traversed, the beam was triggered to mark a line on the sample at about 1/4 inch increments. After several lines were drawn, the table travel was stopped to allow changing parameters, i.e., current and beam velocity. Table VII shows the important parameter in the higher writing speeds is energy per unit length. It also shows that the margin of energy per inch between separated material and that which shows no damage to be between 0.7 and 1.1 joules/inch.

Some of the samples which were separated looked flat and appeared to have no material build up at the edge of the kerf, but micrometer measurements showed a build up of up to several ten thousandths of an inch. To confirm this, metallographic samples were taken at 1.0 and 1.6 joules/inch. These are presented in figure 55. Note the build up of material on the separated edges due to melting and subsequent surface tension forces. Also, next to the separated edge, a region of crystallization is obvious. Sample c shows evidence of melting in the necked down region in the center but not quite separated. At lower energy densities of d and e, only a crystallized region with no necking down is evident.

The desirability of using the electron beam to directly part the material is obvious so an investigation was conducted using energy densities near the upper limit of our equipment and a range of writing speeds to evaluate the possibility of high temperature melting and sublimation material removal. Table VIII is a compilation of the results of these runs and clearly indicates that as energy density is increased the build up along the edge of the kerf also increases. At the highest energy density, spherical particles were observed attached to the parted edge of the sample. It is also noted that with a constant energy density, the build-up increases with increasing beam velocity.

TABLE VII

EFFECT OF BEAM WRITING PARAMETERS

Sample	Accelerating Potential (kv)	Beam Current (ma)	Power (watts)	Velocity (in/sec)	Energy Density (joules/inch)	Condition of Damage
38a	150	1.0	150	60	2.5	Separated
b	150	.5	75	60	1.25	Not Separated
39a	150	2.0	300	120	2.5	Separated
b	150	.6	90	120	.75	Barely Visible
40a	150	2.5	375	120	3.0	Separated
b		1.25	188	120	1.5	Mostly Separated
c		.8	125	120	1.0	Not Separated
41a	150	6.0	900	300	3.0	Separated
b		3.0	450	300	1.5	Separated
c		2.0	300	300	1.0	Not Separated
d		1.0	150	300	.5	Not Visible
42a	150	12.0	1800	600	3.0	Separated
b		6.0	900	600	1.5	Separated
c		4.5	675	600	1.2	Not Separated
d		3.0	450	600	.7	Not Separated
43a	150	12.0	1800	600	3.0	Separated
b		6.0	900	600	1.5	Separated
c		4.5	675	600	1.2	Partly Separated
d		3.0	450	600	.7	Not Separated
44a	150	24.0	3600	1200	3.0	Separated
b		12	1800	1200	1.5	Partly Separated
c		9	1350	1200	1.2	Not Separated
d		6	900	1200	.7	Not Separated
46a	150	21	3150	1200	2.6	Separated
b		18	2700	1200	2.3	Separated
c		15	2250	1200	1.9	Separated
d		12	1800	1200	1.5	Partly Separated

TABLE VIII

BEAD THICKNESS NEXT TO KERF ON MELTED SAMPLES

Sample	Accelerating Potential (kv)	Beam Current (ma)	Power (watts)	Beam Velocity (in/sec)	Energy Density (joules/inch)	Bead Next To Kerf (inch)
54	150	3	450	130	3.5	.0003 → .0005
55	150	6	900	260	3.5	.0003 → .005
56	150	6	900	130	7.0	.007
57	150	3	450	200	2.3	0 (No separation)
58	150	3	450	130	3.5	0 → .0003
59	150	3	450	130	3.5	.0003 → .0005
60	150	6	900	130	7.0	.012
61	150	6	900	260	3.5	.0003 → .0015
62	150	12	1800	520	3.5	.0008
63	150	24	3600	1040	3.5	.0012
64	150	24	3600	520	7.0	.0048
65	150	24	3600	260	14.0	.0064

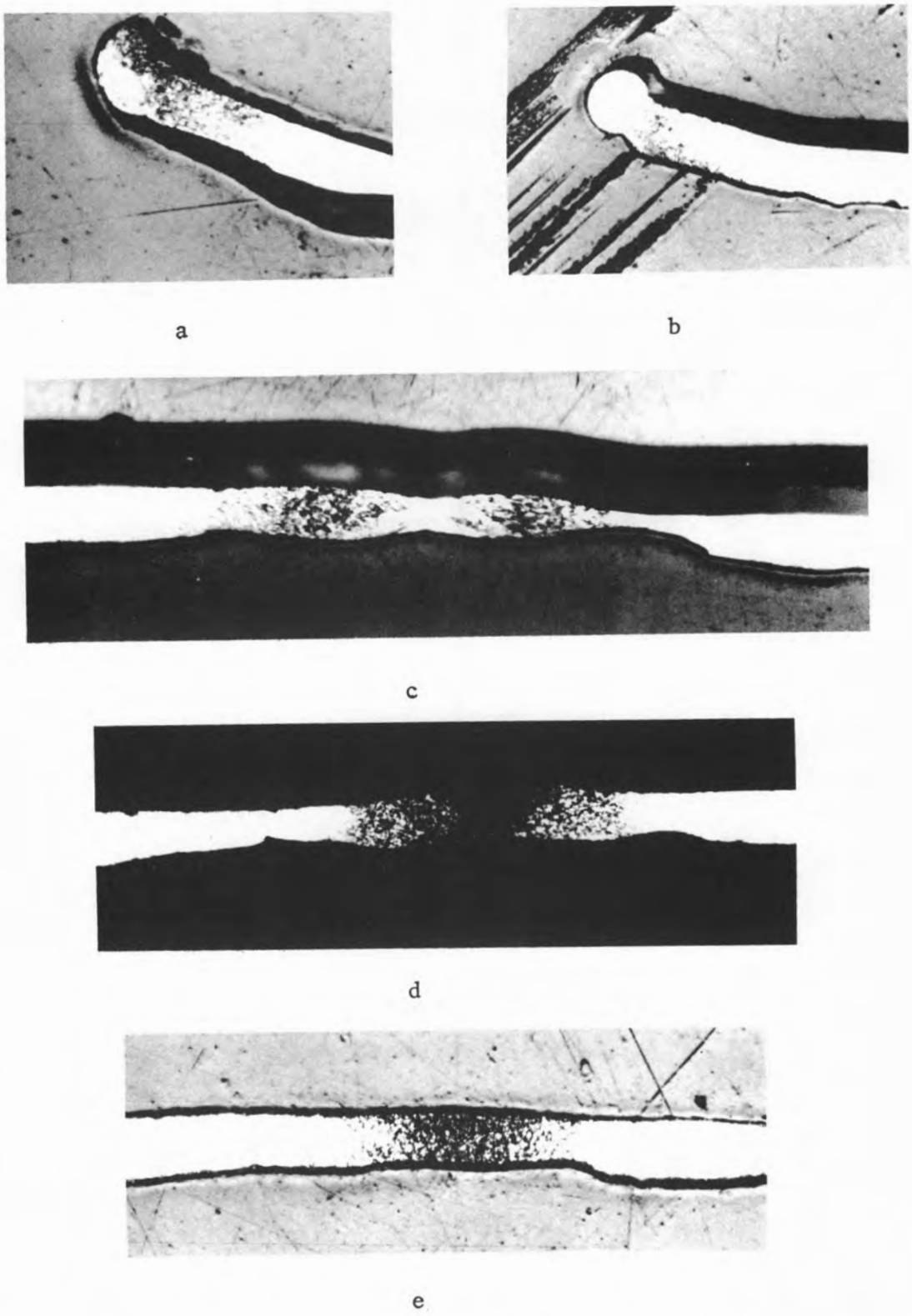

Figure 55. Cross section micrographs of electron beam tracks. (250X)
a, b and c. 1.6 joules/inch
d and e 1.0 joules/inch

We have used energy per unit length as a parameter for evaluating the efficacy of electron beam embrittling when probably energy per unit area is a more definitive variable. In the process of evaluating higher beam velocities at constant energy per unit length, higher currents were required. These higher currents cause a spreading of the beam which reduces the energy density. Samples 73 through 76 were made at velocities an order of magnitude higher than sample 30 and 31 yet require higher energy for the same mark intensity. This is shown in Table IX.

Sample warpage due to e-beam crystallization was of concern until sample separation along the crystallized line was attempted. When the line was fractured, many small flakes, less than the line width in maximum dimension, broke away from the damaged region. The combination of the line fracturing and the material removal invariably relieved the stresses which caused the warpage in the sample and the sample laid flat. Sample 94 in figure 56 displays this stress relief.

Sample separation has been accomplished after electron beam embrittlement by two methods. The line has been "chased" with a ball or dulled pointed rod with a reasonable degree of success. To do this, the sample is placed on a somewhat compliant surface such as the top of a full pad of paper and the chasing tool manually following the line with a nominal pressure (similar to writing with a 2H pencil). The maximum velocity with which this can be done has not been evaluated but is expected to be considerably below the maximum velocity of embrittlement. A second method of break out is to pull the sample over a small diameter rod causing the crystallized region to be strained beyond its elastic limit and thereby fracturing the embrittled region. In all tests performed, the two methods separated the samples equally well. Bending over a small radius rod appears to be capable of more closely matching the electron beam speed than following the line with a chasing tool. Reentrant curves which are part of most motor lamination tooth designs may be more difficult to part completely with the bending technique.

TABLE IX

MARK INTENSITY DECREASING AS BEAM CURRENT IS

INCREASED KEEPING ENERGY CONSTANT

Sample	V (kv)	I (ma)	P (watts)	v (in/sec)	E (joules/in)	Mark Intensity
30a	50	.4	20	40	.5	Very Light
30b	50	.8	40	40	1.0	Moderate
30c	50	.8	40	400	0.1	None
31a	50	.8	40	20	2.0	Heavy
31b	50	1.6	80	80	1.0	Moderate
31c	50	3.2	160	160	1.0	Moderate
73a	100	5	500	550	0.9	Light
73b	100	10	1000	550	1.8	Moderate
73c	100	20	2000	550	3.6	Parted
74a	150	5	750	630	1.2	Light
74b	150	10	1500	630	2.4	Heavy
74c	150	15	2250	630	3.6	Parted
75a	150	5	750	1100	.7	None
75b	150	10	1500	1100	1.4	Light
75c	150	15	2250	1100	2.1	Moderate
76a	150	10	1500	1570	1.0	None
76b	150	15	2250	1570	1.5	Very light
76c	150	20	3000	1570	2.0	Moderate

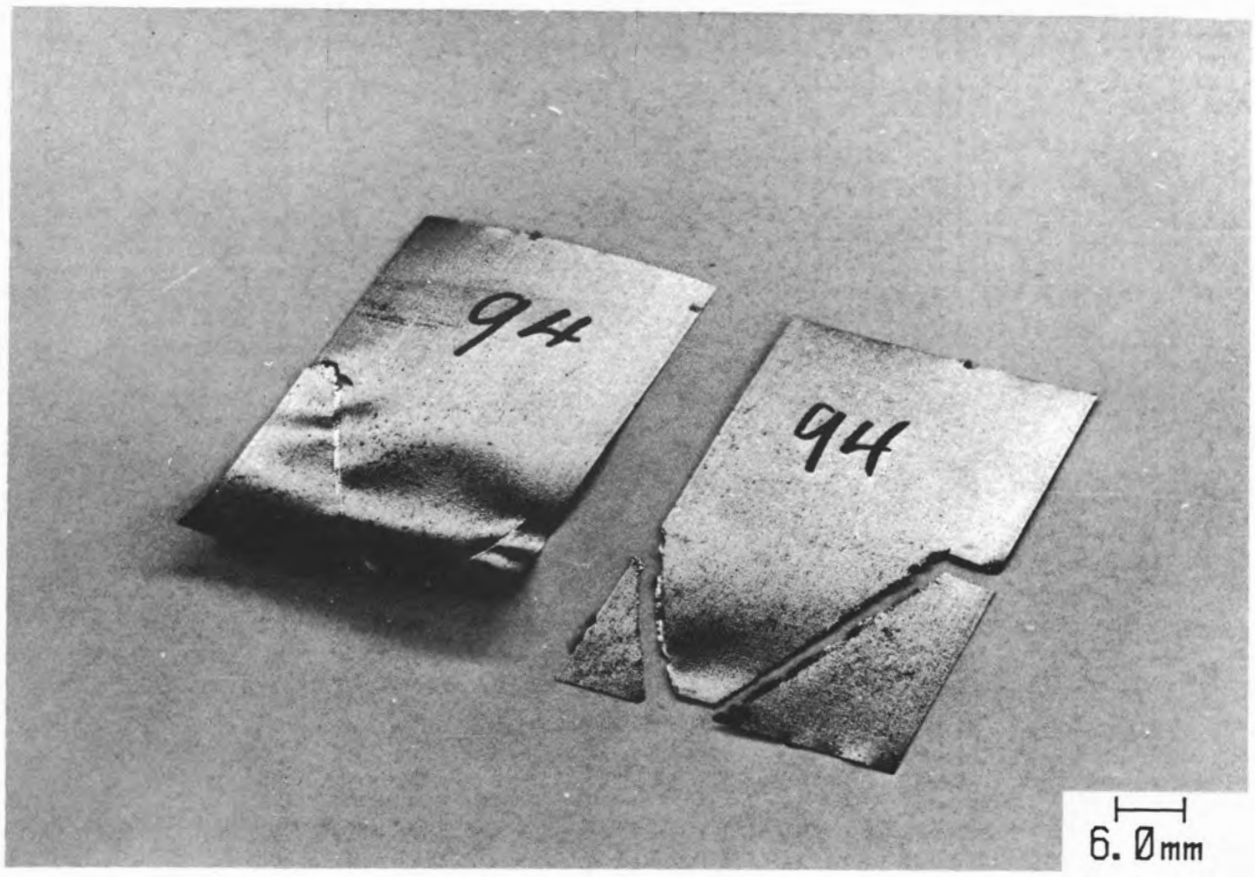

Figure 56. Sample flattening due to stress relief after fracture on crystallized line.

The typical detail of the separated edges of an embrittled line made at 1800 inches/second is shown in figure 57. Although the edge is not as smooth as a conventionally punched lamination, the protrusions are within 0.010 inches of a nominal line. They will stack satisfactorily and not materially alter the motor slot fill factor.

In summary, the forming of embrittling lines with an electron beam at economical speeds is feasible. Good quality, burrless edges can be produced. Further work should be focused on: 1) breakout of re-entrant lines, 2) mechanizing and speeding up the breakout process and 3) developing equipment for transporting the ribbon within the e-beam equipment.

Hot Die Punching

The final method evaluated for forming the conductor slot was not based on the heating to form embrittled regions that was common to the prior three methods. Rather, it is based on the fact that as one heats the amorphous metal the viscosity or resistance to deformation decreases exponentially with temperature. Thus, at some temperature (usually about 100°C below the crystallization temperature) the strength of the amorphous metal drops very rapidly. In this condition the material should be very easy to cut without any detectable tool wear.

It is not possible, however, to simply heat the material to this temperature by normal methods, cut and then cool again. This is because when heated the material also undergoes (with time) internal structural relaxation which causes embrittlement. Thus, heating and cooling must be accomplished very rapidly to avoid the structural relaxation.

To test this approach of hot cutting, a simple die set was made consisting of two brass plates with 1/2 inch holes in them. The ribbon was clamped between these plates with the holes aligned. A steel punch was heated to about 500°C and slowly forced through the holes in the brass plates. The ribbon was heated rapidly from the punch contact, and when it reached its softening temperature the punch went through easily.

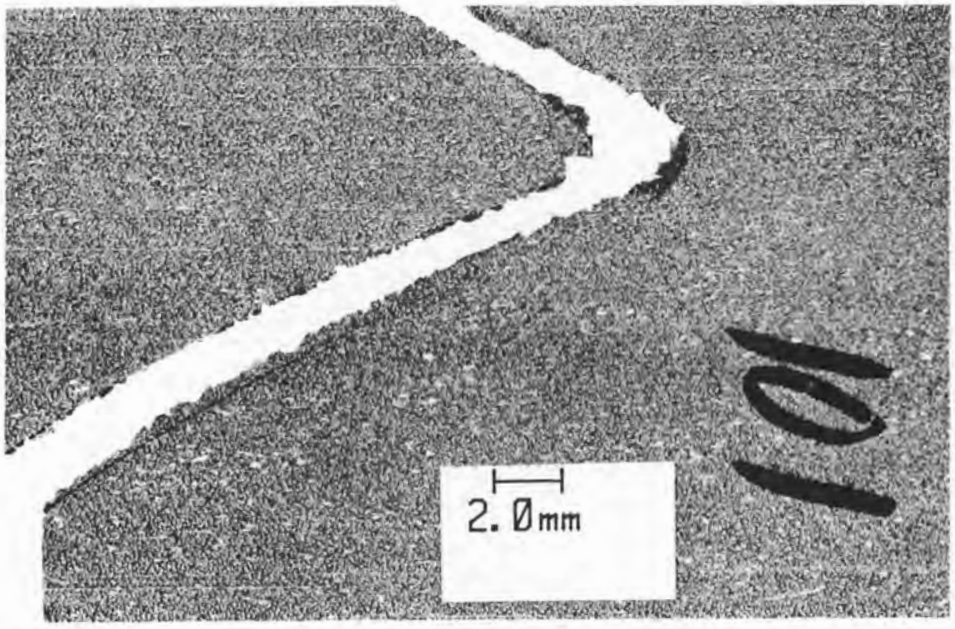

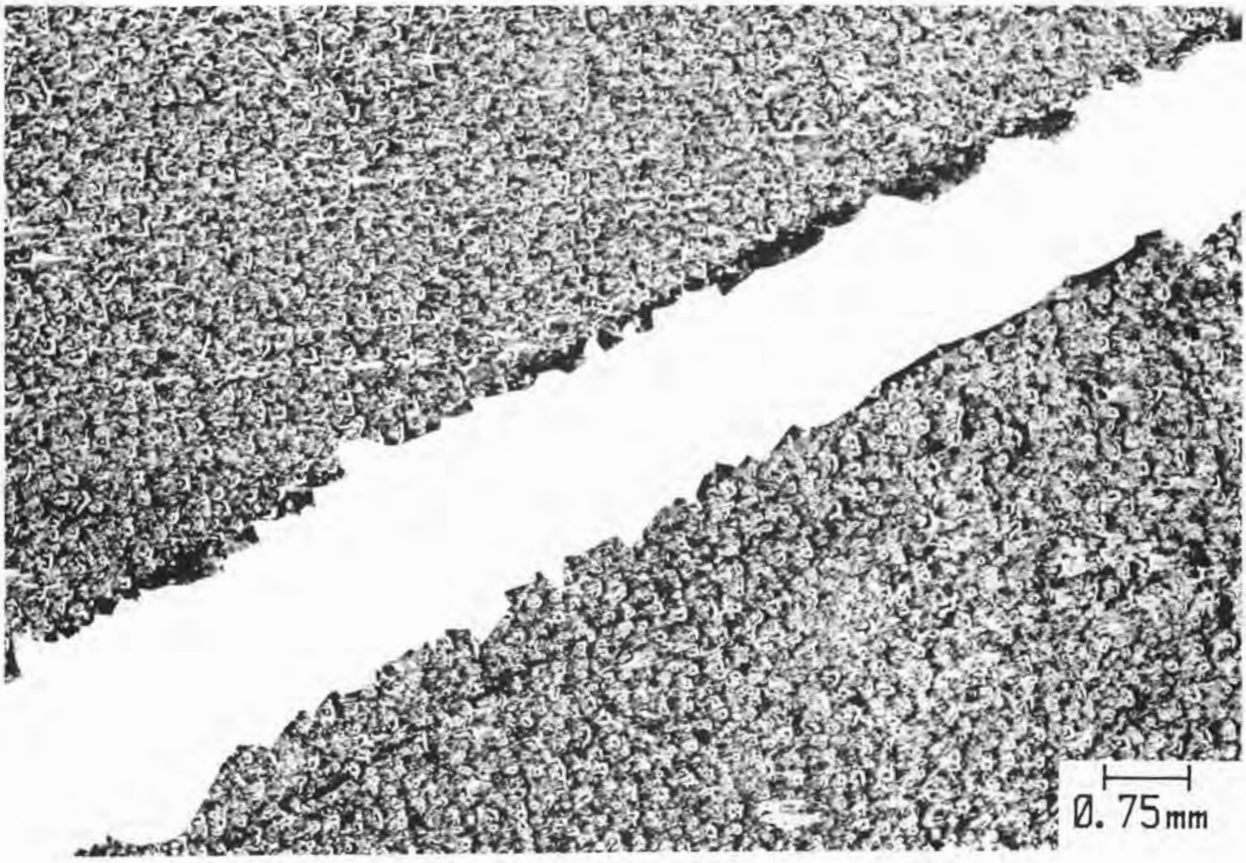

Figure 57. Detail of fractured line written with e-beam at 2.7 joules/inch and 1800 inches/sec.

The punch was rapidly removed so that the ribbon would quench rapidly from its contact with the brass.

Figure 58a shows the ribbon after punching. It can be seen that the ribbon was so soft and ductile when the punch went through that a long deep-draw lip was formed. This lip was easily removed with an abrasive belt as shown in figure 58b. If the die set is made with better tolerance, this ductile lip could be minimized. The key unanswered questions for this approach are: 1) Can the lip be avoided completely? 2) Can the punching go fast enough to be economical? and 3) Are good mechanical and magnetic properties maintained after punching?

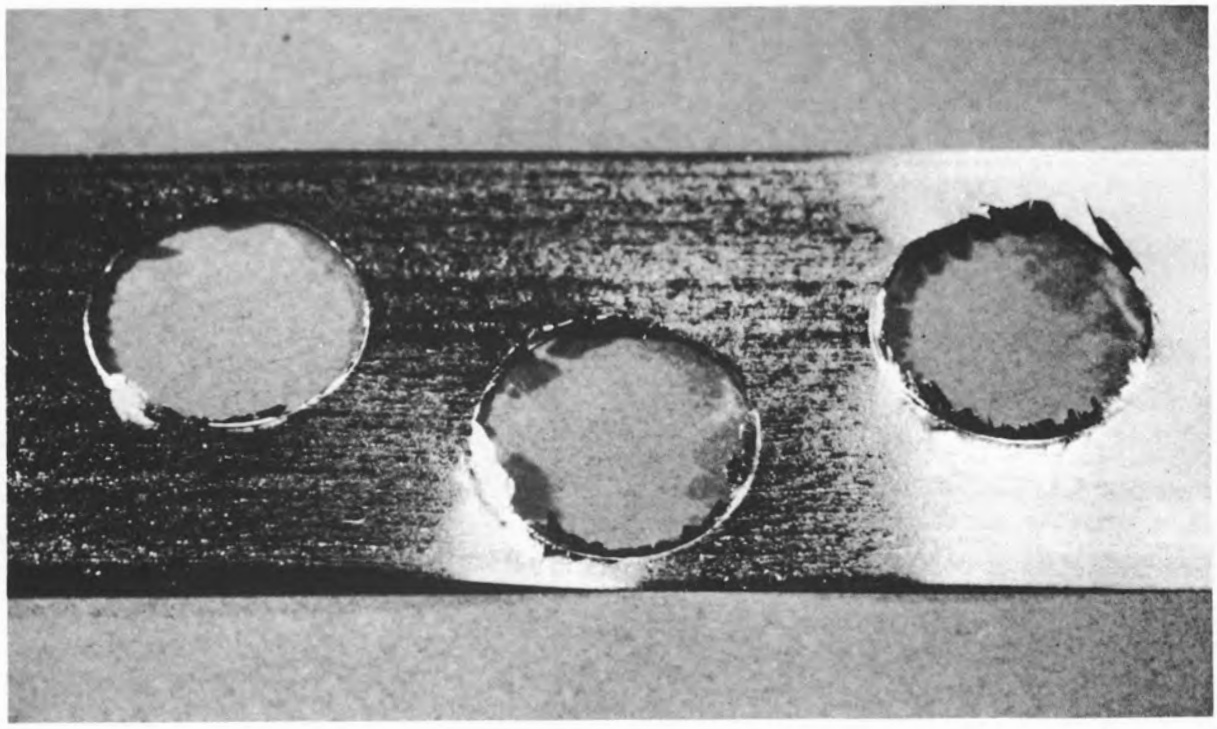

a

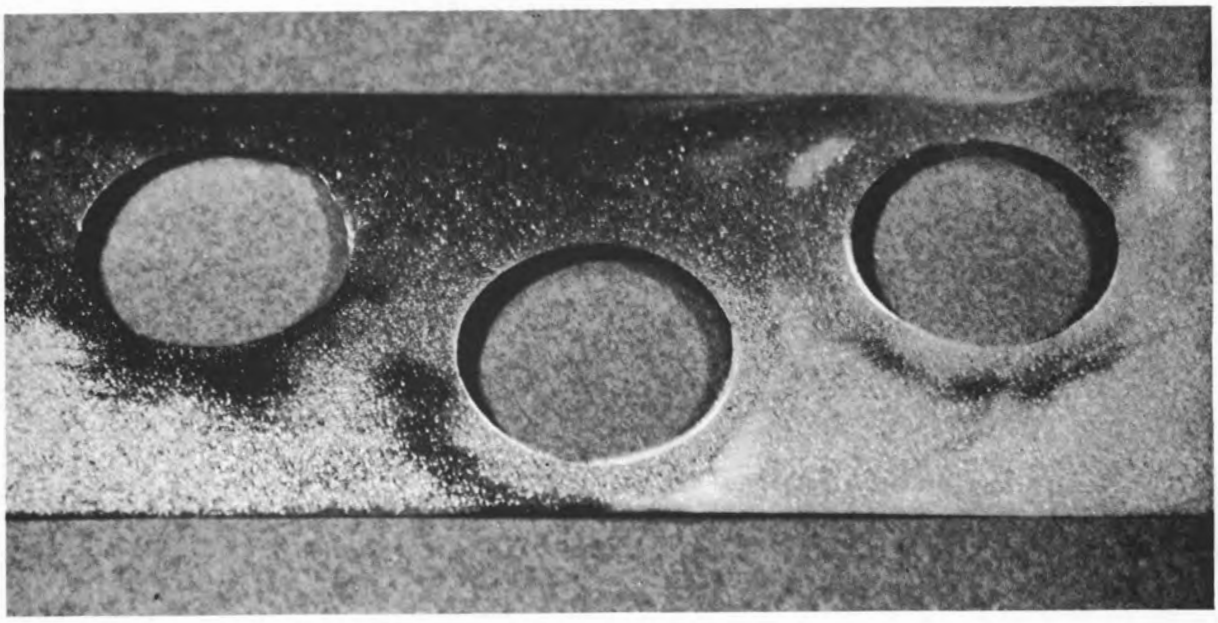

b

Figure 58. Holes made with hot die punch.
a) as punched
b) after abrasive wheel conditioning.

ORNL/Sub-81/70519/1
Dist. Cat. UC-97C

INTERNAL DISTRIBUTION

1. D. B. Allen
2. T. D. Anderson
3. R. S. Carlsmith
4. W. Fulkerson
5-9. P. A. Gnadt
10. D. S. Griffith
11k T. L. Hudson
12. A. F. Johnson
13. M. A. Kuliasha
14. J. W. Michel
15-19. M. C. Miller
20. L. C. Oaks
21. S. L. Purucker
22. T. W. Reddoch
23. M. W. Rosenthal
24. J. P. Stovall
25. R. D. Stulting
26. A. J. Thompson
27. H. E. Trammel
28. D. B. Trauger
29. ORNL Patent Office
30. Central Research Library
31. Document Reference Section
32-33. Laboratory Records Department
34. Laboratory Records (RC)

EXTERNAL DISTRIBUTION

35. G. P. Adams, Niagara Mohawk Power Corp., Research and Development C-1, 300 Erie Boulevard, West, Syracuse, NY 13202

36. S. Annestrand, Bonneville Power Administration, P. O. Box 3621, Portland, OR 97208

37. H. J. Brudner, Research and Development, Power Authority of the State of New York, 10 Columbus Circle, New York, NY 10019

38. J. S. Brushwood, Electric Power Research Institute, 3412 Hillview Avenue, Palo Alto, CA 94304

39. C. Calabrese, Consolidated Edison Co., 4 Irving Place, New York, NY 10003

40. R. D. Caligviri, SRI International, 333 Ravenwood Avenue, Menlo Park, CA 94025

41. O. Compton, VEDCO OJRP15, 700 E. Franklin Street, P. O. Box 2666, Richmond, VA 23261

42. P. Diamant, Medium Motor Division, Siemens-Allis, Inc., 4620 Forrest Avenue, Norwood, OH 45212

43. R. D. Dunlop, Department of Energy, Division of Electric Energy Systems, Forrestal Building, 1000 Independence Avenue, S.W., Washington, DC 20585

43. N. Hingorani, Electric Power Research Institute, P. O. Box 10412, Palo Alto, CA 94304

44. E. T. Horton, Electric Power Research Institute, 3412 Hillview Avenue, Palo Alto, CA 94304

45. L. A. Johnson, General Electric Corporation, Research and Development Center, P. O. Box 8, Building KW, Room D282, Schenectady, NY 12301

46. F. R. Kalhammer, Director, Energy Management and Utilization Division, Electric Power Research Division, P. O. Box 10412, Palo Alto, CA 94304

47. H. Kaufman, Empire State Electric Research Institute, 1271 Avenue of the Americas, Room 33950, New York, NY 10020

48. K. W. Klein, Department of Energy, Division of Electric Energy Systems, Forrestal Building, 1000 Independence Avenue, S.W., Washington, DC 20585

49. B. Kuhn, General Electric Corporation, Research and Development Center, P. O. Box 8, Building KW, Room D282, Schenectady, NY 12301

50. T. R. LaPorte, Institute of Government Studies, University of California, 109 Moses Hall, Berkeley, CA 94720

51. L. Long, Duke Power Company, P. O. Box 2178, Charlotte, NC 28242

52. J. Melcher, Massachusetts Institute of Technology, Department of Electrical Engineering and Computer Science, High Voltage Research Laboratory, Building N-10, 155 Massachusetts Avenue, Cambridge, MA 02139

53. L. I. Moss, Energy/Environmental Design and Policy Analysis, 5769 Longs Peak Route, Estes Park, CO 80517

54. S. Nilson, Electric Power Research Institute, P. O. Box 10412, Palo Alto, CA 94304

55. M. Rabinowitz, Electric Power Research Institute, P. O. Box 10412, Palo Alto, CA 94304

56. M. Russell, Director, Center for Energy, Policy Research, Resources for the Future, 1755 Massachusetts Avenue, N.W., Washington, DC 20036

57. L. Savio, Consolidated Edison Co., 4 Irving Place New York, NY 10003

58. F. Strinsa, New York State Energy Research and Development Authority, Building No. 2, Empire State Plaza, Albany, NY 12223

59. N. Tai, Consolidated Edison Co., 4 Irving Place New York, NY 10003

60. J. V. Vithayathil, Chief Technical Engineer (Network), Bonneville Power Administration, P. O. Box 3621, Portland, OR 97208

61. J. C. White, Electric Power Research Institute, P. O. Box 10412, Palo Alto, CA 94304

62. W. H. Williams, Division Manager, American Bell, Building 83, Room 1B23, Southgate Parkway, Morristown, New Jersey 07960

63. Office of Assistant Manager for Energy Research and Development, Department of Energy, Oak Ridge Operations, Oak Ridge, TN 37831

64-425. Given distribution as shown in DOE/TIC-4500 under category UC-97b (Electric Energy Systems - Power Distribution)

☆U.S. GOVERNMENT PRINTING OFFICE: 1983-646-055/290